

THE SPECTRA OF THE DIETHYNYLBENZENES

THE SPECTRA OF THE DIETWYNYLBENZENES

by

ANTOON A. G. VAN PUTTEN

A Thesis

Submitted to the Faculty of Graduate Studies

in Partial Fulfillment of the Requirements

for the Degree

Doctor of Philosophy

McMaster University

May 1974

DOCTOR OF PHILOSOPHY  
(Chemistry)

McMASTER UNIVERSITY  
Hamilton, Ontario

TITLE: The Spectra of the Diethynylbenzenes

AUTHOR: A. A. G. van Putten

SUPERVISOR: Dr. G. W. King

NUMBER OF PAGES: (viii), 155

SCOPE AND CONTENTS:

The vibrational spectra of the three isomeric diethynylbenzenes (ortho, meta and para) are analyzed and the fundamental frequencies are assigned.

Three electronic absorption systems are observed for each diethynylbenzene. The observed positions and intensities of these three transitions agree closely with the results of CNDO calculations. The transitions show large red shifts with respect to the analogous absorptions in benzene.

Rotational band contour analysis confirms the occurrence of two types of bands, single and double headed, in the lowest-energy transition of the diethynylbenzenes.

It is argued that, at present, nothing definitive can be said about the geometry of the aromatic ring in the ground and first excited electronic state of derivatives of benzene.

## ACKNOWLEDGEMENTS

First I wish to thank Dr. G. W. King for paving the way to the diethynylbenzenes, for allowing me complete freedom in my research and for his comments on the first draft of this thesis.

I acknowledge financial assistance by the Chemistry Department of McMaster University and I am indebted to Mrs. Susan Judge for the skillful typing of this thesis.

During the course of this research I have been influenced by my family, friends and colleagues, and it is a pleasure to thank all those who have helped to put my head where it is at today.

TABLE OF CONTENTS

	Page
INTRODUCTION	1
CHAPTER 1	
THE GROUND STATE GEOMETRY OF THE DIETHYNYLBENZENES	3
CHAPTER 2	
EXPERIMENTAL WORK	14
CHAPTER 3	
THE VIBRATIONAL SPECTRA OF THE DIETHYNYLBENZENES	24
CHAPTER 4	
REVIEW OF U.V. SPECTRA AND MOLECULAR ORBITAL CALCULATIONS	73
CHAPTER 5	
ANALYSIS OF THE ELECTRONIC SPECTRUM	97
CHAPTER 6	
BAND CONTOUR ANALYSIS AND EXCITED STATE GEOMETRY	126
CONCLUSIONS	148
BIBLIOGRAPHY	151

## LIST OF TABLES

Table		Page
1.1	Bondlengths ( $\text{\AA}$ ) and Rotational Constants ( $\text{cm}^{-1}$ ) for Several Structures of $\phi\text{F}$	9
1.2	Bondlengths ( $\text{\AA}$ ) and Rotational Constants ( $\text{cm}^{-1}$ ) for Various Geometries of $\phi\text{CCH}$	10
1.3	Bondlengths ( $\text{\AA}$ ), Bond Angles (degrees) and Rotational Constants ( $\text{cm}^{-1}$ ) for Several Structures of para-DEB	11
1.4	Estimated Rotational Constants ( $\text{cm}^{-1}$ ) and the Asymmetry Parameters for the DEBs	12
3.1	The Symmetries, Descriptions and Frequencies of the 30 Benzene and the 6 Acetylenic Modes of Vibration	28
3.2	Classifications of the Normal Modes of Vibration for ortho-, meta- and para-DEB	30
3.3.A.1	Frequencies ( $\text{cm}^{-1}$ ) and Assignments of the I.R. Bands of the Isotopes of para-DEB	45
3.3.A.2	Frequencies ( $\text{cm}^{-1}$ ) and Assignments of the Raman Bands of the Isotopes of para-DEB	47
3.3.B	Frequencies ( $\text{cm}^{-1}$ ) and Assignments of the I.R. and Raman Bands of meta-DEB	49
3.3.C	Frequencies ( $\text{cm}^{-1}$ ) and Assignments for ortho-DEB	51
3.4.A	Ground State Fundamental Frequencies ( $\text{cm}^{-1}$ ) of the Isotopes of para-DEB	66
3.4.B	Ground State Fundamental Frequencies ( $\text{cm}^{-1}$ ) of the Isotopes of meta-DEB	67
3.4.C	Ground State Fundamental Frequencies ( $\text{cm}^{-1}$ ) of the Isotopes of meta-DEB	68
3.5	Experimental and Theoretical R-T Ratios for the Isotopes of para-DEB	70
3.6	Experimental and Theoretical R-T Ratios for the Isotopes of ortho- and meta-DEB	71
4.1	The $\pi$ Molecular Orbitals of Benzene	74
4.2	Correlation Table	76

Table		Page
4.3.A	The symmetry, energy (eV) and composition of the lowest excited $\pi \rightarrow \pi^*$ states of para-DEB	83
4.3.B	The symmetries and atomic orbital coefficients of the MO's involved in the $\pi \rightarrow \pi^*$ , $\sigma \rightarrow \pi^*$ and $\pi \rightarrow \sigma^*$ single-electron promotions of para-DEB	83
4.3.C	The symmetry, energy (eV) and composition of the $\sigma \rightarrow \pi^*$ and $\pi \rightarrow \sigma^*$ states of para-DEB	84
4.4.A	The symmetry, energy and composition of the lowest $\pi \rightarrow \pi^*$ states of meta-DEB	85
4.4.B	The coefficients of the 2p AO's of the MO's that are important in the single-electron promotions that describe the $\pi \rightarrow \pi^*$ , $\sigma \rightarrow \pi^*$ and $\pi \rightarrow \sigma^*$ transitions of meta-DEB	86
4.4.C	Symmetry, energy and composition of the $\sigma \rightarrow \pi^*$ states of meta-DEB	86
4.5.A.1	Symmetry, energy and composition of the lower $\pi \rightarrow \pi^*$ states of ortho-DEB (40 excited states)	88
4.5.A.2	Symmetry, energy and composition of the lower $\pi \rightarrow \pi^*$ states of ortho-DEB (38 excited states)	88
4.5.B	The coefficients of the 2p AO's of the MO's that are important in the single-electron promotions that describe the $\pi \rightarrow \pi^*$ , $\sigma \rightarrow \pi^*$ and $\pi \rightarrow \sigma^*$ transitions of ortho-DEB	89
4.5.C	Symmetry, energy and composition of the $\sigma \rightarrow \pi^*$ and $\pi \rightarrow \sigma^*$ states of ortho-DEB	89
4.6.A	Energy and composition of the lower $a_1$ excited states of $\phi$ CCH	95
4.6.B	Energy and composition of the lower $a_1$ excited states of $\phi$ CCH, with the exclusion of the $\sigma \rightarrow \sigma^*$ excitation	95
5.1	Wavenumbers ( $\text{cm}^{-1}$ ) and relative intensities of the vibrational bands in the diffuse 261 nm system of para-DEB	103
5.2	Wavenumbers ( $\text{cm}^{-1}$ ) and relative intensities of the bands in the $\tilde{A} \ ^1B_{2u} \leftarrow \tilde{X} \ ^1A_g$ transition of para-DEB	106
5.3	Wavenumbers ( $\text{cm}^{-1}$ ) and relative intensities of the vibrational bands in the 296 nm transition of meta-DEB	113

Table		Page
5.4	Wavenumbers ( $\text{cm}^{-1}$ ) and relative intensities of the vibrational bands in the 256 nm system of ortho- $\text{h}_6$	122
5.5	Wavenumbers ( $\text{cm}^{-1}$ ) and relative intensities of the bands measured in the 298 nm system of ortho-DEB	123
6.1	The changes in the rotational constants (in $\text{cm}^{-1}$ ) for benzene and various benzene derivatives	127
6.2	Calculated ground and excited state geometry for $\phi$ , $\phi\text{F}$ , $\phi\text{CCH}$ and para-DEB	145



LIST OF FIGURES

Figure		Page
1.1	Definition of the coordinate (x,y,z) and inertial (a,b,c) axes and numbering of the C-atoms for $\phi$ CCH and the DEBs	8
3.1.A	Schematic representation of the tangential modes of vibration	31
3.1.B	Schematic representation of the radial modes of vibration	34
3.1.C	Schematic representation of the out-of-plane modes of vibration	37
3.2	Wavenumber range ( $\text{cm}^{-1}$ ) of the frequencies of the normal modes of vibration of the DEBs	43
5.1	The U.V. absorption systems of para- $\text{h}_6$	98
5.2.A	The vacuum U.V. absorption systems of para- $\text{h}_6$ from 180 to 150 nm	99
5.2.B	The vacuum U.V. spectrum of para- $\text{h}_6$ in the region from 135 to 115 nm	100
5.3	The U.V. absorption systems of meta- $\text{h}_6$	110
5.4	The U.V. absorption systems of ortho- $\text{h}_6$	117
6.1	The $0_0^0$ band (B-type) of para- $\text{h}_6$ . Curves A and B are microdensitometer tracings and curve C is a calculated contour.	130
6.2	The $20_0^1$ (A-type) band of para- $\text{h}_6$ . Curve A is a tracing and curve B is a calculated contour.	131
6.3	The $0_0^0$ (B-type) band of $\text{C}_6\text{D}_5\text{CCH}$ . Curve A is a microdensitometer tracing and curve B a calculated contour.	135
6.4	A microdensitometer tracing of the $0_0^0$ band of meta- $\text{h}_6$	136
6.5	A microdensitometer tracing of the $0_0^0$ band of ortho- $\text{h}_6$	137

## INTRODUCTION

In this thesis the results are reported of an investigation of the spectra of the three diethynylbenzenes, ortho-, meta- and para- $C_6H_4(CCH)_2$ , and their deuterated isotopes. The latter are: para- $C_6H_4(CCD)_2$ , para- $C_6D_4(CCH)_2$ , para- $C_6D_4(CCD)_2$ , meta- $C_6H_4(CCH)_2$  or ortho- $C_6D_4(CCH)_2$  and ortho- $C_6D_4(CCD)_2$ .

The diethynylbenzenes belong to a class of derivatives of benzene which has received very little spectroscopic attention in the literature in the past. The analysis made here for the vibrational spectra of the diethynylbenzenes leads to a better understanding of the internal bending modes of the acetylenic and the analogous cyano groups. Previous differences in the assignments of the far infrared frequencies of benzene derivatives with these substituents are resolved in this study.

The ultraviolet spectra of the diethynylbenzenes are of special interest, because of the strong conjugation in these molecules between the ring and the substituents, as is seen from the present work and a review of the literature. Two absorption systems are commonly observed in the ultraviolet spectra of benzene and its derivatives at wavelengths larger than 200 nm. The diethynylbenzenes are unusual in that they display three absorption systems in this region. These observations can be explained qualitatively in terms of the interaction of the  $\pi$ -electrons of the substituent with those of the benzene ring. These interactions are estimated quantitatively via calculations on the energies of the excited electronic states. The calculated and observed positions of the three absorption systems of the diethynylbenzenes provide novel and essential information on the correlations between the higher excited electronic states of benzene and these of its derivatives.

The geometries of the aromatic ring in the ground and excited electronic states of benzene and substituted benzenes have intrigued chemists for many years and many publications have appeared which deal with this topic. The methods employed for elucidating this structural problem are examined critically. Quantitative structural information is derived from the changes in rotational constants for hydrogenic and perdeutero para-diethynylbenzene upon electronic excitation. Open-shell CNDO calculations are also used to gain an insight into the changes that occur in the benzene ring geometry of substituted benzenes upon electronic excitation.

Basic spectroscopic theory is not reviewed here. The reader is referred to the texts on this subject by Herzberg<sup>(1,2)</sup>, King<sup>(3)</sup> and Varsanyi<sup>(4)</sup>. These are only referenced where specific information has been taken from them. Likewise, basic molecular orbital theory is not presented, but can be found in the texts by Parr<sup>(5)</sup> and Dewar<sup>(6)</sup>. Specific reference to these two sources is made where appropriate. Only those equations which are examined in detail are given in this study.

## CHAPTER 1

### The Ground State Geometry of the Diethynylbenzenes

#### Introduction

In this chapter the ground state geometries of the three diethynylbenzenes (DEBs) will be discussed. No structural data is available for these molecules. Therefore correlations are sought with the known structures for the monosubstituted benzenes, fluoro-benzene ( $\phi F$ ) and benzonitrile ( $\phi CN$ ). Three different structures have been proposed for  $\phi F$  and two different geometries have been suggested for  $\phi CN$ . The differences between these geometries are determined by the position of the substituent-carrying C-atom. This nucleus is displaced towards the center of the ring in one geometry and in the other, it is further from the center than in the undistorted benzene ring. No unambiguous choice can be made between these two structures. The rotational constants calculated for these two structures differ slightly from the experimental values, while the geometry calculated from these experimental values is somewhere in between the above two structures.

This makes it possible to set upper and lower limits for the parameters that determine the relative position of the substituent-carrying C-atom. This range includes the parameters for an undistorted benzene ring.

Extrapolation of these findings lead to calculated rotational constants for the DEBs with an uncertainty of about 0.5 to, at most, 1%. This uncertainty is of minor importance in the succeeding chapter, where ratios of rotational constants have been calculated. This uncertainty is important in the final chapter where geometry changes upon electronic excitation will be calculated from differences in rotational constants.

### 1.1. Estimation of Bondlengths

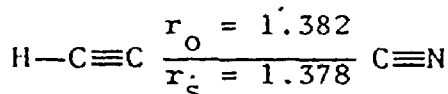
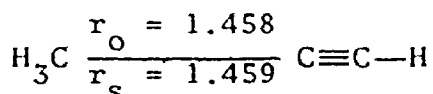
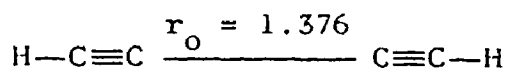
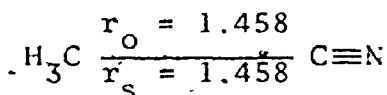
The bondlengths between two nuclei is the distance between these atoms at rest. This equilibrium distance ( $r_e$ ) can be found from the rotational structure of vibrational bands. This procedure has been followed for a few small molecules. Bondlengths for the vibrationless ground state can be determined by microwave spectroscopy, crystallographic analysis and electron diffraction. The resulting effective bondlengths ( $r_o$ ) are different for isotopic molecules and  $r_o$  bondlengths are usually chosen as values which fit best all data for the isotopes studied. An improvement in the  $r_o$  dimensions can be achieved in two ways:

1. by taking into consideration the zero-point vibrations<sup>(7a)</sup>. The resultant interatomic distances ( $r_z$ ) correspond to the corrected average distance between the nuclei.
2. by determining the position of a particular atom in a molecule by isotopic substitution<sup>(7b)</sup>. The resulting molecular substitution structure ( $r_s$ ) is independent of the isotopes studied. The  $r_s$  bondlengths are very nearly equal to the  $r_e$  distances, where these are available for comparison.

Bondlengths will be estimated below for the acetylenic (CCH) group, the bond linking this group to the benzene ring and the benzene ring itself ( $\phi$ ).

Microwave<sup>(8)</sup> and spectroscopic studies<sup>(9-13)</sup> have shown that the effective bondlengths of the acetylenic triple bond and C—H bond occur in the following narrow ranges for any substituted acetylene:  $r_o(\text{C}\equiv\text{C}) = 1.205 \pm 0.003 \text{ \AA}$  and  $r_o(\text{C—H}) = 1.056 \pm 0.004 \text{ \AA}$ . The  $r_s$  values have been shown to fall within the range specified for the  $r_o$  bondlengths<sup>(14)</sup>. The above values of 1.205  $\text{\AA}$  and 1.056  $\text{\AA}$  have been used throughout this study.

The effective bondlength of the  $\phi$ -CCH linkage has been estimated as  $1.44 \pm .02 \text{ \AA}$ <sup>(13)</sup>. This range can be narrowed by comparing analogous CCH and cyano (CN) compounds. Illustrative examples are given below<sup>(2,14)</sup>.



Obviously a very small change in bondlength occurs when a CCH group is replaced by a CN group. This conclusion is supported to some extent by the nearly identical rotational constants for  $\phi$ CN and  $\phi$ CCH.

A microwave study on  $\phi$ CN<sup>(15)</sup> has resulted in a  $r_s$  value of  $1.455 \text{ \AA}$  for the  $\phi$ -CCH linkage. This value is very close to the  $r_s$  bondlengths in acrylonitrile and propyne. It has been assumed in this study that the bond between the  $\phi$  and CCH parts has a value of  $1.455 \text{ \AA}$  for  $\phi$ CCH and the DEBs. Recently, however, the microwave spectra of the isotopes of  $\phi$ CN were re-examined by Casado et al<sup>(16)</sup> and an improved  $r_s$  value of  $1.451 \text{ \AA}$  has been proposed for the  $\phi$ -CCH bond. The difference between this improved and the original value is rather small. The above authors have estimated  $r_z = 1.444 \text{ \AA}$  for this bond. The difference between the  $r_s$  and  $r_z$  bondlengths is closely related to the benzene ring geometry.

The effective C-C and C-H bondlengths of benzene have been estimated<sup>(2)</sup> as  $r_o(\text{C}-\text{C}) = 1.397 \pm 0.004 \text{ \AA}$  and  $r_o(\text{C}-\text{H}) = 1.084 \pm 0.004 \text{ \AA}$ .

The replacement of a hydrogen atom by a substituent will be accompanied by a change in the geometry of the  $\phi$  ring. This change will depend on the nature of the substituent. In what respect a given substituent in-

fluences the geometry of the  $\phi$  ring is largely unknown. Only for  $\phi F$ <sup>(17)</sup> and  $\phi CN$ <sup>(15,16)</sup> have the  $r_s$  structures been determined by microwave spectroscopy. These studies have shown that for both molecules the unsubstituted part of the ring undergoes a very small change in geometry and that the substituent-carrying C-atom is closer to the center of the ring compared to the unsubstituted ring. This follows from the measured shortening by about 0.01 Å of the two benzene C—C bonds that have the substituent-carrying C-atom in common. This shortening is accompanied by an increase in the bond angle between these two C—C bonds by 1.8° and 3.4° for  $\phi CN$  and  $\phi F$  respectively.

The distortion found for  $\phi CN$  can also be expected for  $\phi CCH$  because of the similarities, outlined above, between analogous CCH and CN compounds. This distortion can also be extrapolated to para-DEB, since opposite C-atoms are substituted. For the latter compound, a benzene ring is then predicted with four short and two long C—C bonds and an angle greater than 120° between the two short bonds. This will be called the antiquinoidal structure.

It can also be argued, however, that the benzene ring is distorted in the typical quinoidal manner with four long and two short C—C bonds. According to resonance theory, two CCH groups in para position give rise to increased conjugation resulting in a quinoidal structure. The reference compound then is para-benzoquinone in which the substituent-carrying C-atoms are further away from the center of the ring compared with  $\phi$  and in which the angle between the adjacent C—C bonds has decreased to 118.6°<sup>(18)</sup>.

This hypothetical quinoidal structure is not at all unreasonable if a comparison is made with the  $r_z$  structure of  $\phi CN/\phi CCH$ . This  $r_z$  structure was found<sup>(16)</sup> to deviate from a regular hexagonal benzene ring in a direction opposite to the distortion found for the  $r_s$  structure. The distinction between the  $r_s$  (antiquinoidal) and  $r_z$  (quinoidal) structure is thus determined

by the in- or outward displacement of the substituent-carrying C-atom with respect to the regular hexagonal ring.

It will be clear that the geometry question hinges on the position of the substituent-carrying C-atom. This position is determined by the following parameters: the benzene C—C bondlengths that have in common the substituent-carrying C-atom, the angle between these bonds and the length of the bond between the benzene ring and the substituent. Numerical values for these parameters will be examined in detail in the next section for  $\phi F$  and  $\phi CN/\phi CCH$ .

### 1.2. Estimation of Rotational Constants

It has been demonstrated in the preceding section that the geometry is dependent on the particular set of internuclear parameters used. A distinction should thus be made between the rotational constants calculated for the  $r_o$ ,  $r_s$  and  $r_z$  structures. The estimation of the rotational constants (and the geometry) of the DEBs would be greatly simplified if it could be shown that these constants are very nearly independent of the set of internuclear parameters used. The rotational constants have been calculated for the structures that have been suggested for  $\phi F$  and  $\phi CN/\phi CCH$ . These calculated rotational constants will be compared with the effective rotational constants as determined via microwave spectroscopy. The rotational constants have been calculated by slightly modifying the computer program described by So<sup>(10)</sup>.

#### $\phi F$

Cvitas et al<sup>(19)</sup> have proposed the  $r_o$  geometry for  $\phi F$  given in Table 1.1, set I. (The numbering of the C-atoms for  $\phi F$  is the same as defined for  $\phi CCH$  in Fig. 1.1.) The above authors arrived at this structure by assuming that substituents only affect the position of the substituent-carrying C-atom in monosubstituted benzenes. Of all possible structures those were



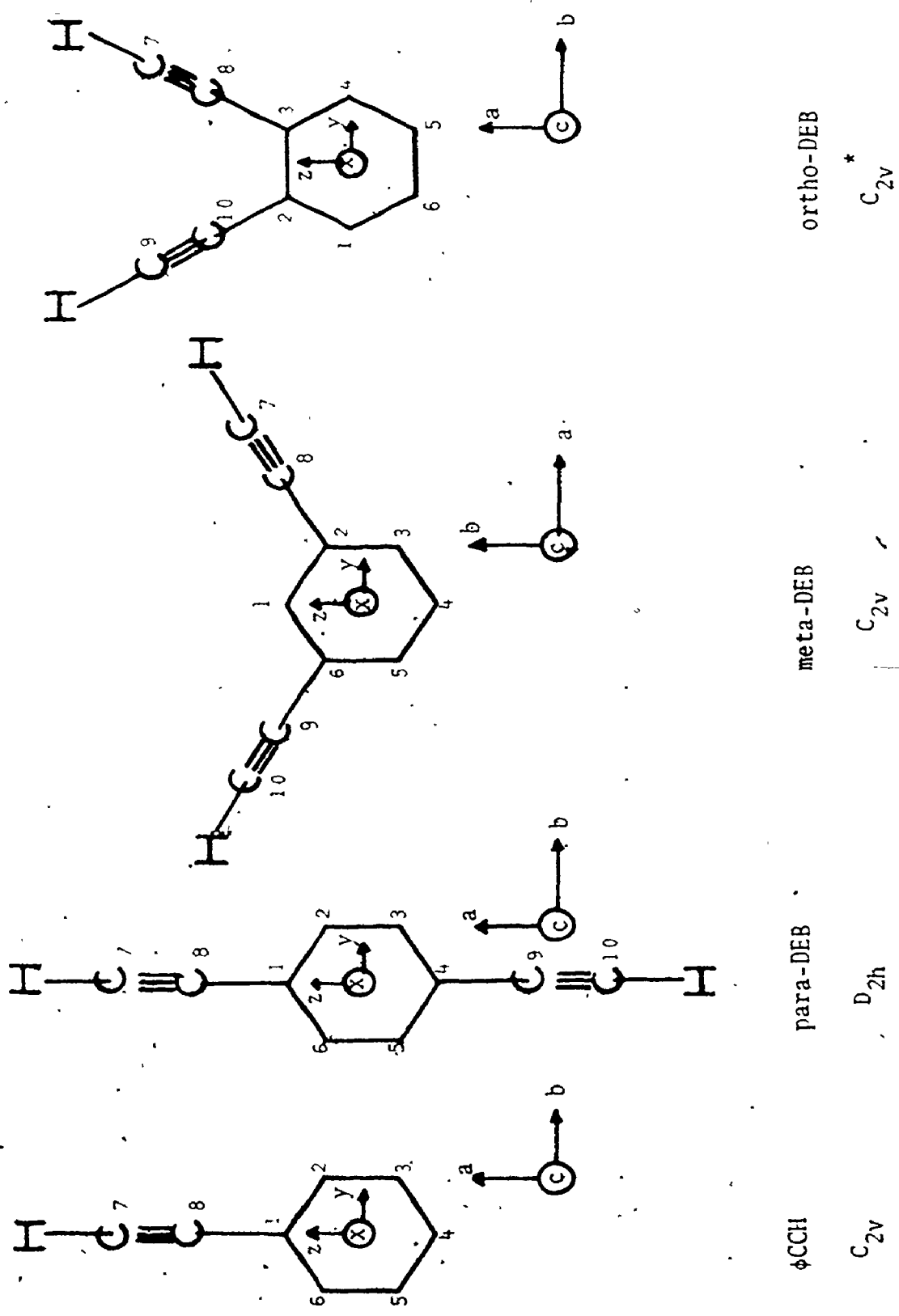


Fig. I.1 Definition of the coordinate (x,y,z) and inertial (a,b,c) axes and numbering of the carbon atoms for  $\phi CCH$  and the DEBs.

chosen, that reproduced satisfactorily the effective rotational constants for variously para-disubstituted benzenes. Set II in Table 1.1 corresponds to the  $r_s$  structure as found from isotopically substituted fluorobenzenes. Set III has been determined theoretically via a calculation of the minimum ground state energy in CNDO approximation by varying bondlengths and bond angles. The details of this calculation will be discussed in a later chapter.

Table 1.1

Bondlengths ( $\text{\AA}$ ) and Rotational Constants ( $\text{cm}^{-1}$ )for Several Structures of  $\phi\text{F}$ 

	$r_{1,2}(\text{\AA})$	$r_{2,3}(\text{\AA})$	$r_{3,4}(\text{\AA})$	$r_{\text{C-F}}(\text{\AA})$	$\angle \text{C}_6\text{C}_1\text{C}_2^\circ$	$A(\text{cm}^{-1})$	$B(\text{cm}^{-1})$	$C(\text{cm}^{-1})$
I	1.397	1.397	1.397	1.319	121.0	0.1889	0.0858	0.0590
II	1.383	1.395	1.397	1.354	123.4	0.1887	0.0862	0.0592
III	1.397	1.395	1.395	1.348	122.5	0.1906	0.0862	0.0594

The data in Table 1.1 reveal that the theoretical and substitution structures are very similar and that the  $r_o$  geometry is quite different from these. The substituent-carrying C-atom is displaced towards the center of the ring by 0.012, 0.044 and 0.028  $\text{\AA}$  for Set I, II and III, respectively, compared to an undistorted benzene ring. The differences between these values are very large in comparison with the differences in  $r_s$  and  $r_o$  values for simpler molecules<sup>(14)</sup>. Cvitas et al<sup>(19)</sup> do not claim a great accuracy for their structure (Set I). The physical significance of the distortions suggested by these authors could therefore be doubtful.

#### $\phi\text{CCH}$

It has been argued earlier in this chapter that the geometries for  $\phi\text{CN}$  and  $\phi\text{CCH}$  should be very nearly identical. This makes it possible to pre-

dict the  $r_s$  and  $r_z$  structures for  $\phi\text{CCH}$ . These and the corresponding rotational constants have been tabulated in Table 1.2, together with an effective and an undistorted structure. The numbering used in Table 1.2 is as given in Fig. 1.1.

Data Set I has been obtained by So<sup>(10)</sup> by matching the C—C bondlengths to the effective rotational constants, assuming a slight, uniform expansion of the benzene ring. Set II is based on the (antiquinoidal)  $r_s$  structure of  $\phi\text{CN}$ <sup>(17)</sup> and the bond between the CCH group and  $\phi$  was assumed to have a length of 1.455 Å. Data Set III corresponds to the theoretical structure obtained via a procedure analogous to the one used for  $\phi\text{F}$ . This theoretical structure possesses typical quinoidal character and is thus similar to the  $r_z$ <sup>(12)</sup> geometry.

Table 1.2

Bondlengths (Å) and Rotational Constants ( $\text{cm}^{-1}$ )

for Various Geometries of  $\phi\text{CCH}$

	$r_{1,2}$ (Å)	$r_{2,3}$ (Å)	$r_{3,4}$ (Å)	$r_{1,8}$ (Å)	$r_{7,8}$ (Å)	$\angle\text{C}_6\text{C}_1\text{C}_2$	A( $\text{cm}^{-1}$ )	B( $\text{cm}^{-1}$ )	C( $\text{cm}^{-1}$ )
I	1.4005	1.4005	1.4005	1.4325	1.205	120.0°	0.1888	0.0510	0.0402
II	1.389	1.396	1.397	1.455	1.205	121.8°	0.1892	0.0512	0.0403
III	1.405	1.395	1.396	1.423	1.209	118.5°	0.1900	0.0509	0.0401
IV	1.397	1.397	1.397	1.455	1.205	120.0°	0.1896	0.0507	0.0400

The data in Table 1.2 show that the quinoidal (Set II) and the antiquinoidal (Set III) geometries do not reproduce the effective moments of inertia. So's procedure (Set I) results in a geometry in between those in Set II and III. The position of the substituent-carrying C-atom is shifted by +0.035, -0.025, and +0.018 Å for Set I, II and III respectively, in comparison to a regular  $\phi$  ring. The differences between these shifts are very much larger than analogous differences for smaller molecules<sup>(11)</sup>. This indicates that these differences

are of a procedural rather than a molecular origin. It is thus impossible to make a physical significant choice between the three structures discussed for  $\phi$ CCH. As a result, the parameters that define the position of the substituent-carrying C-atom cannot be quoted more accurately than  $\angle C_6C_1C_2 = 120 \pm 2^\circ$ ,  $r_{1,2} = 1.397 \pm 0.010 \text{ \AA}$  and  $r_{1,8} = 1.44 \pm 0.02 \text{ \AA}$ .

The data in Table 1.2 reveal that the calculated rotational constants are nevertheless within 0.5% of the experimental values, using  $r_{1,8} = 1.455 \text{ \AA}$ . This value was chosen on the basis of the original value for the analogous  $r_s$  bondlength in  $\phi$ CN<sup>(15)</sup>.

Data Set IV in Table 1.2 shows that the calculated rotational constants for a regular hexagonal benzene ring and  $r_{1,8} = 1.455 \text{ \AA}$  also reproduce the experimental rotational constants within 0.5% error.

We now proceed to discuss the rotational constants of the DEBs. These constants have been calculated for para-DEB for the geometries given in Table 1.3. The numbering of the C-atoms is indicated in Fig. 1.1 and will be used throughout this study.

A comparison of the bondlengths and bond angles in Tables 1.2 and 1.3 shows that Set I corresponds to the antiquinoidal  $r_s$  structure, Set II to the quinoidal  $r_z$  geometry, and Set III to an intermediate, regular hexagonal ring. The  $r_z$  structure has been determined theoretically for para-DEB also.

Table 1.3

Bondlengths ( $\text{\AA}$ ), Bond Angles (Degrees) and Rotational Constants ( $\text{cm}^{-1}$ )

for Several Structures of para-DEB

	$r_{1,2}(\text{\AA})$	$r_{2,3}(\text{\AA})$	$r_{1,8}(\text{\AA})$	$r_{7,8}(\text{\AA})$	$\angle C_6C_1C_2$	$A(\text{cm}^{-1})$	$B(\text{cm}^{-1})$	$C(\text{cm}^{-1})$
I	1.389	1.396	1.455	1.205	121.8°	0.1885	0.0238	0.0211
II	1.406	1.395	1.423	1.209	118.6°	0.1899	0.0235	0.0209
III	1.397	1.397	1.455	1.205	120.0°	0.1896	0.0234	0.0209

The data in Table 1.3 cannot be used to select a best structure, since the rotational constants are not known for any DEB. The above discussion of  $\phi$ CCH suggests that the rotational constants for the DEBs can be determined within 0.5 to, at most, 1%, if a regular ring is assumed and all other parameters as for Set IV.

Finally, the assumed rotational constants for the three DEBs are collected in Table 1.4 together with the asymmetry parameter  $\kappa$   $[(2B-A-C)/(A-C)]$ . These constants have thus been calculated for benzene C—C bondlengths of 1.397 Å, a length of 1.455 Å for the  $\phi$ —CCH linkage, an acetylenic triple bond of 1.205 Å, aromatic C—H distances of 1.084 Å, acetylenic C—H distances of 1.056 Å, benzene bond angles of  $120^\circ$  and acetylenic bond angles of  $180^\circ$ .

Table 1.4

Estimated Rotational Constants ( $\text{cm}^{-1}$ ) and the Asymmetry Parameters

for the DEBs

	A ( $\text{cm}^{-1}$ )	B ( $\text{cm}^{-1}$ )	C ( $\text{cm}^{-1}$ )	$\kappa$
ortho-DEB	0.0684	0.0435	0.0266	-0.19
meta-DEB	0.0894	0.0300	0.0225	-0.78
para-DEB	0.1896	0.0234	0.0209	-0.98

The numerical values of  $\kappa$  show that para-, meta- and ortho-DEB can be described as a very near prolate symmetric top, a near prolate symmetric top and an asymmetric top, respectively.

### Conclusions

In this chapter it is shown that a probable ground state geometry can be estimated for  $\phi$ CCH, but it is too crude to distinguish between a slightly quinoidal or slightly antiquinoidal ring structure. The main difficulty is

the location of the substituent-carrying C-atom. If this atom is positioned in the middle of the above range, that is assuming an undistorted benzene ring, the calculated rotational constants were found to differ about 0.5% from the experimental values. Extrapolation of these results for  $\phi$ CCH to the DEBs resulted in rotational constants with an uncertainty of 0.5 to 1%.

In the next chapter rotational constants will be used to check the analysis of the vibration spectra using Redlich-Teller product ratios. These contain ratios of rotational constants and can thus not be quoted in more than two significant figures. In a later chapter, geometry changes upon electronic excitation will be estimated from differences in rotational constants between the ground and the excited electronic state. In order to be able to say anything meaningful about the geometry of an excited electronic state, the differences in rotational constants should be larger than 1%. This conclusion is thought to hold also for other substituted benzenes, for which the ground state substitution structures have not been determined via microwave spectroscopy.

## CHAPTER 2

### Experimental Work

#### 2.1. Synthesis of the Diethynylbenzenes

Acetylenes are usually prepared by dehydrohalogenation of dibromides or dichlorides of olefines with potassium hydroxide<sup>(20)</sup>. The halogen compounds that yield the DEBs upon dehydrohalogenation have been synthesized in three different ways.

##### 1. Bromination of divinylbenzenes

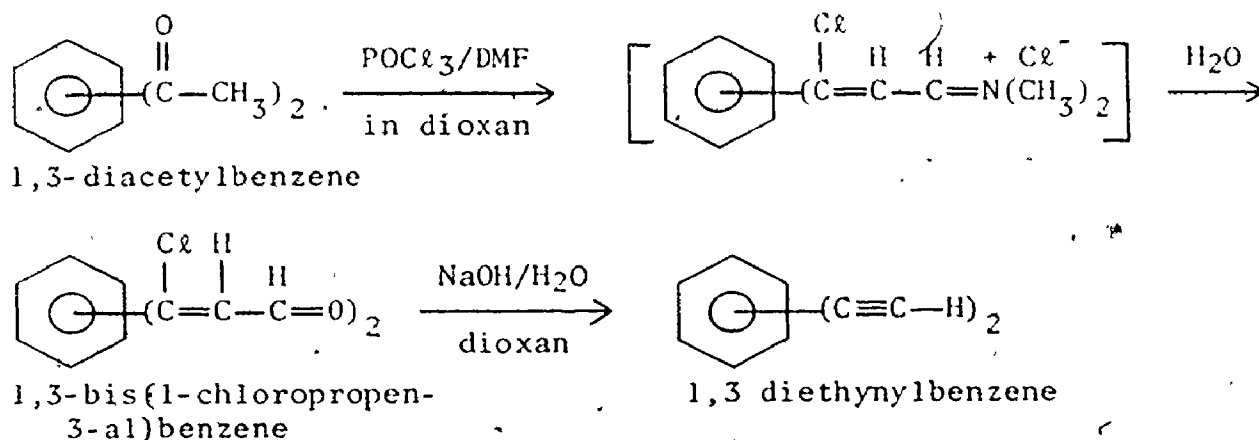
The method given by Hay<sup>(21)</sup> was followed for the synthesis of the DEBs. A commercial mixture of divinylbenzenes and ethylstyrenes was brominated in chloroform solution. On cooling 1,4-bis(1,2-dibromoethyl)benzene crystallized out and was recrystallized from chloroform. The pure material was dehydrobrominated with KOH in tertiary butanol. The resulting solid para-DEB was purified by sublimation. The saturated vapor pressure of para-DEB at room temperature is 0.4 torr. The bromination residue contained 1,3-bis(1,2-dibromoethyl)benzene and considerable quantities of dibromodiethylbenzenes from the ethylstyrenes in the starting material. The former compound was isolated via recrystallization from ethanol and was dehydrobrominated according to the process described for para-DEB. The meta-DEB thus prepared did however contain some para-DEB that could not be removed by distillation. The presence of the para compound indicated that 1,4-bis(1,2-dibromoethyl)benzene does not precipitate completely on cooling the brominated starting mixture of divinylbenzenes and ethylstyrenes. A different route was therefore followed for synthesizing pure meta-DEB (see below).

A small quantity of ortho-DEB was prepared from 1,2-bis(1,2-dibromoethyl)benzene by elimination of hydrogenbromide with KOH in t-butanol. The

starting material was kindly provided by Dr. A. J. Leusink of the Institute of Organic Chemistry, TNO, Utrecht, The Netherlands. The saturated vapour pressure of ortho-DEB was measured as 0.35 torr at room temperature.

### 2. Reaction of diacetylbenzenes with phosphoroxchloride

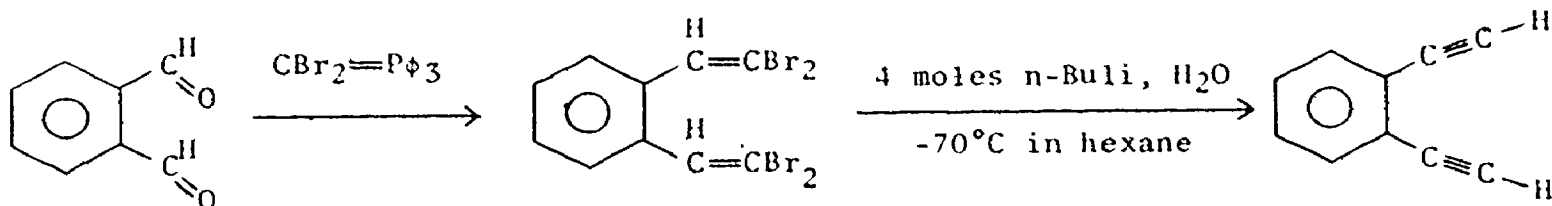
The pure meta compound was prepared from meta-diacetylbenzene, according to the following scheme proposed by Watson<sup>(22)</sup>.



The saturated vapor pressure of the pure meta-DEB was measured as 0.35 torr at room temperature.

### 3. Reaction of phthalaldehyde with $\text{CBr}_2=\text{P}\phi_3$

The synthesis of ortho-DEB was carried out by Dr. R. Bell in these laboratories, starting from phthalaldehyde and dibromomethylenetriphenylphosphorane ( $\text{CBr}_2=\text{P}\phi_3$ ).



The reaction product was isolated by vacuum distillation. The commercial n-butyllithium contained hydrocarbons with a boiling point close to that of ortho-DEB. The presence of these impurities was evident from the NMR spectrum.



The above preparation was done on a small scale, so that only a small quantity of ortho-DEB was available. The sample was vacuum distilled several times to remove the impurities. The distillations were stopped when about 0.5 cc of sample was left.

### Synthesis of the deuterated DLBs

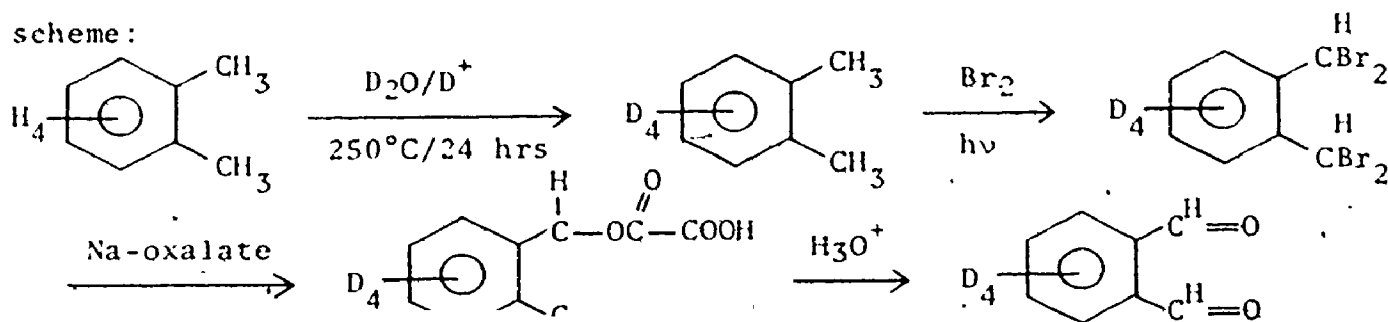
The acetylenic protons were replaced by deuterium atoms by stirring a mixture of the following composition: 0.1 mole triethylamine, 0.05 mole DLB and 1 mole of  $D_2O$ . The deuteration of acetylenic protons is base catalyzed<sup>(23)</sup>. In this study triethylamine has been used, because the DEBs are soluble in this Lewis base, which is immiscible with water. Every hour the  $D_2O/H_2O$  mixture was pipetted off and replaced with fresh  $D_2O$ . The degree of deuteration was followed by recording the NMR spectra. It was found that four to five exchanges were sufficient to deuterate more than 95% of the acetylenic protons.

The above procedure was used to convert para- $C_6H_4(CCH_2)$  (para- $h_6$ ) into para- $C_6H_4(CCD)_2$  (para- $d_2$ ), meta- $C_6H_4(CCH)_2$  (meta- $h_6$ ) into meta- $C_6H_4(CCD)_2$  (meta- $d_2$ ). Ortho- $C_6H_4(CCH)_2$  (ortho- $h_6$ ) could not be deuterated, because no sample was left of the original 0.5 cc, after recording the I.R., Raman and U.V. spectra.

Ring deuterated para-DEB, para- $C_6D_4(CCH)_2$  (para- $d_4$ ), was custom-synthesized by Merck, Sharp and Dohme (Montreal). Perdeutero para-DEB (para- $d_6$ ) was prepared from this compound according to the exchange reaction described above.

Ring deuterated ortho-DEB was prepared by Dr. R. Bell according to the

scheme:



The succeeding steps, leading to ring deuterated ortho-DEB, are identical to the reactions given above for the synthesis of hydrogenic ortho-DEB.

The above synthesis was carried out on a small scale and about 1 cc of sample was obtained. The sample was distilled only twice, although the amount of impurities was about equal to that present in the hydrogenic sample received. After recording the I.R., Raman and U.V. spectra of ortho-C<sub>6</sub>D<sub>4</sub>(CCH)<sub>2</sub> (ortho-d<sub>4</sub>) enough sample was left to synthesize and to record also the spectra of ortho-C<sub>6</sub>D<sub>4</sub>(CCD)<sub>2</sub> (ortho-d<sub>6</sub>).

## 2.2. The Vibration Spectra

### A. The infrared spectra

The infrared spectra of the isotopes of the DEBs were recorded with a Perkin-Elmer 521 double beam grating spectrophotometer in the 250 to 4000 cm<sup>-1</sup> region. The calibration of the instrument was checked by taking the spectra of indene and cyclohexanone. The wavenumber accuracy of intense, sharp bands in the spectra of the DEBs is about ±1 cm<sup>-1</sup> and ±2 to ±5 cm<sup>-1</sup> for broad and/or weak signals.

The spectra of the liquid samples (meta- and ortho-DEB) were recorded with a variable path length cell with KBr windows. Two KBr plates (14 mm each) were placed in the reference beam so that the strongest bands below 500 cm<sup>-1</sup> could be observed. The wavelength region from 250 to 600 cm<sup>-1</sup> was further investigated using liquid cells fitted with polyethylene windows. These windows were replaced for each isotope.

The spectra of the isotopes of the solid para-DEB were recorded in CS<sub>2</sub> (500-1300 cm<sup>-1</sup>), CCl<sub>4</sub> (1600-4000 cm<sup>-1</sup>), CH<sub>2</sub>Cl<sub>2</sub> (1400-1800 cm<sup>-1</sup>) and cyclohexane (below 600 cm<sup>-1</sup>). The spectra at frequencies lower than 600 cm<sup>-1</sup> were also recorded by spraying a thin teflon or Krylon coating over a thin layer of the solid sample on 0.05 mm thick polyethylene. Blanks prepared similarly did

not show any absorption below  $600\text{ cm}^{-1}$ .

A Perkin Elmer 301 double beam grating spectrophotometer was used to examine the region below  $300\text{ cm}^{-1}$ . The instrument was flushed thoroughly before use (48 hours with dry  $\text{N}_2$  at a flow rate of 10 liters/min). During runs a lower flow rate was used. The instrument was equipped with a new Hg lamp and a new Golay detector. It was expected that the instrument could be used down to 50 to  $60\text{ cm}^{-1}$  in this condition. This is the instrumental limit according to the manufacturer. It was found, however, that the available energy is extremely low at wavelengths smaller than about  $100\text{ cm}^{-1}$ . The spectra of the liquid samples were recorded using the above mentioned variable path length cell equipped with polyethylene windows. The spectrum of the para-DEBs were recorded using polyethylene, as a support for a thin layer of the solid sample coated with teflon. The spectra of the DEBs were examined in the single beam mode down to about  $90\text{ cm}^{-1}$ . No absorptions were found for para-DEB in the frequency range from 325 down to  $90\text{ cm}^{-1}$ , while two signals were observed for meta- and ortho-DEB in this region (at 180 and  $120\text{ cm}^{-1}$ ). Polyethylene showed an absorption around  $80\text{ cm}^{-1}$  and the polyethylene support was therefore replaced by TPX<sup>(24)</sup>. This is a new polyolefine with a transmission greater than 60% below  $100\text{ cm}^{-1}$ . Two millimeter thick discs of this material were kindly provided by Dr. J. B. Rose of I.C.I., England. It was impossible however to find any absorption below  $100\text{ cm}^{-1}$  with this material as a support for the solid para-DEB. This result does not necessarily indicate that para-DEB does not have any absorption below  $100\text{ cm}^{-1}$ , because of the extremely low intensity of the Hg-arc in this region.

#### B. The Raman spectra

The Raman spectra were recorded with a laser Raman spectrophotometer.

The exciting radiation was provided either by the red 632.8 nm neon line from a Spectra-Physics Model 125 He/Ne gas laser or by the green 514.5 nm argon line from a Spectra-Physics Model 165 argon gas laser with variable output from 20 to 900 milliwatts. The Raman lines were recorded on a Spex grating monochromator unit with photoelectric recording. The polarized laser light was completely depolarized before it entered the monochromator. The latter was calibrated using a Fe/Ne hollow cathode tube. The estimated uncertainty in the measured frequencies is  $\pm 2$  to  $\pm 5$   $\text{cm}^{-1}$ .

Initially the samples were sealed in pyrex capillary tubes. The sample was found to turn yellow rapidly at the spot where the laser beam was focussed. This yellowish polymer (see below) raised the background radiation to such an extent that the weaker bands of the sample were obscured. The polymerization was prevented by using a spinning cell. This cell was made from a 10 cm vycor flow cell with an internal diameter of 20 mm. The middle part of this flow cell was drawn out conically in a hot flame and provided with a graded seal. The conical part and the lower part of the graded seal were provided with an aluminium cover. A sleeve in this cover made it possible to attach the cell to a rotary motor. No observable polymerization occurred when this cell was used.

### 2.3. The Ultraviolet Absorption Spectra

A low resolution survey of the ultraviolet absorption systems of the DEBs was carried out with a Cary Model 11 double beam recording spectrophotometer in the 200 to 350 nm region. The vacuum ultraviolet spectrum of para-DEB was recorded photoelectrically in the range from 120 to 200 nm using a McPherson Model 225 1 meter double beam scanning monochromator. All these spectra were recorded using 10 cm absorption cells.

Very intense absorption systems were observed at 260 and 180 nm for para-DEB, at 245 and 220 nm for meta-DEB, and at 260 and 220 nm for ortho-DEB. These systems are so intense that they could be recorded using 10 cm cells filled to the saturated vapor pressure of the compounds at about  $-25^{\circ}\text{C}$ .

The intense 260, 245 and 260 nm absorption systems of para-, meta- and ortho-DEB respectively, were also studied with a Hilger large quartz prism spectrograph and a 1.5 m Bausch and Lomb model 11 spectrograph using 10 cm cells with the sample in the side arm at temperatures from  $-20$  to  $-30^{\circ}\text{C}$ . An absorption system with discrete vibrational structure was photographed for each DEB in the 280 to 300 nm region, when 50 cm and 1 m cells were used filled to the saturated vapor pressure at room temperature. In order to observe weak bands in the above region, 1.53 and 6.10 m White type multiple reflection cells were used. Pathlengths varied from 3.6 to 360 meters.

High resolution spectra of the isotopes of the DEBs were photographed on a 6.10 m Ebert plane grating spectrograph in the second order. The second order linear dispersion at the plate of this instrument is about 3.35 mm/A in the region from 270 to 300 nm. The resolving power in second order is about 300,000. The slitwidths were chosen in accordance with the optimum calculated values and varied between 20 and 30 microns. The samples were contained in the 1.83 m White-type multiple reflection cell at room temperature and the maximal pathlengths used were about 100 meters (60 traversals).

It was very difficult to photograph weak bands in the discrete absorption systems of each of the DEBs in the region from 270 to 300 nm, because of some stray light at the plateholder. The following adjustments have been made to the Ebert spectrograph, similar to the one described by King<sup>(25)</sup>, to eliminate this stray light. The standard procedure was followed to line up

the external optics including the 1.83 m multiple reflection cell.

### 1. Baffle

After removal of the grating turntable, the baffle (Fig. 5, ref. 25) was taken out. The lower rectangle was adjusted to a height of 16 mm, corresponding to a baffle position of 76.2 cm from the entrance slit. The baffle was next carefully placed in the proper position and the grating turntable was replaced. Slight baffle adjustments were made until the grating image was evenly illuminated.

### 2. Mirror

The increase in height of the entrance rectangle resulted in a dramatic increase in stray light at the plate holder. In order to eliminate this stray light, a strip of black cardboard (2.54 by 25.4 cm) was positioned horizontally over the middle part of the mirror and was lowered gradually until the grating (top) was just not eclipsed. The proper position of the cardboard strip could be determined easily by observing the zeroth order reflection. A similar procedure was followed with a cardboard strip at the bottom of the mirror. This obstruction was moved upwards until the bottom part of the grating was just not eclipsed.

3. After these adjustments were made, no stray light could be seen with the naked eye. Photographically, however, a slight fogging could still be observed after prolonged exposure times. This light was removed completely by lowering the grating turntable as much as possible (about 1.5 cm) by adjusting very gradually the three long screws below the grating casing. This lowering made it necessary to repeat the final adjustments of the cardboard strips (see 2).

### 2.4. Photography and Reduction of Spectrograms

The spectra were recorded using a 450 Watt high pressure Xe-arc. Kodak

Spectrum Analysis No. 1 film was used in combination with Kodak D-19 developer. Film processing was done according to the recommendations by the manufacturer. Exposed film was developed for 4 minutes at 20°C, except when it was necessary to obtain a higher contrast for very weak bands. In this case exposure times were halved successively and the development time was prolonged to 6 to 10 minutes.

The absorption bands, together with selected iron arc lines, were measured with a McPherson travelling microscope with a precision of  $10^{-4}$  cm. A quadratic dispersion curve was calculated from the wavelengths of the iron arc lines (M.I.T. tables). The wavelengths of the bandheads were obtained from this curve and converted to vacuum wavelengths. The accuracy of the wave numbers so obtained was  $\pm 0.1$  to  $\pm 0.5$   $\text{cm}^{-1}$ , depending on the sharpness of the bands. The features in the origin bands of the isotopes of para-DEB were measured several times from at least three different plates and then averaged in order to obtain a higher accuracy. The wavenumbers of extremely weak or diffuse bands were measured from photographic enlargements of the spectra or were measured by interpolation from microdensitometer tracings recorded on a Joyce-Loebl Model Mk IIIC instrument. The rotational profiles of bands of interest were recorded also on this instrument.

#### 2.5. Polymerization of the DEBs

A yellowish tinge developed when the colorless, pure DEBs were kept at room temperature. The color deepened with time on storage at room temperature or on heating. para-DEB can be detonated with a hammer or by heating to about 120°C.

After the U.V. absorption cells had been used for a few hours, a thin, dark yellow film was formed on the entrance window. A 10 cm cell, containing

some solid para-DEB, was purposely irradiated for a prolonged time. The para-DEB that was not deposited on the windows was removed by evacuation of the cell. No absorption bands could be found with this film in the light path, although the transmitted light intensity was markedly decreased. Similar observations have been made for  $\phi$ CCH and have been ascribed to a polymerization product<sup>(10)</sup>. This product was removed by so by heating the cell windows to about 600°C with the cell containing air. Recently the polymerization product of  $\phi$ CCH and meta-DEB has been shown by Bracke<sup>(26)</sup> to decompose in air at 600°C. The above author found also that the polymer dissolved in chlorinated hydrocarbons.

In this study a U.V. filter, between the light source and the absorption cell, was used to cut down the amount of polymer formed. This was reasonably effective for para- and meta-DEB. For ortho-DEB, however, the cell windows had to be cleaned after irradiating the sample for a few hours. Also some polymer was formed on the mirrors of the multiple reflection cell. This made it necessary to re-aluminize them every few hours.



## CHAPTER 3

### The Vibrational Spectra of the Diethynylbenzenes

#### Introduction

The analysis of the vibrational spectra of the three diethynylbenzenes (DEBs) is presented in this chapter. A total of forty-two normal frequencies will be assigned for each DEB. The analysis is greatly facilitated by subdividing the normal modes of vibration into thirty benzene ( $\phi$ ) modes and six modes for each acetylenic (CCH) group.

The displacements of the C and H nuclei are a basis for the irreducible representations of the point groups to which the DEBs belong. This provides a classification of the normal modes of vibration according to the symmetry classes of the point groups. This method of labelling the vibrations is very helpful for the analysis. It does not make it possible, however, to discuss the general features of the vibrational spectra. An "in" and "out-of-plane" classification is more suitable in this respect, because there are only thirteen out-of-plane vibrations for each relevant point group and most importantly, these vibrations derive from the same benzene and acetylenic modes of vibration. The twenty-nine in-plane vibrations are partitioned according to Varsanyi's definition of radial and tangential vibrations (see below).

The above classifications will be discussed in detail in the first part of this chapter. Most of the material presented in this section is adapted from Varsanyi's authoritative book on the vibrational spectra of benzene derivatives<sup>(4)</sup>.

Each of the above three groups of vibrations (tangential, radial and out-of-plane) is next considered in more detail from the point of view of qualitative analysis. The infrared (I.R.) spectrum of every substituted

acetylene derivative, for instance, shows three characteristic intense bands which correspond to the triple bond stretching mode and the acetylenic hydrogen stretching and bending modes. The normal frequencies of three of the six modes of vibration of the CCH group can therefore be predicted by analogy. Likewise, every benzene derivative has been found to possess a large number of characteristic absorption frequencies. At least fifteen of the thirty fundamentals of the  $\phi$  part can be assigned for each of the three DEBs by analogy with reported studies on other benzene derivatives.

After the assignment of these characteristic absorptions, three groups of vibrations remain for which the assignment is less certain, namely, the (radial) in-plane bending modes of the CCH group, the (tangential) C—C stretches of the  $\phi$  and CCH parts, and, finally, the low frequency out-of-plane vibrations. Each of these three main difficulties is fully discussed in Section 3.1.A, B and C. In this way the analysis of the observed spectra does not have to be interrupted with lengthy arguments on the above issues.

### 3.1. Classification of the Normal Vibrations

The classification used here for the normal modes of vibration of the DEBs is based on the thirty benzene modes and the six modes for each CCH group. The numbering of the thirty  $\phi$  modes, as well as the accompanying displacement diagrams, have been taken from Varsanyi and follow Wilson's notation<sup>(4)</sup>.

The replacement of two benzene H-atoms by CCH groups changes two in and out-of-plane C—H bending modes [ $\beta$ (C—H) and  $\gamma$ (C—H)] into two substituent-sensitive in and out-of-plane bending modes [ $\beta$ (C—CCH) and  $\gamma$ (C—CCH)]. Likewise, two C—H stretching modes [ $\nu$ (C—H)] have to be replaced by two substituent-sensitive stretching modes [ $\nu$ (C—CCH)]. A total of six benzene vibrations is thus changed into substituent-sensitive vibrations. For defining which

benzene modes will be considered substituent-sensitive, a rule is applied that is more general than Varsanyi's conventions. This results in minor differences in the numbering of the substituent-sensitive vibrations.

Definition: The C-atoms adjacent to the substituent-carrying C-atom have to oscillate out-of-phase with respect to the substituted C-nuclei.

For some molecules two benzene vibrations satisfy this criterium. These benzene modes were then considered substituent-sensitive, in which the substituted C-atoms were oscillating with the largest amplitudes.

The CCH group in  $\phi$ CCH gives rise to six modes of vibration<sup>(27)</sup>. These modes are also appropriate descriptions for the DEBs, although each mode occurs twice in the latter. In one mode, the nuclei in the CCH group move in phase and in the other mode, they oscillate out of phase with respect to the atoms in the other CCH group. The following terms and letters will be used for the approximate description of the CCH modes:  $\nu(\equiv\text{C}-\text{H})$  for the acetylenic C—H stretching modes (A and B),  $\beta(\equiv\text{C}-\text{H})$  and  $\gamma(\equiv\text{C}-\text{H})$  for the in and out-of-plane acetylenic C—H bending modes (E, F and I, J),  $\nu(\text{C}\equiv\text{C})$  for the stretching modes of the triple bond (C and D), and, finally,  $\beta(\text{C}-\text{C}\equiv\text{C})$  and  $j(\text{C}-\text{C}\equiv\text{C})$  will indicate the in and out-of-plane acetylenic skeletal bending modes (G, H and K, L). The schematic displacement diagrams, as given in Fig. 3.1, have next been used to classify the 42 normal modes of vibration into the symmetry classes of the point groups of the DEBs. The point groups for para-, meta- and ortho-DEB are given in Fig. 1.1 as  $D_{2h}$ ,  $C_{2v}$  and  $C_{2v}^*$  respectively. An asterisk is usually added to the point group of ortho-disubstituted benzenes,<sup>(4,28)</sup> to indicate that the two-fold symmetry axis bisects opposite C—C bonds of the  $\phi$  ring instead of passing through opposite C-nuclei. The conventional numbering, also given in Fig. 1.1, reveals that the Y and Z axes for meta-DEB corres-

pond to the Z and  $\bar{Y}_1$  axes respectively for ortho-DEB. This interchange results in different symmetries for the same benzene mode for ortho- and meta-DEB. Benzene mode 4, for instance, falls into the  $b_1$  symmetry class in the  $C_{2v}$  point group and in the  $a_2$  class in the  $C_{2v}^*$  point group.

The symmetry, designation, frequency and approximate description of all 42 modes of vibration for the three DEBs have been collected in Table 3.1. This information is reorganized in Table 3.2 according to the spectroscopic convention of listing and numbering the vibrations in order of decreasing symmetry and frequency. This table also contains the abbreviations R, T and O. The symbol O stands for out-of-plane vibration. There are 13 such modes for each DEB. The remaining 29 in-plane vibrations have been split into radial (R) and tangential (T) modes of vibration<sup>(4)</sup>. Radial modes involve only displacements along the lines connecting opposite nuclei of the benzene ring, while tangential modes are characterized by displacements perpendicular to these lines.

The three criteria applied above for subdividing the 42 vibrations will be used in the next section to find the characteristic  $\phi$  and CCH vibrations. The tangential modes will be dealt with first, since these are easiest to understand. The radial modes will be discussed next and they will be found to be more complex. Finally, most difficulties will be encountered for the out-of-plane vibrations and it will prove very fruitfull to examine the out-of-plane modes of  $\phi$ CCH and  $\phi$ CN.

#### A. Tangential vibrations

There are in total 15 tangential vibrations, namely 3, 14, 15 and the degenerate pairs 8, 9, 18, 19, E and F, and G and H. The approximate displacement diagrams for these modes have been depicted in Fig. 3.1.A.

The four acetylenic modes E, F, G and H will be discussed first. The

Table 3.1

The symmetries, descriptions and frequencies of the benzene and acetylenic modes of vibration. An asterisk indicates a substituent-sensitive vibration.

Design.	$\nu$	$D_{6h}$	$D_{2h}$	$C_{2v}$	$C_{2v}^*$	Description
1	993	$a_{1g}$	$a_g$	$a_1$	$a_1$	$\nu(C-C)$
2	3073	$a_{1g}$	$a_g$	$a_1$	$a_1$	$\nu(C-H)$
3	1350	$a_{2g}$	$b_{3g}$	$b_2$	$b_2$	$\beta(C-H)$
4	707	$b_{2g}$	$b_{2g}$	$b_1$	$a_2$	$\phi(C-C)$
5	990	$b_{2g}$	$b_{2g}^*$	$b_1$	$a_2^*$	$\gamma(C-H)$
6a	606	$e_{2g}$	$a_g$	$a_1$	$a_1$	$\alpha(C-C-C)$
6b			$b_{3g}$	$b_2$	$b_2$	
7a	3056	$e_{2g}$	$a_g^*$	$a_1$	$a_1^*$	$\nu(C-H)$
7b			$b_{3g}$	$b_2^*$	$b_2$	
8a	1599	$e_{2g}$	$a_g$	$a_1$	$a_1$	$\nu(C-C)$
8b			$b_{3g}$	$b_2$	$b_2$	
9a	1178	$e_{2g}$	$a_g$	$a_1^*$	$a_1^*$	$\beta(C-H)$
9b			$b_{3g}$	$b_2$	$b_2$	
10a	846	$e_{1g}$	$b_{1g}$	$a_2$	$b_1$	$\gamma(C-H)$
10b			$b_{2g}$	$b_1$	$a_2$	
11	673	$a_{2u}$	$b_{3u}$	$b_1$	$b_1$	$\gamma(C-H)$
12	1010	$b_{1u}$	$b_{1u}$	$a_1$	$b_2$	$\alpha(C-C-C)$
13	3057	$b_{1u}$	$b_{1u}^*$	$a_1^*$	$b_2^*$	$\nu(C-H)$
14	1309	$b_{2u}$	$b_{2u}$	$b_2$	$a_1$	$\nu(C-C)$
15	1146	$b_{2u}$	$b_{2u}^*$	$b_2^*$	$a_1$	$\beta(C-H)$
16a	404	$e_{2u}$	$a_u$	$a_2$	$a_2$	$\phi(C-C)$
16b			$b_{3u}$	$b_1$	$b_1$	

Table 3.1 (cont'd.)

Design.	$\nu$	$D_{6h}$	$D_{2h}$	$C_{2v}$	$C_{2v}^*$	Description
17a	967	$e_{2u}$	$a_u$	$a_2^*$	$a_2$	$\gamma(C-H)$
17b			$b_{3u}$	$b_1^*$	$b_1^*$	
18a	1037	$e_{1u}$	$b_{1u}$	$a_1$	$b_2^*$	$\delta(C-H)$
18b			$b_{2u}$	$b_2$	$a_1$	
19a	1482	$e_{1u}$	$b_{1u}$	$a_1$	$b_2$	$\nu(C-C)$
19b			$b_{2u}$	$b_2$	$a_1$	
20a	3064	$e_{1u}$	$b_{1u}$	$a_1$	$b_2$	$\nu(C-H)$
20b			$b_{2u}$	$b_2$	$a_1$	
A	3300		$a_g$	$a_1$	$a_1$	$\nu(\equiv C-H)$
B			$b_{1u}$	$b_2$	$b_2$	
C	2100		$a_g$	$a_1$	$a_1$	$\nu(C\equiv C)$
D			$b_{1u}$	$b_2$	$b_2$	
E	650		$b_{3g}$	$b_2$	$b_2$	$\delta(C-H)$
F			$b_{2u}$	$a_1$	$a_1$	
G	500		$b_{3g}$	$b_2$	$b_2$	$\delta(C-C\equiv C)$
H			$b_{2u}$	$a_1$	$a_1$	
I	650		$b_{3u}$	$b_1$	$b_1$	$\gamma(C-H)$
J			$b_{2g}$	$a_2$	$a_2$	
K	500		$b_{2g}$	$a_2$	$a_2$	$\gamma(C-C\equiv C)$
L			$b_{3u}$	$b_1$	$b_1$	

Table 3.2

The classifications of the normal modes of vibration  
of ortho-, meta- and para-DLB

	para-DLB ( $D_{2h}$ )	meta-DLB ( $C_{2v}$ )	ortho-DLB ( $C_{2v}^*$ )
1	A $\nu$ (C—H) R	A $\nu$ (C—H) R	A $\nu$ (C—H) R
2	2 $\nu$ (C—H) R	20a $\nu$ (C—H) R	2 $\nu$ (C—H) R
3	C $\nu$ (C $\equiv$ C) R	2 $\nu$ (C—H) R	20b $\nu$ (C—H) R
4	8a $\nu$ (C—C) T	7a $\nu$ (C—H) R	C $\nu$ (C $\equiv$ C) R
5	7a $\nu$ (C—CCH) R	C $\nu$ (C $\equiv$ C) R	8a $\nu$ (C—C) T
6	9a $\nu$ (C—H) T	8a $\nu$ (C—C) T	19b $\nu$ (C—C) T
7	1 $\nu$ (C—CCH) R	19a $\nu$ (C—C) T	14 $\nu$ (C—C) T
8	6a $\nu$ (C—C—C) R	13 $\nu$ (C—CCH) R	7a $\nu$ (C—CCH) R
9	10a $\nu$ (C—H) O	18a $\nu$ (C—H) T	9a $\beta$ (C—H) T
10	10b $\gamma$ (C—H) O	12 $\nu$ (C—C) R	18b $\beta$ (C—H) T
11	4 $\phi$ (C—C) O	1 $\nu$ (C—CCH) R	1 $\nu$ (C—CCH) R
12	7 $\gamma$ (C—H) O	F $\beta$ ( $\equiv$ C—H) T	F $\beta$ ( $\equiv$ C—H) T
13	K $\gamma$ (C—C $\equiv$ C) O	H $\beta$ (C—C $\equiv$ C) T	H $\beta$ (C—C $\equiv$ C) T
14	5 $\gamma$ (C—CCH) O	6a $\alpha$ (C—C—C) R	6a $\alpha$ (C—C—C) R
15	7b $\nu$ (C—H) R	9a $\beta$ (C—CCH) R	15 $\beta$ (C—CCH) T
16	8b $\nu$ (C—C) T	10a $\gamma$ (C—H) O	17a $\gamma$ (C—H) O
17	3 $\beta$ (C—H) T	J $\gamma$ ( $\equiv$ C—H) O	10b $\gamma$ (C—H) O
18	6b $\alpha$ (C—C—C) R	16a $\phi$ (C—C) O	4 $\phi$ (C—C) O
19	L $\beta$ (C—H) T	K $\gamma$ (C—C $\equiv$ C) O	J $\gamma$ ( $\equiv$ C—H) O
20	G $\beta$ (C—C $\equiv$ C) T	17a $\gamma$ (C—CCH) O	16a $\phi$ (C—C) O
21	9b $\beta$ (C—CCH) T	5 $\gamma$ (C—H) O	K $\gamma$ (C—C $\equiv$ C) O
22	17a $\gamma$ (C—H) O	10b $\gamma$ (C—H) O	5 $\gamma$ (C—CCH) O
23	16a $\phi$ (C—C) O	11 $\gamma$ (C—H) O	11 $\gamma$ (C—H) O
24	B $\nu$ (C—H) R	4 $\phi$ (C—C) O	10a $\gamma$ (C—H) O
25	20a $\nu$ (C—H) R	I $\gamma$ ( $\equiv$ C—H) O	I $\gamma$ ( $\equiv$ C—H) O
26	D $\nu$ (C $\equiv$ C) R	16b $\phi$ (C—C) O	16b $\phi$ (C—C) O
27	19a $\nu$ (C—C) T	L $\gamma$ (C—C $\equiv$ C) O	L $\gamma$ (C—C $\equiv$ C) O
28	13 $\nu$ (C—CCH) R	17b $\gamma$ (C—CCH) O	17b $\gamma$ (C—CCH) O
29	18a $\beta$ (C—H) T	B $\nu$ ( $\equiv$ C—H) R	B $\nu$ ( $\equiv$ C—H) R
30	12 $\nu$ (C—CCH) R	20b $\nu$ (C—H) R	20a $\nu$ (C—H) R
31	20b $\nu$ (C—H) R	D $\nu$ (C $\equiv$ C) R	7b $\nu$ (C—H) R
32	19b $\nu$ (C—C) T	8b $\nu$ (C—C) T	D $\nu$ (C $\equiv$ C) R
33	14 $\nu$ (C—C) T	19b $\nu$ (C—C) T	8b $\nu$ (C—C) T
34	15 $\beta$ (C—H) T	3 $\beta$ (C—H) T	19a $\nu$ (C—C) T
35	F $\beta$ ( $\equiv$ C—H) T	14 $\nu$ (C—C) T	3 $\beta$ (C—H) T
36	H $\beta$ (C—C $\equiv$ C) T	9b $\beta$ (C—H) T	13 $\nu$ (C—CCH) R
37	18b $\beta$ (C—CCH) T	18b $\beta$ (C—H) T	9b $\beta$ (C—H) T
38	11 $\gamma$ (C—H) O	7b $\nu$ (C—CCH) R	12 $\nu$ (C—CCH) R
39	I $\gamma$ (C—H) O	E $\beta$ ( $\equiv$ C—H) T	E $\beta$ ( $\equiv$ C—H) T
40	16b $\phi$ (C—C) O	G $\beta$ (C—C $\equiv$ C) T	G $\beta$ (C—C $\equiv$ C) T
41	L $\gamma$ (C—C $\equiv$ C) O	6b $\alpha$ (C—C—C) R	6b $\alpha$ (C—C—C) R
42	17b $\gamma$ (C—CCH) O	15 $\beta$ (C—CCH) T	18a $\beta$ (C—CCH) T

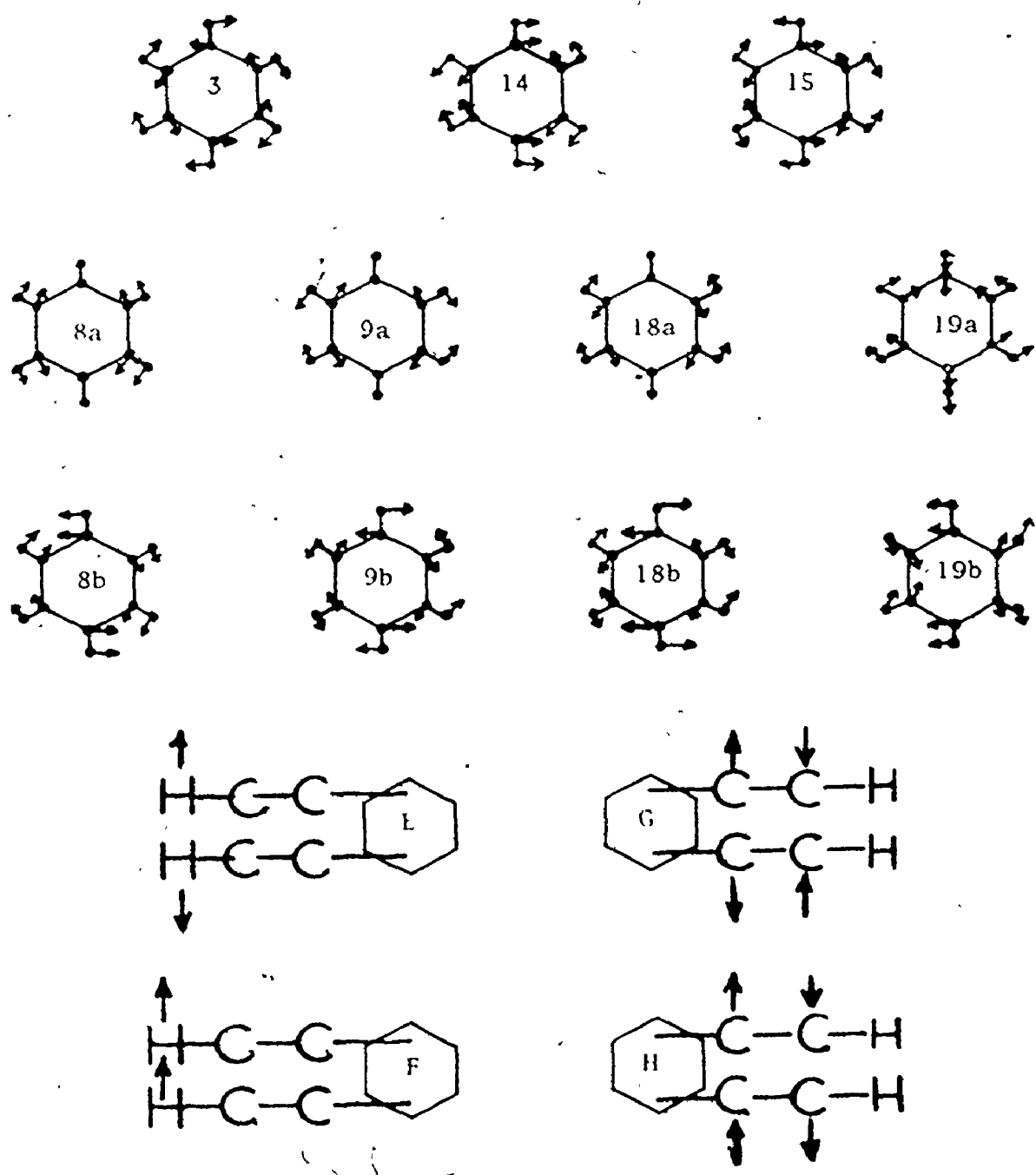


Fig. 3.1.A. Schematic representation of the tangential modes of vibration.



$\beta(\text{C—H})$  fundamentals E and F are very easily recognized in the I.R. spectra by very intense bands around  $650\text{ cm}^{-1}$ . The  $\beta(\text{C—C}\equiv\text{C})$  fundamentals G and H are characterized by weak or medium intense bands around  $500\text{ cm}^{-1}$  for aromatic acetylenes<sup>(27)</sup> and around  $350\text{ cm}^{-1}$  for aliphatic acetylenes<sup>(1,29)</sup>.

The remaining modes derive from benzene vibrations. These vibrations are numbered differently for each DEB and therefore approximate descriptions will be used, such as  $\beta(\text{C—H})$ . The normal frequencies of the four  $\beta(\text{C—H})$  modes occur in narrow wave number ranges for analogous benzene derivatives.<sup>(4,30-34)</sup> These vibrations can thus be assigned easily by analogy. The same procedure can be followed for the C—C stretching modes [ $\nu(\text{C—C})$ ] 8 and 19, that occur also in well defined, narrow frequency ranges. The cyclohexatriene or Kékulé vibration, mode 14, is usually very hard to find in I.R. spectra. For ortho-DEB this mode falls into the totally symmetric class and corresponds to a strong polarized band in the Raman spectrum. In the I.R. spectra of para- and meta-DEB, a weak signal occurs in the same region. This absorption has been assigned to the Kékulé mode by analogy.

The remaining two tangential vibrations are the, in and out-of-phase bending modes of the whole CCH group. The corresponding  $\beta(\text{C—CCH})$  mode for  $\phi\text{CCH}$  and the  $\beta(\text{C—CN})$  vibration for  $\phi\text{CN}$ , have been assigned in a number of ways. King and So<sup>(27)</sup> have agreed with the value of  $350\text{ cm}^{-1}$  proposed by Evans and Nyquist<sup>(35)</sup>. Padhye and Rao<sup>(36)</sup> however preferred a value of  $164\text{ cm}^{-1}$ . This assignment has been supported by Danchinov et al<sup>(37)</sup> on the basis of normal coordinate analysis. The latter authors predicted a value of  $194\text{ cm}^{-1}$  for the  $\beta(\text{C—CN})$  fundamental of  $\phi\text{CN}$ . Jacobson<sup>(38)</sup> on the other hand has proposed the value of  $380\text{ cm}^{-1}$  for  $\phi\text{CN}$ , because the spectra of several aromatic nitriles show a characteristic medium intense absorption around  $400$

$\text{cm}^{-1}$ (39). All these assignments have in common that a medium intense band is chosen for the bending mode of the whole CCH/CN group.

In this study a total of six  $\beta(\text{C}-\text{CCH})$  fundamentals have been assigned, for each DEB two. The (four) nontotally symmetric  $\beta(\text{C}-\text{CCH})$  vibrations were found to correspond to very weak I.R. and Raman bands around  $400 \text{ cm}^{-1}$ . The totally symmetric  $\beta(\text{C}-\text{CCH})$  vibrations for ortho- and meta-DEB have been positively identified with the polarized Raman bands at 440 and  $456 \text{ cm}^{-1}$  respectively. These assignments are supported by the weak and very weak signals found at  $390 \pm 30 \text{ cm}^{-1}$  for a number of para-disubstituted benzonitriles<sup>(40)</sup> in addition to the medium intense band in this region. The latter characteristic fundamental will be further discussed in Section 3.1.C., where the far I.R. spectra of  $\phi\text{CCH}$  and  $\phi\text{CN}$  will be re-examined.

It can be stated conclusively that some difficulty was encountered only in the assignment of the two tangential  $\beta(\text{C}-\text{CCH})$  modes.

#### B. Radial modes

Fourteen radial modes of vibration can be distinguished for each of the DEBs viz. 1, 2, 12, 13 and the degenerate pairs 6, 7, 20, A and B, and C and D. The schematic diagrams for these vibrations are given in Fig. 3.1.B.

The four acetylenic modes can be readily assigned. The  $\nu(\text{C}-\text{H})$  modes A and B are always found around  $3300 \text{ cm}^{-1}$ (1,29) and are very intense. The  $\nu(\text{C}\equiv\text{C})$  modes C and D always occur at  $2110 \pm 5 \text{ cm}^{-1}$  and are weak to medium intense in the I.R. spectra<sup>(1,29,41)</sup>. The ten remaining radial modes will be referred to below by their approximate descriptions. The four  $\nu(\text{C}-\text{H})$  modes (2, 20a, 20b and 7a or 7b) are invariably found at  $3050 \pm 40 \text{ cm}^{-1}$ (4,30-34). Only overlapping bands can cause problems in this region. The two  $\nu(\text{C}-\text{CCH})$  vibrations (13 and 7b or 7a) cannot be discussed separately, because of the

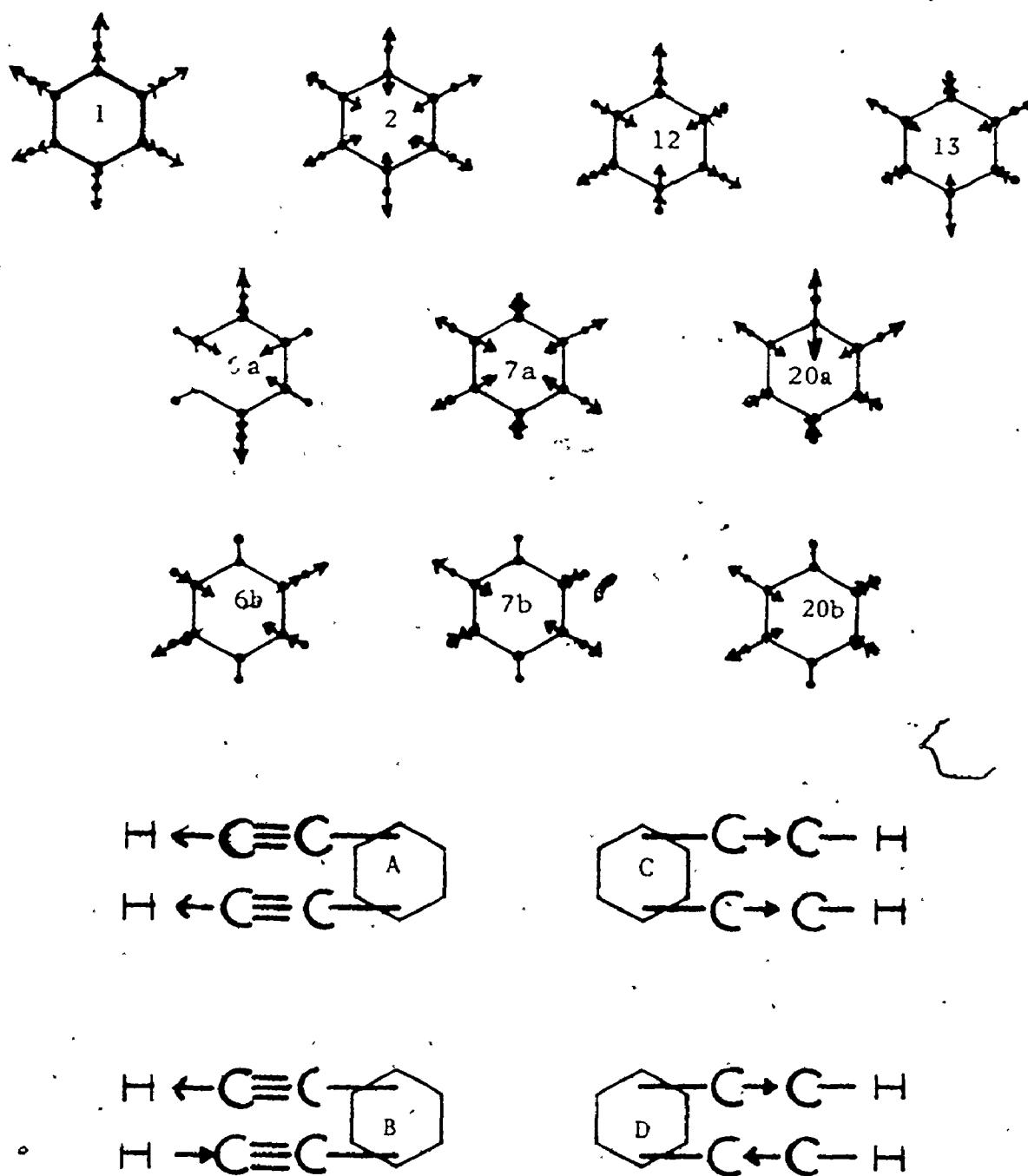


Fig. 3.1.B. Schematic representation of the radial modes of vibration.

coupling of these modes to the benzene  $\nu(\text{C}-\text{C})$  vibrations 1 and 12. This interaction can be explained best by analogy to the coupling occurring for  $\phi\text{CCH}$ . Nyquist and Potts<sup>(29)</sup> have reported that the  $\text{C}-\text{C}\equiv\text{C}$  stretching mode is found always from 900 to 960  $\text{cm}^{-1}$  for a large number of alkylacetylenes.

However,  $\phi\text{CCH}$  does not show the expected absorption in this region<sup>(27,35)</sup>. This can be explained by a coupling to the  $\phi$  modes 1 and/or 12. These two vibrations occur around 1000  $\text{cm}^{-1}$  too and involve also mainly displacements of C-nuclei. The same coupling of radial  $\text{C}-\text{C}$  stretches is possible for meta-DEB. A considerably simpler interaction should be found for para- and ortho-DEB. For these molecules the vibrations 1 and 7a are totally symmetric and the vibrations 12 and 13 fall into the same, nontotally symmetric class (see Table 3.2). The two totally symmetric modes have been found readily from the Raman spectra, by analogy with the Raman spectra of the xylenes<sup>(30)</sup> and the fluorobenzenes<sup>(33,34)</sup>. The above vibrations were observed in this study around 1200 and 800  $\text{cm}^{-1}$  in the Raman as well as in the I.R. spectra. The sum of the observed frequencies is equal to the sum of  $\phi \nu(\text{C}-\text{C})$  mode (1000  $\text{cm}^{-1}$ ) and the  $\nu(\text{C}-\text{C}\equiv\text{C})$  mode for alkylbenzenes<sup>(29)</sup> (950  $\text{cm}^{-1}$ ). This supports the above arguments to some extent.

This coupling could be much more complicated for monosubstitution and meta-disubstitution because the totally symmetric vibrations 1 and 12 can both interact with  $\nu(\text{C}-\text{CCH})$ . Fortunately, a strong polarized band is always found in the Raman spectra at  $1000\pm 10 \text{ cm}^{-1}$  for all mono-, meta- and 1,3,5-substituted benzenes. This result is readily explained by Whiffen's displacement diagram for the  $\phi$  mode 12, in which only the C-nuclei 2, 4 and 6 oscillate with sizeable amplitudes<sup>(42)</sup>. These C-atoms do not carry a substituent in mono-, meta- and 1,3,5-substitution and the frequency of

vibration p (mode 12) is therefore constant.

This implies that vibration 1 couples with  $\nu(\text{C}-\text{CCH})$  in the same way as found for the other types of substitution and that we should find the unperturbed, nontotally symmetric  $\nu(\text{C}-\text{CCH})$  mode for meta-DEB around  $950 \text{ cm}^{-1}$ . Finally only vibrational pair 6 is left to discuss. An inspection of the approximate diagrams in Fig. 3.2.B., reveals that the C-nuclei 1 and 4 have zero amplitudes for vibration 6b. This vibration should thus be found very close to the benzene value of  $606 \text{ cm}^{-1}$  for both  $\phi\text{CCH}$  and para-DEB. Vibration 6b has been found for ortho- and meta-disubstituted benzenes anywhere from 300 to  $500 \text{ cm}^{-1}$  (4,30-34). Likewise, vibration 6a has been found to occur also within a rather wide frequency range. The assignment of vibration 6a is simplified by the fact that this vibration is one of the two or three totally symmetric vibrations below  $600 \text{ cm}^{-1}$ . This completes the discussion of the radial modes.

### C. Out-of-plane vibrations

The out-of-plane vibrations--4, 5, 11 and the degenerate pairs 10, 16, 17, I and J, and K and L--are schematically represented in Fig. 3.1.C. All thirteen fundamentals have been found at frequencies below  $1000 \text{ cm}^{-1}$  for benzene and all its derivatives (4,30-34).

The frequencies of the four  $\gamma(\text{C}-\text{H})$  modes can be assigned readily with the help of their summation bands. For para- and ortho-DEB the assignment of these bending modes has been facilitated by the frequency shifts that occur upon ring deuteration. The summation bands of the  $\gamma(\text{C}-\text{H})$  vibrations occur in the I.R. in the region from  $1600$  to  $2000 \text{ cm}^{-1}$ , the so-called "finger-print" region<sup>(43)</sup>. The skeletal bending mode 4 is the only other benzene vibration that has been assigned by analogy with other substituted benzenes (4,30-34).

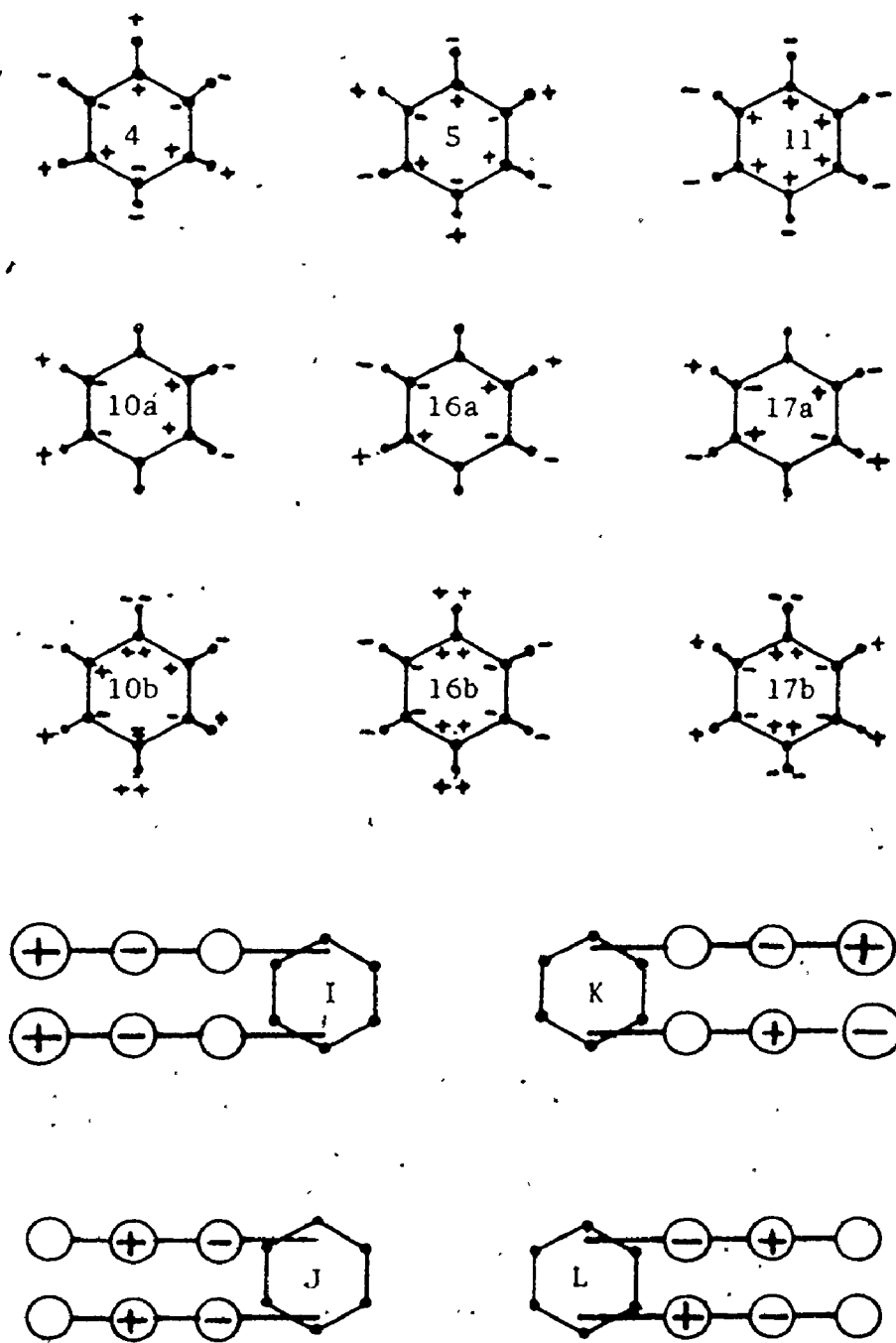


Fig. 3.1.C. Schematic representation of the out-of-plane modes.

This fundamental is found at  $700 \pm 25 \text{ cm}^{-1}$  for the three DEBs.

The fundamentals of the  $\gamma(\text{C—H})$  and  $\phi(\text{C—C})$  modes of vibration are thus found at frequencies higher than  $600 \text{ cm}^{-1}$ . The remaining out-of-plane benzene vibrations occur below  $600 \text{ cm}^{-1}$ , as well as some tangential and radial modes (see above). This region should thus be rather crowded.

The I.R. spectra of all CCH compounds recorded in this study showed very strong bands at  $640$  and  $615 \text{ cm}^{-1}$ . The same pattern was found in the I.R. spectra of liquid  $\phi\text{CCH}^{(27)}$ . The high resolution I.R. spectra of  $\phi\text{CCH}$  vapor have revealed that the  $\beta(\equiv\text{C—H})$  and  $\gamma(\equiv\text{C—H})$  bending modes that correspond to these absorptions are strongly Coriolis coupled<sup>(27)</sup>. Unfortunately, the vapor pressures of the DEBs were too low for recording vapor phase spectra. It has however been assumed that the I.R. active acetylenic hydrogen bending modes of the DEBs are also Coriolis coupled, because of the similarities between the liquid phase spectra of  $\phi\text{CCH}$  and the DEBs. These bending modes will be fully discussed in the next section.

Six out-of-plane vibrations are left unassigned at this point for each DEB. These vibrations are indicated with curly brackets in Table 3.2. It is readily seen there that a group of three similar out-of-plane vibrations is found five times for the three DEBs. The vibrations in question are the benzene skeletal bending mode 16, the acetylenic skeletal bending mode  $\gamma(\text{C—C}\equiv\text{C})$ , and the  $\gamma(\text{C—CCH})$  mode. The same group of three vibrations occurs for  $\phi\text{CCH}$  ( $\nu_{22}, \nu_{23}$  and  $\nu_{24}$ ) and the fundamentals have been assigned to absorptions at  $530, 349$  and  $162 \text{ cm}^{-1}$ <sup>(27)</sup>. A similar pattern of absorptions has been observed a total of four times in the spectra of ortho- and meta-DEB. For para-DEB, the bands at  $530$  and  $350 \text{ cm}^{-1}$  were readily identified in the I.R. spectra. The absorption corresponding to the out-of-plane bending mode of

the whole CCH group, however, could not be found above  $100\text{ cm}^{-1}$ , the practical lower limit of the Perkin-Elmer instrument used (see Chapter 2).

The Raman active group of three vibrations of para-DEB is split into two acetylenic vibrations with  $b_{2g}$  symmetry and mode 16a is seen to have  $a_u$  symmetry (see Table 3.2). The displacement diagram in Fig. 3.1.C. for the latter mode reveals that the C-nuclei 1 and 4 have zero amplitude. The frequency of this vibration can therefore be assigned the value of  $400 \pm 5\text{ cm}^{-1}$  by analogy to  $\phi$  and  $\phi\text{CCH}$  (4,27). A strong band with the lowest frequency in the Raman spectrum of para-DEB was found at  $197\text{ cm}^{-1}$  and has been assigned to the  $\gamma(\text{C}-\text{CCH})$  mode with  $b_{2g}$  symmetry. The other low frequency acetylenic mode with  $b_{2g}$  symmetry has been assigned to the next lowest frequency band with a medium intensity. This signal did not occur around  $350\text{ cm}^{-1}$ , but was found as high as  $477\text{ cm}^{-1}$ . It is important to note that the frequencies of this characteristic group of three vibrations add up to the same total in all cases mentioned. This indicates that considerable interaction occurs between these three vibrations if they fall into the same symmetry class.

It is interesting to note at this point that the in-plane skeletal bending mode for  $\phi\text{CCH}$  occurs at  $513\text{ cm}^{-1}$ , while the "pure"  $(\text{C}-\text{C}\equiv\text{C})$  mode for para-DEB occurs at  $477\text{ cm}^{-1}$ . The skeletal bending modes of the aliphatic molecules  $\text{CH}_3\text{CN}$  and  $\text{CH}_3\text{CCH}$  have been measured at frequencies of 360 and  $330\text{ cm}^{-1}$  respectively (1). Also, the species  $\text{CCN}$  and  $\text{CNC}$  show bending modes around  $325\text{ cm}^{-1}$  (1). The same values have thus been found in the I.R. spectra of  $\phi\text{CCH}$  and the three DEBs. It is suggested, therefore, that the benzene skeletal bending mode 16b--in which the C-atoms 1 and 4 oscillate with large amplitudes--is coupled strongly to the  $\gamma(\text{C}-\text{C}\equiv\text{C})$  and  $\gamma(\text{C}-\text{CCH})$  modes. This coupling is responsible for the high value of the normal frequency of mode 16b,



the low "aliphatic" value for the  $\gamma(\text{C}-\text{C}\equiv\text{C})$  mode and the low value for the bending mode of the whole substituent. The descriptions  $\phi(\text{C}-\text{C})$ ,  $\gamma(\text{C}-\text{C}\equiv\text{C})$  and  $\gamma(\text{C}-\text{CCH})$  indicate, at best, the general features of these coupled vibrations.

The above arguments are in accordance with the assignment for this characteristic group of three vibrations for  $\phi\text{CCH}$ . Jacobson<sup>(38)</sup>, however, has assigned to this group in  $\phi\text{CN}$  the frequencies of 550, 170 and 160  $\text{cm}^{-1}$  and a medium intense band at 380  $\text{cm}^{-1}$  was associated with the  $\beta(\text{C}-\text{CN})$  mode. It is proposed here that the group of three out-of-plane vibrations should be assigned to the absorption bands at 550, 380 and 160  $\text{cm}^{-1}$ . This suggestion introduces two difficulties, namely, the band occurring at 170  $\text{cm}^{-1}$  has to be explained, and the  $\beta(\text{C}-\text{CN})$  mode has to be assigned to some other band. The latter (tangential) mode has been discussed already in Section 3.1.A. It was seen there that this band probably occurs around 400  $\text{cm}^{-1}$  with a rather low intensity<sup>(40)</sup>. It is thus not unreasonable to assume that this weak signal is obscured by the more intense  $\gamma(\text{C}-\text{C}\equiv\text{N})$  fundamental.

The other difficulty--the occurrence of two bands very close in frequency--can best be explained by examining the Raman spectra of the following closely related molecules. Jacobson<sup>(38)</sup> found a shoulder at 170  $\text{cm}^{-1}$  on the 160  $\text{cm}^{-1}$  band of  $\phi\text{CN}$ , while King and So<sup>(27)</sup> found only one broad absorption around 160  $\text{cm}^{-1}$  for  $\phi\text{CCH}$ . Likewise, Laposa and Nalepa found only one broad band in this region for phenylisocyanate ( $\phi\text{NC}$ )<sup>(44)</sup>. In this study, a barely discernable shoulder was found at 201  $\text{cm}^{-1}$  on the broad 197  $\text{cm}^{-1}$  absorption of para-DEB.

The above mentioned molecules have also been studied at low temperatures. Laposa and Nalepa<sup>(44)</sup> were unable to resolve the broad signals for  $\phi\text{CCH}$  and  $\phi\text{NC}$ .

In this study it was found that the  $197\text{ cm}^{-1}$  signal of para-DEB became very much sharper at low temperature ( $-100^\circ\text{C}$ ) and a weak signal appeared very clearly at  $201\text{ cm}^{-1}$ . The observations for para-DEB thus resemble closely the results obtained for  $\phi\text{CN}$ . These observations can readily be accounted for if it is realized that thermal energy ( $1/2\text{ kT}$ ) at room temperature corresponds to about  $200\text{ cm}^{-1}$ . Therefore, the first excited vibrational state of the lowest out-of-plane vibration is appreciably populated. The shoulders on the bands of  $\phi\text{CN}$  and para-DEB, as well as the broad signals for  $\phi\text{CCH}$  and  $\phi\text{NC}$ , can then be ascribed to transitions from the first to the second excited vibrational state, if some anharmonicity is assumed. Even at lower temperatures, the first excited vibrational state is still sufficiently populated to give rise to an observable transition from the first to the second excited vibrational state. This transition should, of course, be much weaker than at room temperature. Unfortunately, the broad signal at room temperature makes it impossible to compare the intensities of the shoulder and the weak band.

It was mentioned above already that the absorption corresponding to the I.R. active  $\gamma(\text{C}-\text{CCH})$  mode of para-DEB could not be found in the far I.R. down to about  $100\text{ cm}^{-1}$ . Steele et al<sup>(45)</sup> have observed that the lowest I.R. active vibration of aromatic molecules is often found to be Raman active in violation of the selection rules. For this reason, the Raman spectrum of para-DEB was examined as close to the exciting line as possible. A strong band was found at  $68\text{ cm}^{-1}$  followed by four progressively weaker bands at intervals of  $10\text{ cm}^{-1}$ . The intensity ratios of these peaks with respect to the  $68\text{ cm}^{-1}$  band are found as 100:66:52:20 at room temperature. At a temperature of  $-100^\circ\text{C}$  these ratios reduce to 100:60:45:12. These observations,

first of all, are consistent with the explanation given above for the occurrence of two bands for the  $\gamma(\text{C}-\text{CCH})$  mode of para-DEB. Secondly, the very low frequency of this Raman forbidden band supports the proposed coupling between the vibrations in the characteristic group of three out-of-plane vibrations. This coupling of the benzene mode 16b with  $\gamma(\text{C}-\text{C}\equiv\text{C})$  and  $\gamma(\text{C}-\text{CCH})$  results in a fundamental with a frequency of  $160\text{ cm}^{-1}$  for  $\phi\text{CCH}$ . The introduction of another CCH group results in a decrease in frequency because of additional coupling. For ortho- and meta-DEB, the frequency is lowered to  $120\text{ cm}^{-1}$ . For para-DEB, however, an even lower frequency can be anticipated because the C-nuclei 1 and 4 oscillate with larger amplitudes than the substituted C-atoms in ortho- and meta-DEB.

This completes the preliminary study of the vibrational spectra of the three DEBs. The methods followed for subdividing the vibrations into groups have been very useful for interpreting the vibrational spectra. The foregoing is illustrated in Fig. 3.2, where the expected frequency ranges are given for the fundamentals of the three DEBs. These ranges are taken from Varsanyi<sup>(4)</sup> and are supplemented with the expected depolarization ratios of the signals in the Raman spectra.

### 3.2. Analysis of the Spectra

The analysis of the spectra of the isotopes of the three DEBs will be presented in five parts. Part A deals with the spectral region from  $3500$  to  $2100\text{ cm}^{-1}$ , in which the C—H and C—D stretches occur. Part B spans the range from  $2100$  to  $1400\text{ cm}^{-1}$  in which most of the C—C stretches occur. Part C involves the frequency range from  $1400$  to  $1000\text{ cm}^{-1}$ , in which the aromatic C—H bending modes are found. In the region from  $1000$  to  $600\text{ cm}^{-1}$ , Part D, five characteristic out-of-plane fundamentals can be easily identified. Finally

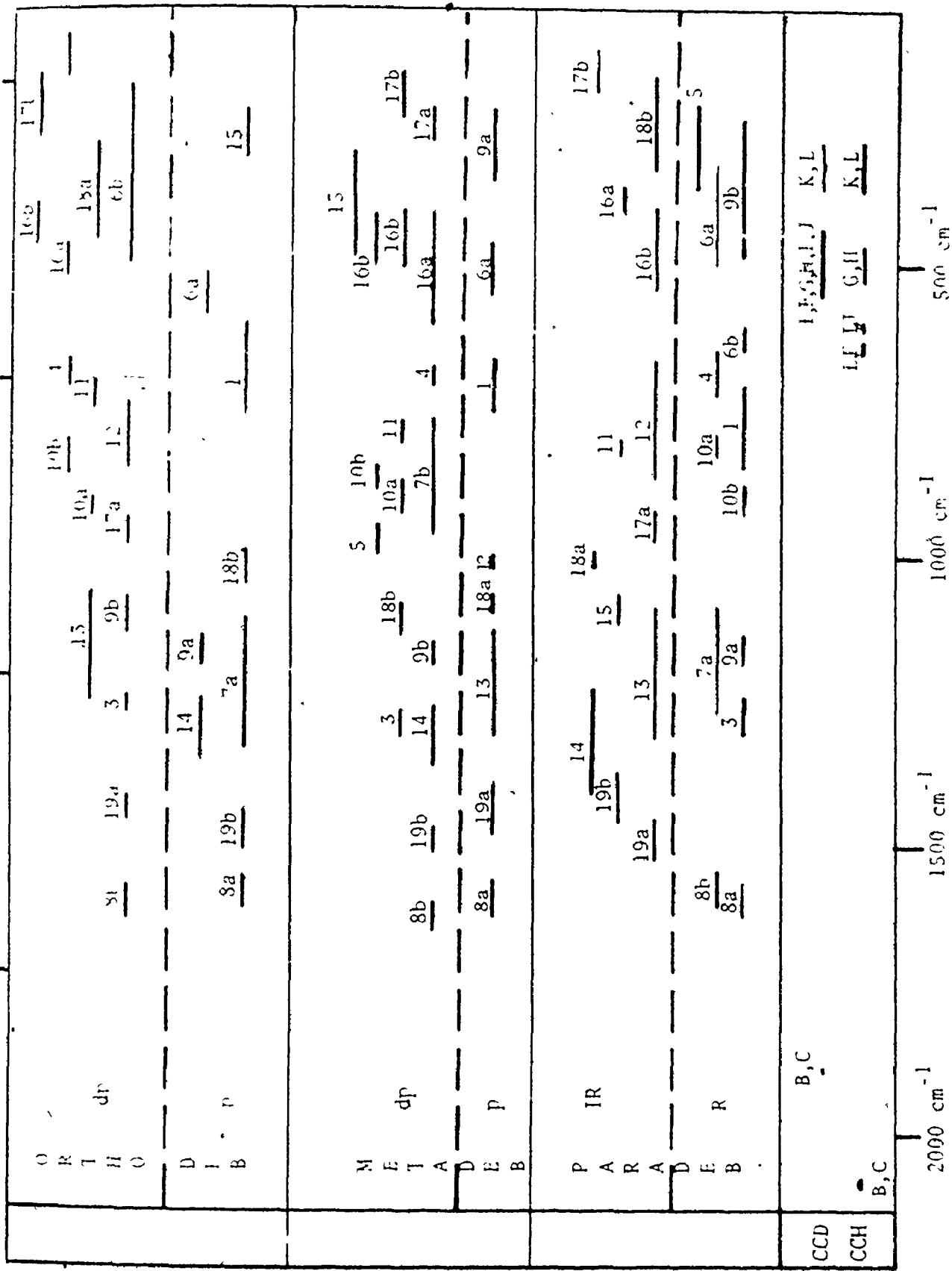


Fig. 3.2. Wavenumber range ( $\text{cm}^{-1}$ ) of the frequencies of the normal modes of vibration of the DEBs.

in Part E, the region below  $600\text{ cm}^{-1}$  will be discussed.

The spectra of a total of nine isotopes of the three DEBs have been recorded. These isotopes and their abbreviations are repeated here (see Chapter 2): para- $\text{C}_6\text{H}_4(\text{CCH})_2$  (para- $h_6$ ), para- $\text{C}_6\text{H}_4(\text{CCD})_2$  (para- $d_2$ ), para- $\text{C}_6\text{D}_4(\text{CCH})_2$  (para- $d_4$ ), para- $\text{C}_6\text{D}_4(\text{CCD})_2$  (para- $d_6$ ), meta- $\text{C}_6\text{H}_4(\text{CCH})_2$  (meta- $h_6$ ), meta- $\text{C}_6\text{H}_4(\text{CCD})_2$  (meta- $d_2$ ), ortho- $\text{C}_6\text{H}_4(\text{CCH})_2$  (ortho- $h_6$ ), ortho- $\text{C}_6\text{D}_4(\text{CCH})_2$  (ortho- $d_4$ ) and ortho- $\text{C}_6\text{D}_4(\text{CCD})_2$  (ortho- $d_6$ ).

The frequencies and intensities of the observed bands have been collected in Tables 3.2.A, B and C for the isotopes of para-, meta- and ortho-DEB respectively. These tables also contain the assignments proposed for these molecules.

Part A. The very intense acetylenic C—H stretches A and B occur in the I.R. at  $3333\text{ cm}^{-1}$  in the gas phase and at  $3300\text{ cm}^{-1}$  in solution. In the Raman spectra medium intense broad signals are observed at  $3300\text{ cm}^{-1}$  for liquid samples and at  $3268\text{ cm}^{-1}$  for the solids. These frequency shifts can be attributed to the interaction of the acetylenic H-atom with its surroundings<sup>(27)</sup>. The vibrations A and B decrease by about  $700\text{ cm}^{-1}$  upon deuteration of the CCH groups. The aromatic C—H stretches are found at  $3050\pm 50\text{ cm}^{-1}$  and bad overlapping occurs in the I.R. for ortho-DEB and in the Raman spectra for meta-DEB. The totally symmetric vibrations could be assigned with the help of the measured depolarization ratios of the Raman bands. The C—H stretching modes decrease in frequency by nearly  $700\text{ cm}^{-1}$  upon ring deuteration. Numerous weak bands are observed in the I.R. spectra in frequency range A, in addition to the above strong fundamentals.

An unambiguous assignment is impossible for most of these signals. However, some regularities have been found. It has been observed, for instance,

Table 3.3.A.1.

Frequencies ( $\text{cm}^{-1}$ ) and assignments of the I.R. bands  
of the isotopes of para-DEB

para-h <sub>6</sub>		para-d <sub>2</sub>		para-d <sub>4</sub>		para-d <sub>6</sub>		assignment
3940	vw			3940	vw			$\nu_{19} + \nu_{24}$
3898	vw			3900	vw			$\nu_{12} + \nu_{24}$
3689	vvw			3689	vvw			$\nu_{21} + \nu_{24}$
3616	vvw			3615	vvw			$\nu_{24} + \nu_{41}$
3480	*vvw			3480	*vvw			$\nu_{14} + \nu_{24}$
3390	sh	3385	vvw	3385	sh	3390	vvw	$\nu_{24} + \nu_{42}$
3305	vs	3306	m	3305	vvs	3305	m	$\nu_{24}$
3112	vw	3110	vw	3120	vw	3125	vw	$\nu_{24} - \nu_{14}$
3080	m	3080	m					$\nu_{31}$
				3065	vvw	3060	vvw	$\nu_7 + \nu_{25}$
3040	m	3039	m					$\nu_{25}$
2976	vvw	2969	vvw					$\nu_{16} + \nu_{33}$
2925	vvw	2928	vvw					$\nu_{27} + \nu_{33}$
2862	vvw	2865	vvw					$\nu_4 + \nu_{28}$
2804	vvw	2802	vvw					$\nu_{17} + \nu_{27}$
				2802	vvw	2804	vvw	$2\nu_{32}$
				2782	vvw	2782	vvw	$\nu_2 + \nu_{40}$
		2591	vs			2590	vs	$\nu_{24}^D$
2500	vvw	2500	vvw					$\nu_{21} + \nu_{26}$
				2422	vvw	2422	vvw	$\nu_4 + \nu_{29}$
2398	vvw	2396	vvw					$\nu_{17} + \nu_{34}$
				2340	vvw	2340	vvw	$\nu_4 + \nu_{38}$
2320	vvw	2324	vvw					$\nu_7 + \nu_{27}$
				2297	m	2296	m	$\nu_{31}$
				2286	m	2285	m	$\nu_{25}$
2275	vvw	2278	vvw					$\nu_5 + \nu_{34}$
				2260	vvw	2259	vvw	$\nu_5 + \nu_{27}$
2110	ms	1980	ms	2110	s	1981	s	$\nu_{26}$
				2024	vvw	2020	vvw	$\nu_7 + \nu_{28}$
1908	m	1910	m					$\nu_{10} + \nu_{22}$
				1868	vvw	1864	vvw	$\nu_{17} + \nu_{29}$
				1820	vvw	1815	vvw	$\nu_{10} + \nu_{34}$
1792	w	1792	w					$\nu_{10} + \nu_{38}$
				1770	vvw	1772	vvw	$\nu_7 + \nu_{17}$
1782	w	1784	w					$\nu_{22} + \nu_{38}$
1719	vvw	1717	vvw					$\nu_{11} + \nu_{34}$
				1688	vvw	1686	vvw	$\nu_5^D + \nu_{34}^D$
1664	m	1665	m					$\nu_9 + \nu_{38}$
1640				1640				} polymer
1662		1600		1600		1598		
				1580		1580		$\nu_{10} + \nu_{40}$
1499	vs	1500	s					$\nu_{27}$
1489	vs	1490	s					
1455	vvw	1456	vvw	1438	vw	1433	vvw	$\nu_{14} + \nu_{28}$

\* An asterisk indicates a broad band.

Table 3.3.A.1. (cont'd.)

para-h <sub>6</sub>	para-d <sub>2</sub>	para-d <sub>4</sub>	para-d <sub>6</sub>	assignment
		1404 vs	1403 vs	v <sub>27</sub> <sup>D</sup>
1401 s	1401 s			v <sub>32</sub>
1375 vw	1374 w			v <sub>33</sub>
1345 vvw	1350 vvw	1350 vvw	1350 vw	v <sub>9</sub> + v <sub>40</sub>
		1320 m	1320 m	v <sub>18</sub> <sup>D</sup> + v <sub>38</sub> <sup>D</sup>
1305 vw	1303 vvw		1300 vvw	v <sub>32</sub> <sup>D</sup> , v <sub>33</sub> <sup>D</sup>
1293 vw	1292 vvw	1295 *vw		} v <sub>19</sub> +v <sub>35</sub> , v <sub>19</sub> +v <sub>39</sub>
1260 w	1260 m	1258 w	1258 ms	v <sub>28</sub>
1225**vs	1231 *vw	1222**vs	1220 *vw	v <sub>19</sub> + v <sub>39</sub>
1197 sh	1198 w			v <sub>19</sub> + v <sub>40</sub>
1174 sh	1170 vw	1170 vvw	1170 vvw	v <sub>20</sub> + v <sub>35</sub>
				v <sub>8</sub> <sup>D</sup> + v <sub>38</sub> <sup>D</sup>
1122 vvw	1115 sh	1096	1085	v <sub>9</sub> + v <sub>41</sub>
		1045 vvw	1045 vvw	v <sub>21</sub> <sup>D</sup> + v <sub>30</sub> <sup>D</sup>
1100 ms	1100 m			v <sub>34</sub>
1054 vvw	1058 vvw			v <sub>30</sub> <sup>D</sup> + v <sub>41</sub> <sup>D</sup>
1015 m	1014 m			v <sub>18</sub> + v <sub>23</sub>
	980 m	948 vvw	980 s	v <sub>29</sub>
	934 m		954 vw	} v <sub>19</sub> <sup>D</sup> + v <sub>35</sub> <sup>D</sup>
950 vw	955 sh		930 m	v <sub>12</sub> <sup>D</sup> + v <sub>19</sub> <sup>D</sup>
908 vvw	884 w			v <sub>12</sub> <sup>D</sup> + v <sub>39</sub> <sup>D</sup>
		866 sh	861 sh	v <sub>22</sub>
		851 m	851 m	2v <sub>6</sub>
				v <sub>19</sub> + v <sub>41</sub>
				v <sub>21</sub> <sup>D</sup> + v <sub>40</sub> <sup>D</sup>
834 s	835 s			v <sub>29</sub> <sup>D</sup>
834 s	812 w			v <sub>38</sub>
		820 m	819 m	v <sub>30</sub>
				v <sub>34</sub> <sup>D</sup>
804 vw		804 vvw	800 vvw	v <sub>14</sub> + v <sub>39</sub>
		780 vw	780 *sh	v <sub>22</sub> <sup>D</sup>
763 vvw	760 vvw	760 vw	760 sh	v <sub>21</sub> + v <sub>37</sub>
		741 s	740 s	v <sub>38</sub> <sup>D</sup>
724 vvw	720 vvw	725 vs	722 vs	v <sub>23</sub> + v <sub>41</sub>
		690 sh	685 sh	v <sub>30</sub> <sup>D</sup>
646 vs	650 vw	648 vs	650 vw	v <sub>14</sub> + v <sub>40</sub>
		615 vs	614 vw	v <sub>35</sub>
615 vs	617 vw		630 vw	v <sub>9</sub> , v <sub>18</sub>
	573 vw		614 vw	v <sub>39</sub>
547 ms	545 s		575 vvw	v <sub>40</sub>
		536 vvw	528 sh	v <sub>36</sub>
486 ms	520 s	484 s	520 s	v <sub>35</sub>
	482 s		486 vs	v <sub>40</sub>
		469 s	486 vs	v <sub>39</sub>
	464 s		464 s	v <sub>23</sub>
399 vvw	400 vvw			v <sub>37</sub> <sup>D</sup>
370 vvw	370 vvw	350 sh	350 vvw	v <sub>23</sub>
		315 m	309 s	v <sub>41</sub>
325 m	312 m			

Table 3.3.A.2.

Frequencies ( $\text{cm}^{-1}$ ) and assignments of the Raman bands  
of the isotopes of para-DEB

para-h <sub>6</sub>	para-d <sub>2</sub>	para-d <sub>4</sub>	para-d <sub>6</sub>	assignment
3300 *vw p		3300 *vw p		v <sub>1</sub>
3064 vw p	3066 vw p(.2)			v <sub>2</sub>
3054 w dp	3053 w dp(.7)			v <sub>15</sub>
2985 vvw	2983 vvw			v <sub>27</sub> +v <sub>32</sub>
	2596 m p(.4)		2598 m	v <sub>1</sub> <sup>D</sup>
	2566 w		2565 w	v <sub>3</sub> +v <sub>20</sub>
		2291 m p(.1)	2291 s	v <sub>2</sub> <sup>D</sup> , v <sub>15</sub> <sup>D</sup>
		2273 vw	2271 vw	v <sub>6</sub> +v <sub>17</sub> +v <sub>21</sub>
		2257 vw	2253 vw	v <sub>27</sub> +v <sub>29</sub>
2108 vs p(.1)	2104 vvw p(.3)	2108 vs p(.4)		v <sub>3</sub>
	1985 s p(.2)		1985 vs	v <sub>3</sub> <sup>D</sup>
	1973 s p(.2)			v <sub>6</sub> +v <sub>7</sub>
	1926 vvw		1925 vvw	v <sub>3</sub> <sup>D</sup> -v <sub>42</sub>
1606 sh	1605 sh	1575 s	1575 s	v <sub>4</sub>
1601 s p(.4)	1600 m p(.5)	1570 s p(.4)	1568 m	v <sub>16</sub>
1306 vvw	1305 vvw			v <sub>17</sub>
1207 vw p(.2)	1205 vvw	1202 vw p(.1)		2v <sub>12</sub>
1195 vw p(.3)	1196 vw p(.2)			v <sub>18</sub> +v <sub>20</sub>
1176 s p(.3)	1171 s p(.2)	1175 s p(.1)	1168 s	v <sub>5</sub>
1176 s p(.3)	1171 s p(.2)			v <sub>6</sub>
		1122 vvw	1120 vvw	v <sub>8</sub> +v <sub>11</sub>
		1018 vvw	1018 vvw	v <sub>17</sub> <sup>D</sup>
			985 vvw*	2v <sub>12</sub> <sup>D</sup> , 2v <sub>18</sub> <sup>D</sup>
				v <sub>12</sub> <sup>D</sup> +v <sub>18</sub> <sup>D</sup>
957 vvw	954 vvw			v <sub>10</sub>
		949 vvw	948 vvw	v <sub>7</sub> +v <sub>14</sub>
		869 s p(.1)	870 s	v <sub>5</sub> <sup>D</sup>
		862 vw p(.1)	863 vw	v <sub>37</sub> +v <sub>40</sub>
		837 vvw	840 vvw	v <sub>23</sub> +v <sub>40</sub>
812 w p(.1)	809 w			v <sub>7</sub>
		810 vw	811 vw	v <sub>10</sub> <sup>D</sup>
797 vw	796 vw			v <sub>9</sub>
		773 vw p(.1)	775 vw	v <sub>37</sub> +v <sub>40</sub>
		766 m p(.1)	763 m	v <sub>7</sub>
724 vw	724 vw dp(.7)			v <sub>11</sub>
676 vw		677 vw		v <sub>39</sub> +v <sub>42</sub>
		652 vw	651 vwr	v <sub>11</sub> <sup>D</sup>
653 m dp(.8)	650 w dp(.9)	631 w dp(.8)	630 m	v <sub>18</sub>
632 *w	626 *vw	631 w dp(.8)	630 m	v <sub>19</sub>
618 m dp(.7)		619 ms dp(.8)		v <sub>12</sub>
535 vw	547 sh	511 w dp(.7)	547 vw	v <sub>20</sub>
477 m dp(.7)	542 m dp(.8)	466 m dp(.8)	534 m	v <sub>13</sub>
	506 sh		505 sh	v <sub>19</sub> <sup>D</sup>
	498 s dp(.8)		496 s	v <sub>12</sub> <sup>D</sup>



Table 3.3.A.2. (cont'd.)

para-h <sub>6</sub>	para-d <sub>2</sub>	para-d <sub>4</sub>	para-d <sub>6</sub>	assignment
460 vvw	458 vvw	( )	450 vvw	v <sub>8</sub>
385 *vvw	380 *vvw	370 *vvw	390 *vvw	v <sub>21</sub>
375 *vvw	362 *vvw	370 *vvw	370 *vvw	2v <sub>14</sub>
201 sh	189 sh	193 sh	186 sh	v <sub>14</sub> (14 <sup>2</sup> <sub>1</sub> )
197 s dp(.8)	182 s dp(.8)	186 s dp(.7)	177 s	v <sub>14</sub> (14 <sup>1</sup> <sub>0</sub> )
109 vvw	93 vw	92 vvw	92 vvw	v <sub>42</sub> (42 <sup>3</sup> <sub>3</sub> )
98 w		83 w	83 w	v <sub>42</sub> (42 <sup>2</sup> <sub>2</sub> )
77 sh	74 sh	72 m	72 m	v <sub>42</sub> (42 <sup>1</sup> <sub>1</sub> )
68 s	68 s	64 s	63 s	v <sub>42</sub> (42 <sup>0</sup> <sub>0</sub> )

Table 3.3.B.

Frequencies ( $\text{cm}^{-1}$ ) and intensities of the I.R. and Raman bands  
of meta-DEB

meta-h <sub>6</sub>		meta-d <sub>2</sub>		Assignment
I.R.	Raman	I.R.	Raman	
3940	vw	3940	vvw	$\nu_{12}+\nu_{29}, \nu_1+\nu_{39}$
3904	vw	3910	vvw	$\nu_{17}+\nu_{29}, \nu_1+\nu_{25}$
3416	vvw	3620	vvw	$\nu_{19}+\nu_{29}$
3303	vvs	3302	m	$\nu_{29}+\nu_1$
3088	vw	3088	vw	$\nu_2$
3065	w	3064	w	$\nu_3+\nu_{20}$
3028	vw	3028	vw	$\nu_4$
2963	sh	2965	sh	polymer
2930	vw	2928	vw	
2825	vw	2924	vw	
		2590	vs	2588 w p(.2)
2858	vvw	2454	vvw	$\nu_1, \nu_{29}$
2400	vvw	2400	vvw	$\nu_{33}+\nu_{34}$
2340	vvw	2340	vvw	$2\nu_7$
2260	vvw	2260	vvw	
2108	s	2108	vw	2107 vw p(.2)
		1979	s	1978 vw p(.1)
1945	vw	1948	sh	$\nu_5, \nu_{31}$
1885	w	1884	w	$\nu_5^D, \nu_{31}^D$
1820	vw	1822	vw	$2\nu_{21}$
1790	vw	1790	vw	$\nu_{16}+\nu_{21}$
1705	vw	1707	vw	$\nu_{21}+\nu_{22}$
1672	vw	1678	vw	$2\nu_{16}$
		1641	vvw	$\nu_{16}+\nu_{23}$
1600	sh	1602	sh	$\nu_{22}+\nu_{23}$
1592	vs	1592	vs	impurity?
1570	vs	1570	vs	$2\nu_{23}$
		1520	vvw	$\nu_{32}$
1495	vvw	1493	vvw	$\nu_6$
1475	vs	1473	vs	
1450	vvw	1435	vvw	$\nu_{33}$
1404	vs	1405	vs	1406 vw
1372	vvw			$\nu_7$
1348	vvw	1342	vvw	$\nu_{34}$
1310	vw	1308	vw	$\nu_{35}$
1284	sh	1288	vw	$2\beta(\equiv\text{C}-\text{H}), 2\gamma(\equiv\text{C}-\text{H})$
1260	sh	1262	vw	$\beta+\gamma(\equiv\text{C}-\text{H})$
1250	**vs.	1226	vw	
				$\nu_8$
				$2\nu_{18}$
		1177	vvw	$\nu_{18}+\nu_{26}$
1165	vw	1166	vw	$\nu_{10}+\nu_{13}$
		1142	vw	$\nu_{36}$

Table 3.3.B. (cont'd.)

meta-h <sub>6</sub>		meta-d <sub>2</sub>		Assignment
I.R.	Raman	I.R.	Raman	
1111	vw			intensity $\alpha$ bands at 2900
1090	s	1088	s	v <sub>9</sub>
1078	sh	1080	sh	v <sub>37</sub>
998	vw			v <sub>10</sub>
	998 vs p(.1)		997 vs p(.1)	v <sub>15</sub> +v <sub>18</sub>
	986 vw		988 vw	2 $\beta$ , 2 $\gamma$ , 8+ $\gamma$
		980	*vvs	
		950	w	
976	vw			v <sub>21</sub>
966	vw			v <sub>38</sub>
894	vs	894	vs	v <sub>16</sub>
865	s			v <sub>15</sub> +v <sub>40</sub>
835	vw	834	w	v <sub>22</sub>
	812 vw			v <sub>14</sub> +v <sub>41</sub>
	797 vw			v <sub>41</sub> +v <sub>29</sub>
793	vs	794	vs	v <sub>23</sub>
760	vw	760	sh	2v <sub>15</sub> , 2v <sub>42</sub>
	703 m p(.1)			v <sub>11</sub>
683	s	682	s	v <sub>4</sub>
	690 vw			2v <sub>19</sub>
647	vs	650	w	v <sub>12</sub> , v <sub>39</sub>
618	vs			v <sub>17</sub> , v <sub>25</sub>
603	sh	607	vw	v <sub>18</sub>
557	vw	561	vw	v <sub>26</sub>
525	vw			v <sub>19</sub> +v <sub>28</sub>
				v <sub>15</sub> +v <sub>20</sub>
480	m	522	ms	v <sub>40</sub>
		497	vs	v <sub>12</sub> , v <sub>39</sub> , v <sub>19</sub> <sup>D</sup>
	480 m p(.3)			v <sub>13</sub> , v <sub>14</sub>
		470	ms	v <sub>25</sub>
		464	ms	v <sub>17</sub>
	(.....)			v <sub>41</sub>
455	m	440	m	v <sub>14</sub>
( )	456 w p(.2)	385	vw	v <sub>42</sub>
	386 *vw	355	ms	v <sub>27</sub>
363	s			v <sub>19</sub>
	366 vw dp(.7)			v <sub>28</sub>
	343 m dp(.7)	170	m dp(.8)	v <sub>20</sub>
180	185 *m dp(.7)	110	117 s dp(.7)	
120	122 *s dp(.8)			

Table 3.3.C.

Frequencies ( $\text{cm}^{-1}$ ) and assignments for ortho-DEB

ortho-h <sub>6</sub>		ortho-d <sub>4</sub>		ortho-d <sub>6</sub>		Assignment
I.R.	Raman	I.R.	Raman	I.R.	Raman	
3936 vw						$\nu_1 + \nu_{12}, \nu_{39}; \nu_{29} + \nu_{12}, 39$
3905 vw						$\nu_1 + \nu_{19}, \nu_{25}; \nu_{29} + \nu_{19}, 25$
3302 vs	3297 *w p(<.1)	3300 vvs	3296 *w p(<.1)	3300 w		$\nu_1, \nu_{29}$
	3182 vw					$\nu_1 - \nu_{22}$
3118 vw	3120 w p					$\nu_{29} - \nu_{28}$
3080 w	3078 vs p(<.1)					$\nu_2, \nu_3$
3064 *m						$\nu_{30}, \nu_{31}$
3020 vw						$\nu_{33} + \nu_{34}$
2975 s		2975 vs	2930 *vs p	2975 vs	2930 *vs p	hydrocarbon(s)
2930 s	2900 *w	2930 vs	2916 *vs p	2930 vs	2915 *vs p	
2870 s		2870 vs	2870 *vs p	2870 vs	2870 *vs p	$\nu_1^D, \nu_{29}^D$
		2286 m	2287 s } p(.2)	2589 vvs	2587 vs p(.1)	$\nu_2^D, \nu_3^D$
		2278 m	2280 sh } p(.1)	2285 m	2289 s } p(<.1)	$\nu_{30}^D, \nu_{31}^D$
		2106 m	2105 vs p(.1)	2277 m	2281 sh } p(<.1)	$\nu_4, \nu_{32}$
2108 w	2108 vs p(.1)		2092 w p(<.1)		2107 vw	$\nu_1 - 2\nu_{25}$
	2076 vw p		2060 vw p			$\nu_1 - 2\nu_{12}$
	2060 vw p			1980 s	1972 vs p(.2)	$\nu_4, \nu_{32}$
1850 vvw*		1860 *vvw				$\nu_{16} + \nu_{23}$
1820		1810 *vvw		1706 vs		2 $\nu_{23}$
1698 *m		1708 vs				phthaldehyde
1670 *m		1640 vvw		1638 vvw		$\nu_{23} + \nu_{24}$
1622 *w						polymer
		1595 vw		1595 vw		$\nu_{17} + \nu_{24}$
		1560 vw		1562 vw		phthaldehyde
1593 vw	1592 vs dp(.8)		1562 vs dp(.8)		1563 s p(.7)	$\nu_{33}$

Table 3.3.C. (cont'd.)

ortho-h <sub>6</sub>		ortho-d <sub>4</sub>		ortho-d <sub>6</sub>		Assignment	
I.R.	Raman	I.R.	Raman	I.R.	Raman	I.R.	Raman
1558 vw	1562 s p(.3)	1528 w	1530 s p(.1)	1528 w	1530 s p(.1)	v <sub>5</sub>	
1508 vw		1490 w		1490 w		2v <sub>24</sub>	
1472 s	1474 s p(.1)	1462 s		1462		v <sub>6</sub>	hydrocarbon(s)
1460 w	1460 vw	1455 sh		1452 sh		v <sub>34</sub>	hydrocarbon(s)
1452 vw		1424 vvw		1424 vvw		v <sub>6D</sub>	hydrocarbon(s)
1436 s	1439 vw	1408 vvw		1404 vvw		v <sub>7</sub>	hydrocarbon(s)
1400 vvw		1389 s	1388 s p(.1)		1390 vs p(.1)	v <sub>13+v<sub>38</sub></sub>	
1374 vw	1378 s p(.1)	1377 m	1372 w p(.1)	1379 s	1378 s p(.1)	v <sub>34</sub>	
1360 vw		1340 s	1338 vw	1339 m	1338 vw	v <sub>13+v<sub>38</sub></sub>	
1290 w		1306 vvw		1303 vvw		v <sub>35</sub>	
1240**w	1260 *vw p	1270 vw	1272 ms	1268 vw	1271 s p(.3)	v <sub>7D</sub>	
	1226 w	1250**w	1216 vw } p(<.1)		1213 vvw	v <sub>7</sub>	comb. of v <sub>12</sub> , v <sub>19</sub> , v <sub>25</sub> , v <sub>3</sub>
	1204 vs p(.1)		1200 vw }		1198		
	1204 vs p(.1)						
1180 vw	1182 vw	1140 w	1139 vw	1138 w	1137 vw	v <sub>8</sub>	
1159 vvw	1163 s p(.4)					v <sub>36</sub>	
1137 vvw						v <sub>9</sub>	
1089 w		1130 vvw	1128 s p(<.1)	1120 vvw	1124	v <sub>37</sub>	
1030 w	1037 vs p(.1)	1040 *vw		1040 *vw		v <sub>8D</sub>	
	1026 w p					v <sub>14+v<sub>20</sub></sub>	
950 vw		1008 m		1006 m		v <sub>10</sub>	
		940 w		1030 to 900	998 vvw	2v <sub>14</sub>	comb. of v <sub>12</sub> , v <sub>19</sub> , v <sub>25</sub>
910 w				vs **		v <sub>35D</sub>	and v <sub>39</sub>
875 w						v <sub>16</sub>	

Table 3.3.C. (cont'd.)

ortho-h <sub>6</sub>		ortho-d <sub>4</sub>		ortho-d <sub>6</sub>		Assignment
I.R.	Raman	I.R.	Raman	I.R.	Raman	
806 w	807 w dp(.7)	871 w 860 vw 852 vw 832 vw	873 vvw 856 s p(.1) 833 w p(.3)	871 w 859 vw 852 vw 828 vw	874 vvw 857 s p(.1) 832 w p(.3)	v <sub>37</sub> <sup>D</sup> v <sub>9</sub> <sup>D</sup> phthaldehyde v <sub>10</sub> <sup>D</sup>
782 m		789 w		789 w		v <sub>38</sub> <sup>D</sup> v <sub>16</sub> <sup>D</sup>
760 s		776 w		775 w		v <sub>24</sub> <sup>D</sup> v <sub>23</sub> <sup>D</sup> v <sub>24</sub>
	760 m p(.1)		760 vw p(<.1)			v <sub>19</sub> +v <sub>22</sub> v <sub>38</sub> <sup>D</sup> v <sub>17</sub> <sup>D</sup>
705 m		760 m 740 w		750 m 740 w		v <sub>18</sub> v <sub>11</sub>
	706 vs p(.1) 666 s p(.1)		678 m p(.1) -----		674 s p(<.1) 666 s p(.1)	impurity
640 vs 615 vs	630**ms	640 vs 618 vs	630**ms	630**w		v <sub>12</sub> , v <sub>39</sub> v <sub>19</sub> , v <sub>25</sub> v <sub>24</sub> <sup>D</sup>
		(-----)	(-----)	608 s	642 w dp(.8) 606 m (dp.8)	v <sub>18</sub> <sup>D</sup> v <sub>20</sub> ?
586 w		563 s 540 vw		546 vvw	543 s p(.1)	v <sub>13</sub> v <sub>26</sub>
552 vvw 552. vvw	552 s p(.3)		542 s p(.2)			v <sub>19</sub> , v <sub>40</sub> v <sub>40</sub>
506 w	511 w p 505 s dp(.7)	500 vw 500 vw	508 sh p 500 m dp(.6) 500 m dp(.8)	505 } *vs 495 }	517 s dp(.8) 500 *s dp(.8)	v <sub>12</sub> , v <sub>19</sub> , v <sub>20</sub> , v <sub>25</sub> , v <sub>26</sub> , v <sub>39</sub> v <sub>21</sub> +v <sub>22</sub> ?
476 w		472 vw 462 m 438 w 410 w 390 vvw	462 m dp(.7) 440 s p(.4) 410 m dp(.8)	429 w 409 w 390 vvw	428 m p(.4) 408 w dp(.7)	v <sub>15</sub> v <sub>41</sub> v <sub>42</sub>
442 vw 414 vw	440 s p(.4) 415 w dp(.8)	333 *s	337 m dp(.8) 325 m dp(.7)	330 *s	338 w dp(.7) 316 w dp(.8)	v <sub>27</sub> v <sub>21</sub>
395 vvw 370 m 335 vw	371 m dp(.7) 335 m dp(.7) 182 w dp(.7) 130 vs dp(.8)		170 vw dp(.8) 130 s dp(.7)		162 w dp(.7) 123 s dp(.8)	v <sub>28</sub> v <sub>22</sub>

that the very strong  $3300\text{ cm}^{-1}$  band in the I.R. has associated with it the characteristic vibrations of the CCH group, namely  $\beta$  and  $\gamma(\equiv\text{C}-\text{H})$ ,  $\gamma(\text{C}-\text{CCH})$ ,  $\beta(\text{C}-\text{CCH})$  as well as the  $\gamma(\text{C}-\text{C}\equiv\text{C})$  mode. For para-DEB, the smallest difference in frequency with the  $3300\text{ cm}^{-1}$  band is found, namely  $80\text{ cm}^{-1}$ . This supports the discussion given in Section 3.1.C. Also a band is found at  $382\text{ cm}^{-1}$  from the  $\nu(\equiv\text{C}-\text{H})$  fundamental for para-DEB. This signal is assigned to the  $\beta(\text{C}-\text{CCH})$  fundamental on the basis of the discussion in Section 3.1.A. and the very weak signal in the Raman spectrum at  $380\text{ cm}^{-1}$ .

The region from  $2800$  to  $3000\text{ cm}^{-1}$  showed bands for all isotopes that have to be attributed to impurities. For para-DEB and meta-DEB, these signals were of very low intensity for freshly distilled samples. For ortho-DEB, however, very strong bands were observed that decreased only slightly in intensity upon distillation. This observation cannot be explained by a polymerization of the sample. As discussed in Section 2.1, the N.M.R. spectrum of ortho-DEB indicated the presence of hydrocarbons with a high boiling point. These originate in the commercial n-butyllithium solution in a mixture of hydrocarbons, of which n-hexane was the major component. In order to find other I.R. bands arising from this impurity, the n-butyllithium--in 10 cc of the hydrocarbon solution--was decomposed with water. The lithium hydroxide was removed by filtration and the n-hexane was distilled off. The residue, dissolved in  $\text{CCl}_4$ , showed very strong bands in the I.R. at the same frequencies as recorded for ortho-DEB in the region from  $2800$  to  $3000\text{ cm}^{-1}$ . When the intensities of these bands in the spectrum of the residue were matched to those for ortho-DEB using a variable path length cell, it became immediately apparent that the following bands in the spectrum of ortho-DEB arise from the hydrocarbon impurity:  $1462(\text{s})$ ,  $1452(\text{sh})$ ,  $1424(\text{vvw})$ ,  $1405(\text{vvw})$  and  $1378(\text{m})\text{ cm}^{-1}$ .

Part B. The triple bond stretches C and D have been found as strong bands at  $2105 \pm 5 \text{ cm}^{-1}$  for the CCH isotopes and  $1980 \pm 5 \text{ cm}^{-1}$  for the CCD derivatives in the I.R. and Raman spectra. The fundamentals of vibrations 8a, 8b, 19a and 19b are easily identified in all spectra. A small drop in frequency ( $25 \text{ cm}^{-1}$ ) occurs for pair 8 and a slightly larger decrease ( $75 \text{ cm}^{-1}$ ) is found for pair 19 upon ring deuteration. The vibrations 8a and 8b are Raman active only for para-DEB and differ very little in frequency. The  $1600 \text{ cm}^{-1}$  band is slightly broader than other Raman bands and a shoulder has been detected at  $1605 \text{ cm}^{-1}$  with difficulty for para- $\text{h}_6$  and para- $\text{d}_2$ . A unique assignment for the vibrational pairs 8 and 19 has been possible for all DEBs with the aid of the depolarization ratios of the signals in the Raman spectra.

In the I.R., the summation bands of the  $\gamma(\text{C—H})$  modes are found in the so-called "fingerprint" region from  $1600$  to  $2000 \text{ cm}^{-1}$ . These weak bands could be assigned readily in all cases with the help of Whiffen's generalizations<sup>(42)</sup>.

Some evidence is found for impurities in bands at  $1602$  and  $1640 \text{ cm}^{-1}$  in the I.R. spectra of para- and meta-DEB. These signals probably arise from an ethylenic type bond in the polymerization products. In the I.R. spectrum of the polymerization product of  $\phi\text{CCH}$  and meta-DEB for instance, strong signals are found around  $1600$  and  $1500 \text{ cm}^{-1}$  and a weak absorption occurs at  $1700 \text{ cm}^{-1}$ <sup>(26)</sup>. A medium intense, broad band is found in the I.R. spectrum of the multiple distilled ortho- $\text{h}_6$  isotope at  $1700 \text{ cm}^{-1}$ . The less pure, ring deuterated compounds show a strong absorption at  $1708 \text{ cm}^{-1}$ . This signal is caused by some unreacted starting material (phthalaldehyde). The I.R. spectrum of phthalaldehyde did not show any other impurity bands except the very weak signals at  $1595$  and  $852 \text{ cm}^{-1}$ .

Part C. The region from  $1400$  to  $1000 \text{ cm}^{-1}$  is more complex than the above two spectral ranges (see Fig. 3.2). Apart from the  $\beta(\text{C—H})$  modes and the Kékulé



mode 14, we can expect in this region also some of the coupled radial C—C stretching modes, discussed in Section 3.1.B. The situation is further complicated for the CCH isotopes by the strong combination band(s) of the acetylenic bending modes E, F, I and J. Notwithstanding the large number of CCH isotopes studied, nothing can be said about the summation band(s), because one broad hump is observed in the solution spectra. The vapor pressure of the compounds is too low to enable observation in the gas phase. Below each DEB will be considered separately.

para-DEB. The I.R. active  $\beta(\text{C—H})$  modes can be identified easily in the spectra of the four isotopes by analogy to the halogenobenzenes<sup>(30,33,34)</sup>. The totally symmetric Raman active  $\beta(\text{C—H})$  vibration is found as a strong polarized band at 1176 and 1171  $\text{cm}^{-1}$  for para- $\text{h}_6$  and para- $\text{d}_2$ . The nontotally symmetric Raman active C—H bending mode could be recorded only at a high laser output (700 milliwatt). These Raman active  $\beta(\text{C—H})$  vibrations show similar decreases in frequency upon ring deuteration as the halogenobenzenes<sup>(33,34)</sup>.

In the Raman spectra of para- $\text{d}_4$  and para- $\text{d}_6$ , strong polarized signals occur at 1175 and 1168  $\text{cm}^{-1}$ . These have been assigned to the substituent-sensitive C—C stretching mode 7a. Strong polarized bands are found at 1176 and 1171  $\text{cm}^{-1}$  in the Raman spectra of para- $\text{h}_6$  and para- $\text{d}_2$ . These signals have been attributed to the totally symmetric  $\nu(\text{C—C})$  mode 7a, because the bands at 1206 and 1196  $\text{cm}^{-1}$  are too weak to be likely candidates. The totally symmetric  $\nu(\text{C—H})$  vibration is thus assumed to be accidentally degenerate with the  $\nu(\text{C—C})$  vibration for para- $\text{h}_6$  and para- $\text{d}_2$ . The data in Table 3.2.A.1. reveal that all I.R. signals in the region from 1200 to 1300  $\text{cm}^{-1}$  decrease significantly in intensity upon deuteration of the CCH groups, except the band at 1260  $\text{cm}^{-1}$ . This absorption is largely unaffected by ring deuteration and has therefore been assigned to a substituent-sensitive radial C—C stretching mode ( $\nu_{28}$ ).

The remaining I.R. active vibration, the Kékulé or cyclohexatriene mode, can be assigned to either of the weak bands at 1375 and 1345  $\text{cm}^{-1}$ . The former value has been chosen by analogy to ortho-DEB (see below).

meta-DEB. In the Raman spectrum of meta- $\text{h}_6$  and meta- $\text{d}_2$ , only one strong polarized band is found at 1236 and 1233  $\text{cm}^{-1}$  respectively, and is assigned to the totally symmetric substituent-sensitive  $\nu(\text{C}-\text{C})$  mode  $\nu_8$ . The Kékulé vibration,  $\nu_{34}$ , has been assigned to the very weak band at 1348  $\text{cm}^{-1}$ , because it is the signal closest in frequency to the strong 1378  $\text{cm}^{-1}$  band measured for ortho- $\text{h}_6$ . This value also agrees with the proposed assignment for  $\phi\text{CCH}$  (1330  $\text{cm}^{-1}$ ). By analogy to other meta-disubstituted benzenes<sup>(4,33,34)</sup>, the  $\beta(\text{C}-\text{H})$  fundamental with the highest frequency should occur in the range from about 1250 to 1300  $\text{cm}^{-1}$ . No definite assignment can be made, however, because of the summation band(s) of the in and out-of-plane bending modes of the acetylenic hydrogen atom found in this region as a broad, very strong band. The chosen frequency of 1310  $\text{cm}^{-1}$  can be verified only with the spectra of the ring deuterated meta compounds. The fundamentals of the other two non-totally symmetric  $\beta(\text{C}-\text{H})$  vibrations could be identified readily in the I.R. spectra. The totally symmetric C-H bending modes did not give rise to a strong polarized Raman band. Only a very weak signal could be observed in the expected narrow frequency range and no depolarization ratio could be measured.

ortho-DEB. The Raman active  $\beta(\text{C}-\text{H})$  modes for ortho- $\text{h}_6$  have been assigned to the strong polarized signals at 1037 and 1163  $\text{cm}^{-1}$ , by analogy to other ortho-disubstituted benzenes<sup>(4,30)</sup>. No data is available for comparison for the ring deuterated isotopes. However, a decrease in frequency of 250 to 300  $\text{cm}^{-1}$  occurs commonly for the  $\beta(\text{C}-\text{H})$  modes upon ring deuteration<sup>(4,33,34)</sup>. The totally symmetric Raman active  $\beta(\text{C}-\text{D})$  fundamentals can thus be expected in

the region from 700 to 900  $\text{cm}^{-1}$ . Only two strong, polarized bands are found in this region for ortho- $\text{d}_4$  and ortho- $\text{d}_6$  and these can thus be identified unambiguously. The nontotally symmetric I.R. active  $\beta(\text{C-H})$  and  $\beta(\text{C-D})$  fundamentals have been assigned by similar arguments.

In the Raman spectrum of ortho- $\text{h}_6$ , two other strong polarized signals are found at 1378 and 1204  $\text{cm}^{-1}$ . The latter has been identified with the substituent-sensitive  $\nu(\text{C-C})$  vibration, by analogy to para- and meta-DEB. The 1378  $\text{cm}^{-1}$  signal then must be assigned to the remaining Kékulé mode ( $\nu_7$ ). The above two fundamentals are shifted less than 100  $\text{cm}^{-1}$  upon ring deuteration. It should be noted here the Kékulé mode is readily identified for ortho-DEB and that this cyclohexatriene mode has been assigned to a weak band, closest to 1378  $\text{cm}^{-1}$ , for para- and meta-DEB. The remaining I.R. active vibration can be expected to occur around 1200  $\text{cm}^{-1}$ , by analogy to the substituent-sensitive  $\nu(\text{C-C})$  mode for para- and meta-DEB. The assignment is straightforward because only one band is observed in this region.

Part D. The region from 1000 to 600  $\text{cm}^{-1}$  possesses the following features. In the I.R. the lower part of this range is dominated by very strong bands at 645 and 615  $\text{cm}^{-1}$  for all CCH isotopes. These signals correspond to the fundamentals of the vibrations E and F, and I and J and have been discussed already. For the CCD isotopes, the strong summation band(s) of these fundamentals appear at 950  $\text{cm}^{-1}$ . For para- $\text{d}_2$  and para- $\text{d}_6$ , however, two strong bands are found at 930 and 980  $\text{cm}^{-1}$ . These signals are probably overtones of the in and out-of-plane bending modes I and F at 464 and 482  $\text{cm}^{-1}$  respectively (see below). The Raman spectra of the DEBs contain a very weak, broad signal around 950  $\text{cm}^{-1}$  for the CCD and CCH isotopes. For the latter isotopes, the wavelength region from 600 to 650  $\text{cm}^{-1}$  is obscured by a broad absorption hump, corresponding to the  $\beta$  and  $\gamma(\equiv\text{C-H})$  fundamentals.

The aromatic out-of-plane C—H bending modes have been assigned for all isotopes by analogy to the fundamentals reported for the halogenobenzenes and the xylenes<sup>(30)</sup>. Whiffen's generalizations on the  $\gamma$ (C—H) fundamentals<sup>(42)</sup> have also been very helpful. Deuterium substitution results in a decrease in frequency of about 15% for para-disubstituted halogenobenzenes<sup>(33,34)</sup>. With the help of the data available for these molecules, the  $\gamma$ (C—D) fundamentals could be identified readily for para-d<sub>4</sub> and para-d<sub>6</sub>. When it was assumed that a similar drop in frequency does occur for the ring deuterated isotopes of ortho-DEB, three of the four fundamentals could be identified.  $\nu_{24}^D$ , however, is predicted to occur in the region of the intense bands at 615 and 640  $\text{cm}^{-1}$ . This fundamental could not be observed in the I.R. and has been assigned to the weak depolarized Raman band at 642  $\text{cm}^{-1}$ . This is the only example that the depolarized Raman bands did not only confirm the I.R. data for the out-of-plane modes of vibration. The benzene skeletal bending mode 4 could be identified uniquely for all isotopes, because its position is defined within a very small range for all types of disubstitution<sup>(4,33,34)</sup>. Below the remaining C—C stretching modes will be discussed for each DEB separately. The assignment of these is greatly simplified by the fact that they correspond to the few polarized Raman bands in this range.

In the Raman spectrum of para-DLB, only one polarized signal is found in region D, namely at 812  $\text{cm}^{-1}$ . The Raman active substituent-sensitive (C—C) vibrations have thus been found at 1176 and 812  $\text{cm}^{-1}$  for para-h<sub>6</sub>. The data in Table 3.2.A reveal that small frequency changes occur upon deuteration of the CCH groups and the benzene ring. In the I.R. spectrum of para-h<sub>6</sub>, very weak bands only were found in the region where the  $\nu$ (C—C) fundamental can be expected, apart from the strong band at 834  $\text{cm}^{-1}$ . Upon deuteration of the CCH groups, a sharp peak appears on the low frequency side of the strong

band at  $834\text{ cm}^{-1}$ . It has been assumed that the  $\nu(\text{C}-\text{C})$  fundamental is obscured by this strong band in the spectrum of para- $\text{h}_6$ . The two substituent-sensitive  $\nu(\text{C}-\text{C})$  vibrations thus occur at  $1260$  and  $835\text{ cm}^{-1}$  in the I.R. spectrum of para- $\text{h}_6$ .

In the Raman spectrum of meta- $\text{h}_6$  and meta- $\text{d}_2$ , two strong polarized signals are found in the region  $1000$  to  $600\text{ cm}^{-1}$ , namely at  $998$  and  $702\text{ cm}^{-1}$ . The former frequency is found for all mono-, meta- and 1,3,5-substituted benzenes and can be described best with Whiffen's vibration p (see Section 3.1.B)<sup>(43)</sup>. The Raman active  $\nu(\text{C}-\text{C})$  fundamentals for meta-DEB are thus found at frequencies of  $1235$  and  $702\text{ cm}^{-1}$ . The I.R. active  $\nu(\text{C}-\text{C}\equiv\text{C})$  stretching mode has been assigned to a weak band with a frequency of  $966\text{ cm}^{-1}$  by analogy to alkylacetylenes<sup>(29)</sup>.

The above results have been explained already in Section 3.1.B. and it was seen there that para- and ortho-DEB should show a close similarity.

In the Raman spectrum of ortho- $\text{h}_6$ , one of the  $\nu(\text{C}-\text{C})$  stretches has been assigned a frequency of  $1204\text{ cm}^{-1}$  in Part C. Upon ring deuteration this frequency is shifted down to  $1126\text{ cm}^{-1}$ . This is a rather large shift compared to the decrease found for para-DEB. The drop in frequency upon ring deuteration of the  $\nu(\text{C}-\text{C})$  mode in range D should thus preferably be chosen as small as possible. This condition is met satisfactorily by the  $706\text{ cm}^{-1}$  band of ortho- $\text{h}_6$  and the  $678$  and  $674\text{ cm}^{-1}$  bands of ortho- $\text{d}_4$  and ortho- $\text{d}_6$ . A similar argument has been applied in assigning the I.R. active substituent-sensitive stretching modes.

In the above parts A, B, C and D, the frequencies have been assigned of the C-H stretching and bending modes, as well as the C-C stretching modes. The latter class of vibrations has been discussed thoroughly here, because of its importance in the U.V. spectra.

Part E. It has been outlined in Section 3.1. why ten to fifteen fundamentals can be expected in the region below  $600\text{ cm}^{-1}$ . This region will thus be rather crowded. With the aid of the discussion in Section 3.2.C., however, it is possible to discuss separately the in and out-of-plane vibrations in this range. The latter will be examined first. It should be noted that the Raman spectra in this region are not as useful as in the parts discussed above, because of the very small number of polarized bands and the large number of depolarized signals. The latter only confirm the I.R. data.

For all isotopes of ortho- and meta-DEB two fundamentals with very low frequencies have been found, namely at  $125$  and  $175\text{ cm}^{-1}$ . Also, two medium strong bands occur at about  $330$  and  $370\text{ cm}^{-1}$  for these molecules. Finally, at least two absorptions can always be found in the region from  $500$  to  $600\text{ cm}^{-1}$ , that can be correlated with the fundamentals of the vibrations 16a and 16b. The same pattern has been found for  $\phi\text{CCH}$  and  $\phi\text{CN}$ . The above bands have been explained in Section 3.2.C. by a coupling between the vibrations  $\gamma(\text{C}-\text{C}\equiv\text{C})$  and  $\gamma(\text{C}-\text{CCH})$ . It was argued there also that there should be strong coupling between the three I.R. active out-of-plane vibrations for para-DEB. The vibrations of the other set of three out-of-plane vibrations have different symmetries. Vibration 16a falls into the  $a_u$  class and the frequency of the fundamental has been predicted at  $400\text{ cm}^{-1}$ . This prediction was based on the displacement diagrams for vibrations 16a and the frequency of this fundamental for  $\phi$ ,  $\phi\text{CN}$  and  $\phi\text{CCH}$ . The substituent vibrations  $\gamma(\text{C}-\text{C}\equiv\text{C})$  and  $\gamma(\text{C}-\text{CCH})$  fall into the  $b_{2g}$  symmetry class and have been assigned to the medium intense bands at  $197$  and  $477\text{ cm}^{-1}$  for para- $h_6$ . It is important to note that the spectral region between these frequencies shows only two very weak signals. No medium intense band is thus found around  $350\text{ cm}^{-1}$  as in all other cases. It can be concluded then that the  $\gamma(\text{C}-\text{C}\equiv\text{C})$  vibration has a normal frequency close to

the analogous in-plane vibration, 477 and 530  $\text{cm}^{-1}$  respectively. These observations have confirmed the coupling scheme proposed in Section 3.2.C. Further support has been provided by the frequencies of the I.R. active out-of-plane vibrations namely 545, 325 and 68  $\text{cm}^{-1}$  for para- $\text{h}_6$ . This assignment has been discussed in detail in Section 3.1.C. and is not repeated here. Deuteration of the CCH groups results in a small drop in frequency ( $<10 \text{ cm}^{-1}$ ) of one or two of the fundamentals of this group of three out-of-plane vibrations. Upon ring deuteration a shift of about 60  $\text{cm}^{-1}$  is found for the vibration with the highest frequency. Therefore, this vibration is assumed to derive from the benzene skeletal bending mode 16. These isotopic shifts have been observed for all compounds studied, except for the "pure"  $\gamma(\text{C}\equiv\text{C})$  vibration with  $b_{2g}$  symmetry for para- $\text{d}_2$  and para- $\text{d}_6$ . This will be explained below, during the discussion of the in-plane fundamentals below 600  $\text{cm}^{-1}$ . The corresponding vibrations are indicated with square brackets in Table 3.2 and it is seen there that a very similar pattern should be found in the spectra of meta- and ortho-DEB.

The assignment of the in-plane vibrations is complicated by the fact that deuteration of the CCH groups reduces the fundamentals of the acetylenic hydrogen bending modes (E, F, I and J) by nearly 125  $\text{cm}^{-1}$  to about 500  $\text{cm}^{-1}$ . In the same region the fundamentals are found of the  $\beta(\text{C}\equiv\text{C})$  vibrations. These two types of bending vibrations are thus nearly degenerate and both are localized on the substituent. If these vibrations fall into the same symmetry class, significant interaction can occur (fermi-resonance). The data in Table 3.2 reveal that this interaction might occur between the modes F and H, and E and G for all three DEBs. The same interaction can be expected between the out-of-plane acetylenic deuterium bending mode and the "pure"  $\gamma(\text{C}\equiv\text{C})$  mode, both with  $b_{2g}$  symmetry for para- $\text{d}_2$  and para- $\text{d}_6$ . It was seen above that the

fundamentals of the group of three out-of-plane vibrations were only very slightly affected by deuteration of the CCH groups. It does not seem likely therefore that the  $\gamma(\equiv\text{C}-\text{D})$  vibration influences significantly the coupling between these three out-of-plane vibrations. The spectra of each DEB will now be considered separately.

para-DEB. A comparison of the data in Table 3.2.A. reveals that two new strong I.R. bands appear in the region of 450 to 520  $\text{cm}^{-1}$  upon deuteration of the CCH groups. The total of three strong bands in this range have to be assigned to the fundamentals of the vibrations I, F and H. It is assumed that the strong signal at 464  $\text{cm}^{-1}$  corresponds to the  $\gamma(\equiv\text{C}-\text{D})$  vibration, because out-of-plane acetylenic fundamentals occur always at slightly lower frequencies than the frequencies of the analogous in-plane vibrations<sup>(29)</sup>. The strong bands at 482 and 520  $\text{cm}^{-1}$  for para- $\text{d}_2$  and para- $\text{d}_6$  can then be assigned to the vibrations F and H. Strong bands are found at 930 and 980  $\text{cm}^{-1}$ . These can be neatly identified as overtones of the fundamentals at 464 and 482  $\text{cm}^{-1}$ . Therefore the  $\gamma(\equiv\text{C}-\text{D})$  and  $\beta(\equiv\text{C}-\text{D})$  vibrations have been assigned to the absorptions at the latter frequencies. The 520  $\text{cm}^{-1}$  band is consequently assigned to the fundamental of the  $\beta(\text{C}-\text{C}\equiv\text{C})$  vibration.

It is important to note that the separation between the  $\beta(\equiv\text{C}-\text{D})$  and  $\gamma(\equiv\text{C}-\text{D})$  fundamentals is equal to the separation for the analogous hydrogenic vibrations. The difference for these  $\beta(\equiv\text{C}-\text{H})$  and  $\gamma(\equiv\text{C}-\text{H})$  vibrations has been explained by valence bond arguments by Nyquist and Potts. Only one summation band is found for the  $\beta$  and  $\gamma(\equiv\text{C}-\text{H})$  vibrations. The acetylenic deuterium bending modes, however, give rise to overtones for both fundamentals. It is suggested that this is due to the resonance between the  $\beta(\text{C}-\text{C}\equiv\text{C})$  and  $\beta(\equiv\text{C}-\text{D})$  vibrations.

A splitting of 40  $\text{cm}^{-1}$  between these fundamentals is thus found in the



I.R. The occurrence of resonance is supported by the Raman spectra of the CCD isotopes of para-DEB. Here, two sets of bands are also found that have the same separation of  $40 \text{ cm}^{-1}$ . These bands have been assigned to the fundamentals of the  $\beta(\equiv\text{C}-\text{D})$  and  $\beta(\text{C}-\text{C}\equiv\text{C})$ , and to those of the  $\gamma(\equiv\text{C}-\text{D})$  and the  $\gamma(\text{C}-\text{C}\equiv\text{C})$  modes of vibration.

The assignment of the fundamentals of para-DEB is completed by identifying the very weak signals at  $370 \text{ cm}^{-1}$  in the Raman and I.R. spectra with the bending modes of the whole CCH group and by assigning the very weak signal at  $455 \pm 5 \text{ cm}^{-1}$  in the Raman spectra to the totally symmetric ring deformation  $\nu_8$ . The assignment of this fundamental is identical for para-DEB and  $\phi\text{CCH}$ . This is in accordance with the displacement diagram for this vibration (see Fig. 3.2).

meta-DEB. The data in Table 3.2.B. reveal that two new bands appear at  $470$  and  $464 \text{ cm}^{-1}$  in the I.R. spectra of meta-DEB upon deuteration of the CCH groups. These absorptions have been attributed to the  $\gamma(\equiv\text{C}-\text{D})$  bending modes by analogy to the bands observed at  $464 \text{ cm}^{-1}$  for para- $d_2$  and para- $d_6$ . The strong bands at  $497$  and  $522 \text{ cm}^{-1}$  in the I.R. spectrum of meta- $d_2$  indicate that the  $\beta(\equiv\text{C}-\text{D})$  and  $\beta(\text{C}-\text{C}\equiv\text{C})$  vibrations  $\nu_{39}$  and  $\nu_{40}$  interact in the same way as the analogous vibrations of para-DEB (fermi resonance). The nontotally symmetric ring deformation  $\nu_{41}$  can be seen clearly at  $457 \text{ cm}^{-1}$  in the spectrum of meta- $d_2$ . For meta- $h_6$  this signal is obscured by the stronger band at  $455 \text{ cm}^{-1}$ . The nontotally symmetric bending mode of the whole CCH group has been assigned to the very weak band at  $385 \text{ cm}^{-1}$ . The totally symmetric counterpart of this vibration is assigned to the polarized Raman line at  $456 \text{ cm}^{-1}$  for meta- $h_6$ . For meta- $d_2$  this frequency decreases  $14 \text{ cm}^{-1}$ , as expected for a fundamental of such a vibration. In the Raman spectrum of meta- $h_6$  and meta- $d_2$  only one more polarized signal could be detected, namely at  $480$  and  $475 \text{ cm}^{-1}$ .

For meta- $h_6$  no other signal occurs close to this frequency of  $480\text{ cm}^{-1}$  and it has been assumed therefore that the  $\beta(\text{C}-\text{C}\equiv\text{C})$  and  $\alpha(\text{C}-\text{C}-\text{C})$  vibrations ( $\nu_{13}$  and  $\nu_{14}$  respectively) are accidentally degenerate. For meta- $d_2$ , however, a very broad signal occurs at  $495\text{ cm}^{-1}$  with a half width of about  $30\text{ cm}^{-1}$ . It is not unreasonable to assume that the vibrations F and H are coupled and that the corresponding fundamentals are hidden in this broad absorption. The totally symmetric ring deformation  $\nu_{14}$  has therefore been assigned to the absorption at  $475\text{ cm}^{-1}$ , and the fundamentals of F and H have been arbitrarily put equal to  $495\text{ cm}^{-1}$ , the frequency of the absorption maximum.

ortho-DEB. The analysis of the region around  $500\text{ cm}^{-1}$  for ortho-DEB is greatly complicated by the observation of only one very strong and broad absorption in the I.R. at  $500\text{ cm}^{-1}$  and of only two strong infrared bands, namely at  $517$  and  $500\text{ cm}^{-1}$ , in the spectrum of ortho- $d_6$ . This implies that the fundamentals of the vibrations F and H, E and G, and I and J have frequencies of either  $517$  or  $500\text{ cm}^{-1}$  for ortho- $d_6$ . By analogy to the CCD isotopes of para- and meta-DEB, the higher value has been assumed only for the frequency of the  $\beta(\text{C}-\text{C}\equiv\text{C})$  fundamental.

With this assumption, the totally symmetric vibrations can be readily assigned to the polarized Raman bands for the three isotopes. The frequency of vibration G ( $\nu_{40}$ ) has been assigned to the absorption at  $505$  and  $500\text{ cm}^{-1}$  for ortho- $h_6$  and ortho- $d_4$  respectively. The bending mode of the whole CCH group has been associated with the very weak absorptions at  $390\text{ cm}^{-1}$ . The frequencies of these two acetylenic vibrations thus correspond closely to the frequencies found for para- and meta-DEB. Finally the frequency of the ring deformation  $\nu_{41}$  has been assigned to the infrared absorptions at  $414$ ,  $410$  and  $409\text{ cm}^{-1}$  for ortho- $h_6$ , ortho- $d_4$  and ortho- $d_6$  respectively. This completes the assignment for ortho-DEB, but it leaves unexplained the medium intense signals

Table 3.4.A.

Ground State Fundamental Frequencies ( $\text{cm}^{-1}$ )  
of the Isotopes of para-DEB

				para-h <sub>6</sub>	para-d <sub>2</sub>	para-d <sub>4</sub>	para-d <sub>6</sub>	sym.
1	A	$\nu(\equiv\text{C}-\text{H})$	R	3303	2596	3303	2597	
2	2	$\nu(\text{C}-\text{H})$	R	3064	3066	2291	2291	
3	C	$\nu(\text{C}\equiv\text{C})$	R	2108	1984	2108	1985	
4	8a	$\nu(\text{C}-\text{C})$	T	1606	1605	1575	1575	
5	7a	$\nu(\text{C}-\text{CCH})$	R	1176	1171	1175	1168	a <sub>g</sub>
6	9a	$\beta(\text{C}-\text{H})$	T	1176	1171	869	870	
7	1	$\nu(\text{C}-\text{CCH})$	R	812	809	768	763	
8	6a	$\alpha(\text{C}-\text{C}-\text{C})$	R	460	458	452	450	
9	10a	$\gamma(\text{C}-\text{H})$	O	797	796	631	630	b <sub>1g</sub>
10	10b	$\gamma(\text{C}-\text{H})$	O	957	954	810	811	
11	4	$\phi(\text{C}-\text{C})$	O	727	724	652	651	
12	J	$\gamma(\equiv\text{C}-\text{H})$	O	618	498	619	496	b <sub>2g</sub>
13	K	$\gamma(\text{C}-\text{C}\equiv\text{C})$	O	477	542	466	534	
14	5	$\gamma(\text{C}-\text{CCH})$	O	197	182	186	177	
15	7b	$\nu(\text{C}-\text{H})$	R	3054	3053	2291	2291	
16	8b	$\nu(\text{C}-\text{C})$	T	1601	1600	1570	1568	
17	3	$\beta(\text{C}-\text{H})$	T	1306	1305	1018	1018	
18	6b	$\alpha(\text{C}-\text{C}-\text{C})$	R	653	650	631	630	b <sub>3g</sub>
19	E	$\beta(\equiv\text{C}-\text{H})$	T	632	506	631	505	
20	G	$\beta(\text{C}-\text{C}\equiv\text{C})$	T	535	547	511	547	
21	9b	$\beta(\text{C}-\text{CCH})$	T	375	380	370	380	
22	17a	$\gamma(\text{C}-\text{H})$	O	950	950	782	780	
23	16a	$\phi(\text{C}-\text{C})$	O	399	400	350	350	a <sub>u</sub>
24	B	$\nu(\equiv\text{C}-\text{H})$	R	3305	2591	3305	2590	
25	20a	$\nu(\text{C}-\text{H})$	R	3040	3039	2286	2285	
26	D	$\nu(\text{C}\equiv\text{C})$	R	2110	1980	2110	1981	
27	19a	$\nu(\text{C}-\text{C})$	T	1489	1490	1404	1403	b <sub>1u</sub>
28	13	$\nu(\text{C}-\text{CCH})$	R	1260	1260	1258	1258	
29	18a	$\beta(\text{C}-\text{H})$	T	1015	1014	850	850	
30	12	$\nu(\text{C}-\text{CCH})$	R	835	812	725	725	
31	20b	$\nu(\text{C}-\text{H})$	R	3080	3080	2297	2296	
32	19b	$\nu(\text{C}-\text{C})$	T	1401	1401	1320	1320	
33	14	$\nu(\text{C}-\text{C})$	T	1375	1374	1320	1320	
34	15	$\beta(\text{C}-\text{H})$	T	1100	1101	820	819	b <sub>2u</sub>
35	F	$\beta(\equiv\text{C}-\text{H})$	T	646	482	648	486	
36	H	$\beta(\text{C}-\text{C}\equiv\text{C})$	T	486	520	484	520	
37	18b	$\beta(\text{C}-\text{CCH})$	T	370	370	370	370	
38	11	$\gamma(\text{C}-\text{H})$	O	834	835	742	740	
39	I	$\gamma(\equiv\text{C}-\text{H})$	O	615	464	615	464	
40	16b	$\phi(\text{C}-\text{C})$	O	545	547	484	486	b <sub>3u</sub>
41	L	$\gamma(\text{C}-\text{C}\equiv\text{C})$	O	325	312	315	310	
42	17b	$\gamma(\text{C}-\text{CCH})$	O	68	68	64	63	

Table 3.4.B.

Ground State Fundamental Frequencies ( $\text{cm}^{-1}$ )  
of the Isotopes of meta-DEB

				meta-h <sub>6</sub>	meta-d <sub>2</sub>	sym.
1	A	$\nu(\equiv\text{C}-\text{H})$	R	3303	2590	
2	20a	$\nu(\text{C}-\text{H})$	R	3088	3088	
3	2	$\nu(\text{C}-\text{H})$	R	3062	3064	
4	7a	$\nu(\text{C}-\text{H})$	R	3028	3028	
5	C	$\nu(\text{C}\equiv\text{C})$	R	2108	1979	
6	8a	$\nu(\text{C}-\text{C})$	T	1571	1571	
7	19a	$\nu(\text{C}-\text{C})$	T	1405	1405	
8	13	$\nu(\text{C}-\text{CCH})$	R	1236	1233	a <sub>1</sub>
9	18a	$\beta(\text{C}-\text{H})$	T	1090	1088	
10	12	$\nu(\text{C}-\text{C})$	R	998	997	
11	1	$\nu(\text{C}-\text{CCH})$	R	703	700	
12	F	$\beta(\equiv\text{C}-\text{H})$	T	647	495	
13	H	$\beta(\text{C}-\text{C}\equiv\text{C})$	T	480	495	
14	6a	$\alpha(\text{C}-\text{C}-\text{C})$	R	480	475	
15	9a	$\beta(\text{C}-\text{CCH})$	T	456	442	
<hr/>						
16	10a	$\gamma(\text{C}-\text{H})$	O	894	894	
17	J	$\gamma(\equiv\text{C}-\text{H})$	O	618	464	
18	16a	$\phi(\text{C}-\text{C})$	O	606	606	a <sub>2</sub>
19	K	$\gamma(\text{C}-\text{C}\equiv\text{C})$	O	343	333	
20	17a	$\gamma(\text{C}-\text{CCH})$	O	122	119	
<hr/>						
21	5	$\gamma(\text{C}-\text{H})$	O	976	976	
22	10b	$\gamma(\text{C}-\text{H})$	O	865	864	
23	11	$\gamma(\text{C}-\text{H})$	O	793	794	
24	4	$\phi(\text{C}-\text{C})$	O	683	681	b <sub>1</sub>
25	I	$\gamma(\equiv\text{C}-\text{H})$	O	618	470	
26	16b	$\phi(\text{C}-\text{C})$	O	559	560	
27	L	$\gamma(\text{C}-\text{C}\equiv\text{C})$	O	366	358	
28	17b	$\gamma(\text{C}-\text{CCH})$	O	185	172	
<hr/>						
29	B	$\nu(\equiv\text{C}-\text{H})$	R	3303	2588	
30	20b	$\nu(\text{C}-\text{H})$	R	3088	3088	
31	D	$\nu(\text{C}\equiv\text{C})$	R	2106	1979	
32	8b	$\nu(\text{C}-\text{C})$	T	1593	1592	
33	19b	$\nu(\text{C}-\text{C})$	T	1475	1473	
34	3	$\beta(\text{C}-\text{H})$	T	1310	1310	
35	14	$\nu(\text{C}-\text{CCH})$	T	1348	1342	b <sub>2</sub>
36	9b	$\beta(\text{C}-\text{H})$	T	1142	1142	
37	18b	$\beta(\text{C}-\text{H})$	T	1078	1079	
38	7b	$\nu(\text{C}-\text{CCH})$	R	966	966	
39	E	$\beta(\equiv\text{C}-\text{H})$	T	697	497	
40	G	$\beta(\text{C}-\text{C}\equiv\text{C})$	T	480	522	
41	6b	$\alpha(\text{C}-\text{C}-\text{C})$	R	455	457	
42	15	$\beta(\text{C}-\text{CCH})$	T	388	382	

Table 3.4.C.

Ground State Fundamental Frequencies ( $\text{cm}^{-1}$ )

of the Isotopes of ortho-DEB

				ortho-h <sub>6</sub>	ortho-d <sub>4</sub>	ortho-d <sub>6</sub>	sym.
1	A	$\nu(\equiv\text{C}-\text{H})$	R	3297	3296	2587	
2	2	$\nu(\text{C}-\text{H})$	R	3078	2288	2289	
3	20b	$\nu(\text{C}-\text{H})$	R	3078	2288	2289	
4	C	$\nu(\text{C}\equiv\text{C})$	R	2108	2109	1972	
5	8a	$\nu(\text{C}-\text{C})$	T	1562	1530	1530	
6	19b	$\nu(\text{C}-\text{C})$	T	1474	1388	1390	
7	14	$\nu(\text{C}-\text{C})$	T	1378	1272	1271	
8	7a	$\nu(\text{C}-\text{CCH})$	R	1204	1128	1124	a <sub>1</sub>
9	9a	$\beta(\text{C}-\text{H})$	T	1163	856	857	
10	18b	$\beta(\text{C}-\text{H})$	T	1037	833	832	
11	1	$\nu(\text{C}-\text{CCH})$	R	706	678	674	
12	F	$\beta(\equiv\text{C}-\text{H})$	T	640	640	500	
13	6a	$\alpha(\text{C}-\text{C}-\text{C})$	R	552	542	543	
14	H	$\beta(\text{C}-\text{C}\equiv\text{C})$	T	511	508	517	
15	15	$\beta(\text{C}-\text{CCH})$	T	440	439	428	
16	17a	$\gamma(\text{C}-\text{H})$	O	950	789	789	
17	10b	$\gamma(\text{C}-\text{H})$	O	875	740	740	
18	4	$\phi(\text{C}-\text{C})$	O	706	605	605	
19	J	$\gamma(\equiv\text{C}-\text{H})$	O	615	618	500	a <sub>2</sub>
20	16a	$\phi(\text{C}-\text{C})$	O	586	500	500	
21	K	$\gamma(\text{C}-\text{C}\equiv\text{C})$	O	335	325	316	
22	5	$\gamma(\text{C}-\text{CCH})$	O	130	130	123	
23	10a	$\gamma(\text{C}-\text{H})$	O	910	776	775	
24	11	$\gamma(\text{C}-\text{H})$	O	760	642	642	
25	I	$\gamma(\equiv\text{C}-\text{H})$	O	615	618	500	b <sub>1</sub>
26	16b	$\phi(\text{C}-\text{C})$	O	552	500	500	
27	L	$\gamma(\text{C}-\text{C}\equiv\text{C})$	O	371	337	338	
28	17b	$\gamma(\text{C}-\text{CCH})$	O	182	170	162	
29	B	$\nu(\equiv\text{C}-\text{H})$	R	3302	3300	2590	
30	20a	$\nu(\text{C}-\text{H})$	R	3078	2278	2277	
31	7b	$\nu(\text{C}-\text{H})$	R	3064	2278	2277	
32	D	$\nu(\text{C}\equiv\text{C})$	R	2108	2106	1980	
33	8b	$\nu(\text{C}-\text{C})$	T	1592	1562	1563	
34	19a	$\nu(\text{C}-\text{C})$	T	1436	1340	1338	
35	3	$\beta(\text{C}-\text{H})$	T	1290	1008	1006	b <sub>2</sub>
36	13	$\nu(\text{C}-\text{CCH})$	R	1181	1140	1137	
37	9b	$\beta(\text{C}-\text{H})$	T	1137	872	872	
38	12	$\nu(\text{C}-\text{CCH})$	R	807	760	750	
39	E	$\beta(\equiv\text{C}-\text{H})$	T	640	640	500	
40	G	$\beta(\text{C}-\text{C}\equiv\text{C})$	T	506	500	517	
41	6b	$\alpha(\text{C}-\text{C}-\text{C})$	R	414	411	408	
42	18a	$\beta(\text{C}-\text{CCH})$	T	395	390	390	

at 563 and 462  $\text{cm}^{-1}$  for ortho- $\text{d}_4$ .

A study of the vibrational spectra of ortho-, meta- and para-dicyanobenzene would be very valuable for confirming the interpretation of the spectra of the DEBs, presented above. The fundamentals for the DEBs are collected in Table 3.4 and they will be used to calculate experimental Redlich-Teller product ratios (R-T ratios). These R-T ratios will be compared with the theoretical values for these ratios. This procedure provides an easy qualitative check on the proposed assignments. First of all the uncertainties in the experimental and theoretical R-T ratios will be examined.

The theoretical R-T ratios are dependent on the rotational constants for those symmetry classes that transform as the rotations. The uncertainty in the rotational constants was estimated in Chapter 1 to be at most 1%. An uncertainty of maximally 1.5% can then be expected for the R-T ratios of the vibrations that belong to the same symmetry classes as the rotations. More than two significant figures can thus not be given for these R-T ratios. For calculating product ratios at all, it has to be assumed that isotopic substitution does not affect the force field. Generally this assumption is valid, but it can not be expected to hold for the cases in which fermi-resonance was found to occur between the  $\beta(\equiv\text{C}-\text{D})$  and  $\beta(\text{C}-\text{C}\equiv\text{C})$  vibrations. The calculated R-T ratios are then based on an invalid criterium and it is impossible to say what accuracy these theoretical quantities have in these cases (the vibrations with  $b_{2g}$ ,  $b_{3g}$  and  $b_{2u}$  symmetry for para-DEB and the vibrations with  $a_1$  and  $b_2$  symmetry for ortho- and meta-DEB). The theoretical R-T ratios for these symmetry classes are not given in more than two significant figures. The remaining product ratios have been quoted in two significant figures also for consistency in notation.

The uncertainty in the experimental R-T ratios is determined by the

accuracy with which frequencies have been measured. Several recordings of the same spectra have learned that this error is  $\pm 1 \text{ cm}^{-1}$  for strong sharp bands, 1 to 2  $\text{cm}^{-1}$  for medium intense bands, 2 to 3  $\text{cm}^{-1}$  for weak or broad signals, and 2 to 5  $\text{cm}^{-1}$  for weaker and/or broader bands. Major contributions to the uncertainty in the experimental R-T ratios are made by broad and/or weak low frequency absorptions. An appreciable error can also result from the accumulation of a large number of small uncertainties. It is estimated that an uncertainty of a few percent (2-3%) could occur in the most unfavourable cases.

The theoretical and experimental R-T ratios have been reported in Table 3.5 for para-DEB. An agreement to within the estimated error is found for all isotopic pairs and symmetry classes, except for the  $b_{2g}$ ,  $b_{3g}$  and  $b_{2u}$  vibrations of para- $d_2$  and para- $d_6$  with respect to para- $h_6$ .

Table 3.5

Experimental and theoretical R-T ratios for the isotopes  
of para-DEB

Sym.	para- $d_2$ para- $h_6$		para- $d_4$ para- $h_6$		para- $d_6$ para- $h_6$		para- $d_2$ para- $d_6$	
	th.	exp.	th.	exp.	th.	exp.	th.	exp.
$a_g$	.71	.73	.50	.51	.35	.37	.50	.51
$b_{1g}$	1.00	1.00	.78	.79	.78	.79	.78	.79
$b_{2g}$	.73	.86	.71	.71	.52	.63	.72	.74
$b_{3g}$	.73	.83	.51	.52	.37	.46	.51	.55
$a_u$	1.00	1.00	.71	.72	.71	.72	.71	.72
$b_{1u}$	.71	.72	.51	.51	.36	.38	.51	.53
$b_{2u}$	.71	.80	.51	.50	.36	.40	.51	.51
$b_{3u}$	.71	.72	.72	.72	.51	.53	.72	.73

The differences for these symmetry classes are pathological. The following argument learns that the discrepancies are caused by the interaction between the  $\beta(-C-D)$  and  $\beta(C-C\equiv C)$  vibrations. It was found above that an excellent agreement existed between the theoretical and experimental R-T ratios for para-d<sub>4</sub> with respect to para-h<sub>6</sub>. In other words, ring deuteration does not affect the force field significantly. The same excellent correspondence can be expected for the product ratios of the para-d<sub>2</sub> and para-d<sub>6</sub> isotopes, if the  $\beta(-C-D)$  and  $\beta(C-C\equiv C)$  vibrations interact to the same extent in both isotopes. The theoretical and experimental ratios in Table 3.5 for this pair of isotopes shows that this interaction is the same in first approximation. Only for the vibrations with b<sub>3g</sub> symmetry is the difference slightly larger than the estimated error. It should be noted also that the experimental R-T ratios are consistently larger than the theoretical quantities for the a<sub>g</sub> and b<sub>1u</sub> symmetry classes for the isotopic pairs para-d<sub>2</sub>/para-h<sub>6</sub> and para-d<sub>6</sub>/para-h<sub>6</sub>. These differences can be explained by some interaction between the acetylenic modes A and C, if at least this difference is physically significant.

The calculated and experimental R-T ratios for the two isotopes of meta-DEB are given in Table 3.6. Also tabulated are the ratios of the two ring deuterated isotopes of ortho-DEB with respect to ortho-h<sub>6</sub>.

Table 3.6

Experimental and theoretical R-T ratios for the isotopes  
of meta- and ortho-DEB

Symm. class	$\frac{\text{meta-d}_2}{\text{meta-h}_6}$		$\frac{\text{ortho-d}_4}{\text{ortho-h}_6}$		$\frac{\text{ortho-d}_6}{\text{ortho-h}_6}$	
	th.	exp.	th.	exp.	th.	exp.
a <sub>1</sub>	.50	.53	.25	.25	.13	.13
a <sub>2</sub>	.72	.71	.52	.52	.37	.38
b <sub>1</sub>	.69	.69	.52	.54	.38	.39
						.17



A satisfactory agreement is found for all cases, except for the  $a_1$  and  $b_2$  symmetry classes of the CCD isotopes. The large differences indicate that interaction of  $\beta(C-D)$  and  $\beta(C-C\equiv C)$  also occurs for meta- and ortho-DEB.

### Conclusions

The agreement between the theoretical and experimental R-T ratios, Tables 3.5 and 3.6, supports the coupling schemes suggested in the preceding paragraphs for the radial C—C stretches and for the low frequency out-of-plane vibrations. The first group of vibrations is very important for the analysis of the U.V. spectra. The proposed assignment of the low frequency out-of-plane fundamentals has led to a new understanding of the internal bending modes of the CCH/CN groups.

Fermi-resonance has also been firmly established for the CCD isotopes between the  $\beta(C-D)$  and  $\beta(C-C\equiv C)$  vibrations. These vibrations play an important role in the U.V. spectrum of para-DEB.

## CHAPTER 4

### Review of U.V. Spectra and Molecular Orbital Calculations

#### Introduction

In this chapter the electronic spectra of benzene and its derivatives will be reviewed briefly. The purpose of this review is to outline clearly the unique position of the DEBs among the benzene derivatives studied to date.

First it will be argued qualitatively that the interaction of the  $\pi$ -electrons of the CCH groups with the benzene  $\pi$ -electrons results in appreciable differences between the U.V. spectra of the DEBs and the spectra of benzene and its derivatives with weakly perturbing substituents. These differences will be estimated quantitatively later with the help of CNDO-calculations (Jaffé and Del Bene), which include extensive configuration interaction (CI). The parametrization of the Jaffé and Del Bene CNDO/CI program will be critically examined.

#### 4.1. The U.V. Spectrum of Benzene

Benzene is the most extensively studied aromatic molecule. The excited electronic states of benzene have been the subject of many theoretical and experimental investigations. Notwithstanding this, only a few excited states have been positively identified.

#### Singlet states

The electronic energy levels of benzene have been calculated in a variety of approaches (see ref. 5, 46-49 and references therein). The simplest picture is provided by  $\pi$ -electron theory. The  $\pi$ -orbitals of benzene are completely determined by symmetry and are given below (Table 4.1), in order of decreasing energy upwards. Excitation of an electron from the bonding  $e_{1g}$  orbitals to the antibonding  $e_{2u}$  orbitals, gives the configuration

Table 4.1

The  $\pi$ -Molecular Orbitals of Benzene

$1/\sqrt{6} (\phi_1 - \phi_2 + \phi_3 - \phi_4 + \phi_5 - \phi_6)$	$b_{2g}$
$1/2 (\phi_2 - \phi_3 + \phi_5 - \phi_6)$	} $e_{2u}$
$1/\sqrt{12}(2\phi_1 - \phi_2 - \phi_3 + 2\phi_4 - \phi_5 - \phi_6)$	
$1/\sqrt{12}(2\phi_1 + \phi_2 + \phi_3 - 2\phi_4 - \phi_5 - \phi_6)$	} $e_{1g}$
$1/2 (\phi_2 + \phi_3 - \phi_5 - \phi_6)$	
$1/\sqrt{6} (\phi_1 + \phi_2 + \phi_3 + \phi_4 + \phi_5 + \phi_6)$	$a_{2u}$

$(a_{2u})^2 (e_{1g})^3 (e_{2u})^1$ . The four corresponding excited states have the symmetries  $B_{2u}$ ,  $B_{1u}$ , and  $E_{2u}$ . The energies of these states have been calculated to increase in this order<sup>(5,46-49)</sup>. The configuration  $(a_{2u})^2 (e_{1g})^3 (b_{2g})^1$  has been calculated, in a few instances<sup>(5,49)</sup>, to have an energy comparable to the above four excited states. Also,  $\sigma_{\pi}^*$  states have been predicted to lie at 5 to 6 eV above the ground state<sup>(48,50)</sup>. The singlet-singlet lower  $\pi \rightarrow \pi^*$  transitions of benzene correspond to the absorption systems at 260, 210 and 185 nm. A rotational analysis of the 260 nm absorption system has established  $B_{2u}$  symmetry for the lowest-energy excited electronic state<sup>(51)</sup>. The vibrational analysis of this 260 nm absorption system has been discussed by Herzberg<sup>(2)</sup> and King<sup>(3)</sup>. The origin band is not observed of this forbidden transition. The transition is made allowed by intensity borrowing from the  ${}^1E_{1u} + X, {}^1A_{1g}$  transition at 185 nm, mainly via a nontotally symmetric vibration (a ring deformation) with  $e_{2g}$  symmetry. The most intense bands in the spectrum can be identified as a progression in the totally symmetric ring breathing mode, in combination with one quantum of the above-mentioned  $e_{2g}$  vibration.

The 210 nm absorption is diffuse and is thus difficult to analyze. Recently, Katz et al<sup>(52)</sup> have observed some vibrational structure in this

absorption system, using solid rare gases as host matrices at very low temperatures (4-40°K). These authors have assigned the second singlet state as  $^1B_{1u}$  on the basis of the vibrational structure observed. This assignment is consistent with the result of two-photon absorption spectroscopy and thus seems settled<sup>(46)</sup>.

The 185 nm absorption system is diffuse and very intense. This system is always assumed to correspond to the  $^1E_{1u} \leftarrow X \ ^1A_{1g}$  transition because calculations predict this allowed transition in the region around 180 nm. Transitions from the ground state to singlet states with higher energies than the  $^1E_{1u}$  state, have been observed, but the assignments are uncertain<sup>(46)</sup>.

#### Triplet states

Each of the above singlet  $\pi \rightarrow \pi^*$  states is accompanied by a triplet  $\pi \rightarrow \pi^*$  state. These states increase in energy in the order  $^3B_{1u}$ ,  $^3E_{1u}$  and  $^3B_{2u}$  (5,46). The lowest-energy triplet state of benzene lies at 3.6 eV above the ground state. King and Pennington<sup>(53)</sup> and recently Gwaiz et al<sup>(54)</sup> have reviewed briefly the experimental results obtained for this state. The evidence for the assignment  $^3B_{1u}$  is very convincing. Transitions to triplet states at higher energies above the ground state have been observed in the condensed phase, but assignments are still a matter of debate<sup>(46,49)</sup>.

#### 4.2. Substituted Benzenes

The effects of chemical substitution on the electronic spectrum of benzene derivatives were studied by Sklar as early as 1942<sup>(55)</sup>, and more recently by Petrushka<sup>(56)</sup>. The changes in the spectra produced by substitution will be briefly discussed below. The excited electronic states will be indicated with their group theoretical symbols, instead of Platt's notation (Table 4.2).

Table 4.2  
Correlation Table

Platt	D <sub>6h</sub>	D <sub>2h</sub>	C <sub>2v</sub>	C <sub>2v</sub> *
<sup>1</sup> L <sub>b</sub>	<sup>1</sup> B <sub>2u</sub>	<sup>1</sup> B <sub>2u</sub>	<sup>1</sup> B <sub>2</sub>	<sup>1</sup> A <sub>1</sub>
<sup>1</sup> L <sub>a</sub>	<sup>1</sup> B <sub>1u</sub>	<sup>1</sup> B <sub>1u</sub>	<sup>1</sup> A <sub>1</sub>	<sup>1</sup> B <sub>2</sub>
<sup>1</sup> B <sub>ab</sub>	<sup>1</sup> E <sub>1u</sub>	<sup>1</sup> B <sub>1u</sub> + <sup>1</sup> B <sub>2u</sub>	<sup>1</sup> A <sub>1</sub> + <sup>1</sup> B <sub>2</sub>	<sup>1</sup> B <sub>2</sub> + <sup>1</sup> A <sub>1</sub>
<sup>3</sup> L <sub>a</sub>	<sup>3</sup> B <sub>1u</sub>	<sup>3</sup> B <sub>1u</sub>	<sup>3</sup> A <sub>1</sub>	<sup>3</sup> B <sub>2</sub>

### Monosubstituted benzenes

Numerous computations have been reported for the energies and symmetries of the lower excited electronic states of monosubstituted benzenes (ref. 57 and 58 and references therein). The most frequently studied molecules are phenol, aniline, the halogenobenzenes,  $\phi$ CN,  $\phi$ CCH and styrene. Some calculations are limited to the  $\pi$ -electrons, while others<sup>(57,58)</sup> include all valence electrons.

All calculations predict that the lowest-energy excited  $\pi \rightarrow \pi^*$  state lies at about 4.5 eV above the ground state and that this state possesses B<sub>2</sub> symmetry. The calculations also agree that the second excited  $\pi \rightarrow \pi^*$  state has A<sub>1</sub> symmetry. The energy of this state is calculated to be at 5 to 6 eV above the ground state, depending on the molecule studied and the approximations made. The third and fourth excited  $\pi \rightarrow \pi^*$  states are predicted to lie very close in energy at about 6.5 eV above the ground state. The CNDO/CI calculations have resulted in two low-lying A<sub>2</sub> states ( $\sigma \rightarrow \pi^*$  and  $\pi \rightarrow \sigma^*$ ) for  $\phi$ CCH and  $\phi$ CN<sup>(57)</sup>, but not for  $\phi$ NH<sub>2</sub> and styrene<sup>(58)</sup>. These A<sub>2</sub> states involve bonding and antibonding orbitals, that are almost entirely derived from the in-plane  $\pi$ -atomic orbitals. We have argued elsewhere<sup>(57)</sup> that these results cannot be

considered definitive and some more doubt will be raised in Section 4.4.

The predicted  $B_2$  symmetry of the lowest-energy excited state has been confirmed by rotational analysis of the spectra of about 10 monosubstituted benzenes. This topic has been reviewed recently by Ross<sup>(59)</sup> and will be discussed in detail in a later chapter. A detailed vibrational analysis of the lowest-energy singlet transition has been reported for aniline<sup>(60)</sup>, phenol<sup>(61,62)</sup>, and  $\phi CCH$ <sup>(63)</sup>. About 200 bands have been measured and assigned in the absorption systems, extending from 240 to 280 nm, of toluene<sup>(64)</sup> and  $\phi F$ <sup>(65)</sup>. Less detailed information has been reported for the vibrational structure in the lowest-energy transitions of  $\phi CN$ <sup>(66)</sup>, styrene<sup>(67)</sup>, phenylisocyanate ( $\phi NC$ )<sup>(68)</sup>, and the halobenzenes,  $\phi Br$ <sup>(69)</sup> and  $\phi Cl$ <sup>(70)</sup>. The above studies make it possible to make some general observations. The lowest-energy absorption system of monosubstituted benzenes is composed of two components. One of these, the forbidden subsystem, results from the excitation of totally symmetric vibrations in combination with one quantum of an antisymmetric vibration ( $b_2$ ). In particular a ring deformation that compares with the  $e_{2g}$  benzene vibration is very active in the forbidden component.

The allowed subsystem is formed by the excitation of totally symmetric vibrations. The most intense bands in the spectrum arise from the excitation of the two substituent sensitive C—C stretching modes and the ring breathing vibration.

The electronic origin for all the above monosubstituted benzenes is redshifted with respect to benzene. The following sequence has been found: F(5),  $CH_3$ (7), Cl(10), Br(10), OH(15),  $CH=CH_2$ (20), NC(22),  $NH_2$ (24), CN(24) and CCH(28). The quantities in brackets indicate the redshifts in nm. The intensities of the allowed and forbidden components are rather different for

the molecules at the ends of this redshift scale. For  $\phi F$ , the intensity of the forbidden part is very much weaker than the allowed subsystem, while the reverse holds for  $\phi CCH$ .

The redshifts for the second absorption system have been tabulated by Petrushka<sup>(56)</sup>. Here also, the smallest shifts are found for  $\phi F$  and  $\phi CH_3$  and the largest for styrene and  $\phi CCH$ . The calculated  $A_1$  symmetry of the second excited electronic state is supported by the observation that the intensity of the forbidden component in the first system increases with a decreasing energy separation of the first and second excited states. This is expected from perturbation theory. The first excited state possesses  $B_2$  symmetry and the forbidden component is built on one quantum of a  $b_2$  vibration. These observations can be neatly explained by the Herzberg-Teller formulation of vibronic coupling, if the second excited state is designated as  $\tilde{B}^1A_1$ . Kimura and Nagakura<sup>(71,72)</sup> have described the electronic spectra of a series of monosubstituted benzenes at wavelengths lower than 200 nm. In all spectra a very intense, broad absorption was observed around 180 nm. The high intensity of the transitions suggest a correlation with the benzene  ${}^1E_{1u} + X^1A_{1g}$  transition. The almost continuous absorption around 180 nm does not make it possible to distinguish two components, except perhaps for styrene and  $\phi CCH$ . The red shifts in the liquid phase spectra of these molecules are about 10 nm. This is an important observation because it can be used to argue that larger redshifts should occur for more strongly conjugated systems. It might then be possible to distinguish the  $\tilde{C}$  and  $\tilde{D}$  absorption systems for the DEBs.

Stark effect measurements on the rotational structure in the lowest-energy absorption system of aniline<sup>(73)</sup> and  $\phi CN$ <sup>(74)</sup>, have indicated the presence of a low-lying singlet state with  $B_1$  symmetry. The position of this

state has been calculated at 6.7 eV for  $\phi\text{NH}_2$ <sup>(58)</sup> and at 6.5 eV for  $\phi\text{CN}$ <sup>(57)</sup> with the modified Jaffé and Del Bene CNDO/CI program in these laboratories.

The lowest-energy triplet state has been observed in phosphorescence studies at low temperatures for  $\phi\text{CN}$ <sup>(75)</sup>,  $\phi\text{CCH}$ <sup>(76)</sup>,  $\phi\text{NC}$ <sup>(77)</sup>,  $\phi\text{NH}_2$ <sup>(78)</sup> and  $\phi\text{N}(\text{CH}_3)_2$ <sup>(78)</sup>. The method of photoselection has been used to determine the polarization of this transition for all molecules mentioned. The lowest-energy triplet state was found to have  $^3A_1$  symmetry for all monosubstituted benzenes studied:

#### disubstituted benzenes

The data in Table 4.2 indicate what symmetries can be expected for the lowest excited electronic states of disubstituted benzenes. Unfortunately, very little theoretical and experimental evidence is available to prove these correlations. The few calculations that have been performed are of the  $\pi$ -electron type and are limited to dihalogeno-<sup>(79)</sup> and dicyanobenzenes<sup>(80)</sup>. In these studies, the calculated energies of the excited electronic states did agree satisfactorily with the experimental values, but the symmetries of the states were not given. The experimental evidence for these symmetries will be briefly discussed below for each type of disubstituted benzene.

para-disubstitution. A rotational analysis of the electronic spectrum of five para-disubstituted benzenes has revealed  $B_2$  symmetry for the lowest-energy singlet state<sup>(59)</sup>. An analysis of the highest wavelength absorption system of para-xylene<sup>(81)</sup> and para-difluorobenzene<sup>(82)</sup> (DFB) has established that these systems are composed of an allowed and a forbidden subsystem.

The forbidden part is mainly based on excitation of one quantum of a nontotally symmetric ring deformation ( $b_2$ ) and the most intense bands in the spectrum arise from the excitation of the two totally symmetric substituent



sensitive C—C stretching modes.

The symmetry of the second excited singlet state of para-xylene has been assigned as  $\tilde{B}^1B_{1u}$  by Katz et al<sup>(83)</sup> on the basis of the observed vibrational structure at very low temperatures.

Polarization measurements of the phosphorescence spectra of para-phenylene diamine and N,N,N',N'-tetramethyl-para-phenylene diamine<sup>(78)</sup> have resulted in the assignment  $^3B_{1u}$  for the lowest-energy triplet state of these molecules.

meta-disubstitution. A rotational analysis of meta-DFB only has been carried out. The symmetry of lowest-energy singlet state was shown to be  $^1B_2$  in that study<sup>(84)</sup>. The vibrational structure in the first absorption system of meta-DFB<sup>(85)</sup> and meta-xylene<sup>(28)</sup> has been analyzed in some detail. The first absorption system for these molecules was found to consist of two components, namely a strong allowed part and a weak forbidden subsystem based on one quantum of an antisymmetric ring deformation ( $b_2$ ). The totally symmetric  $\nu(C-C)$  vibrations were found to be prominent in these spectra.

ortho-disubstitution. The symmetry of the lowest-energy singlet state of ortho-DFB has been assigned as  $A_1$  on the basis of a rotational analysis using the band contour method<sup>(84)</sup>. The vibrational structure in the first absorption system of ortho-xylene<sup>(28)</sup> and ortho-DFB<sup>(86)</sup> has been analyzed in terms of a strong allowed component and a very weak forbidden part. The most intense bands in the spectrum can be described in terms of the excitation of the two totally symmetric  $\nu(C-C)$  vibrations based on the electronic origin or in combination with one quantum of a ring deformation with  $b_2$  symmetry.

The above outline shows that a close resemblance exists between the first absorption systems of mono- and disubstituted fluoro and methylbenzenes.

For all these molecules the first absorption system contains an allowed and a forbidden component and the  $\nu(\text{C}-\text{C})$  vibrations ( $a_1$ ) play an important role. Also small redshifts have been found for the absorption systems of these molecules with respect to benzene<sup>(56)</sup>. One of the aims of this study is to find out if the first absorption system of the DEBs has some features in common with the first system of  $\phi\text{CCH}$ . Also large redshifts were found for the absorptions of  $\phi\text{CCH}$  and it was hoped that analysis of the spectra of the DEBs would shed further light on the symmetries of the second and perhaps the higher excited states of benzene and its derivatives.

In order to aid the analysis of the electronic spectrum of the DEBs, the CNDO method has been used to predict the energy and symmetry of the lower excited electronic states. The results of these calculations will be presented in the next section.

#### 4.3. CNDO/CI Calculations

The energies and symmetries of the lowest 40 excited states of the DEBs have been calculated with a modified version of the Jaffé and Del Bene CNDO/CI program. The calculations were carried out for the geometries estimated in Chapter 1. The program used has been described in detail elsewhere<sup>(57)</sup>. The Jacobi diagonalization procedure in this program was very time-consuming for the large basis set of atomic orbitals (46) of the DEBs. One iteration, for instance, required two minutes computation time. In order to examine the dependence of the calculated energies and oscillator strengths on the number of iterations, some of the previously studied molecules were re-investigated, namely  $\phi\text{CN}$ ,  $\phi\text{CCH}$  and styrene<sup>(57,58)</sup>. It was found that small differences did exist between the SCF-orbitals and the orbitals obtained after 3 or 4 iterations. The latter orbitals reproduced the reported SCF-energies

and oscillator strengths to within a few percent. This was considered to be within the limits of the calculation and therefore the transition energies and oscillator strengths for the DEBs have been calculated with the MO's obtained after four iterations. (It should be noted here that good agreement between theory and experiment was obtained in the Fifties with crude Hückel molecular orbitals and an extensive CI treatment<sup>(5)</sup>.) The results of the calculations will be presented below for each DEB.

para-DEB       $\pi \rightarrow \pi^*$  states

The calculated transition energies and oscillator strengths (f) for the lowest  $\pi \rightarrow \pi^*$  transitions are given in Table 4.3.A. Also reported is the composition of the excited electronic states in terms of single-electron promotions between the orbitals given in Table 4.3.B. The experimental values of 4.25, 4.75 and 6.5 eV given in Table 4.3.A., correspond to the wavelengths (291.97, 261 and 190 nm) of the origin band of the 292 nm system, the first strong band of the 261 nm absorption and the onset of the very intense, continuous system extending from 190 to 160 nm. The composition of the  $\pi \rightarrow \pi^*$  transitions shows that these consist almost completely of excitations between the bonding orbitals 22 and 23, and the antibonding orbitals 24 and 25 (see Table 4.3.B.). The calculation predicts that the introduction of a second CCH group in para-position in  $\phi$ CCH, results in a small redshift of the  $\tilde{A}^1B_2 \leftarrow \tilde{X}^1A_1$  transition and a large shift for the  $\tilde{B}^1A_1 \leftarrow \tilde{X}^1A_1$  transition. The  $\tilde{B}^1B_{1u}$  state of para-DEB is predicted to lie at 4.75 eV above the ground state, while the  $\tilde{B}^1B_{1u}$  state of benzene lies at 6.0 eV. The  $\tilde{B}^1B_{1u}$  state of para-DEB is predicted to have almost the same energy as the  $\tilde{A}^1B_{2u}$  state of benzene. The calculations thus predict a very large redshift for the second absorption system of para-DEB.

Table 4.3.A.

The symmetry, energy (in eV) and composition of the lowest excited  $\pi \rightarrow \pi^*$  states of para-DEB

Sym.	$\Delta E$ (eV)	Composition	Exptl. $\Delta E$ (eV)
${}^1B_{2u}$	4.30(0.004)	$0.783(23 \rightarrow 25) + 0.599(22 \rightarrow 24)$	4.25 ( $5 \times 10^{-4}$ )
${}^1B_{1u}$	4.86(0.45)	$0.985(23 \rightarrow 24)$	4.75 (0.40)
${}^1B_{2u}$	6.15(0.40)	$0.616(23 \rightarrow 25) + 0.783(22 \rightarrow 24)$	6.5 (1.5)
${}^1B_{1u}$	6.45(0.50)	$0.970(22 \rightarrow 25)$	

Table 4.3.B.

The symmetries and atomic orbital coefficients of the MO's involved in the  $\pi \rightarrow \pi^*$ ,  $\sigma \rightarrow \pi^*$  and  $\pi \rightarrow \sigma^*$  single-electron promotions of para-DEB

Sym.	No.	Descr.	Composition
$b_{3g}$	20	$\sigma_{loc}$	$0.486(\phi_7^Y - \phi_{10}^Y) + 0.425(\phi_8^Y - \phi_9^Y)$
$b_{2u}$	21	$\sigma_{loc}$	$0.506(\phi_7^Y + \phi_{10}^Y) + 0.440(\phi_8^Y + \phi_9^Y)$
$b_{1g}$	22	$\pi_{loc}$	$-0.500(\phi_2^X + \phi_3^X - \phi_5^X - \phi_6^X)$
$b_{2g}$	23	$\pi_d$	$-0.435(\phi_1^X - \phi_4^X) - 0.246(\phi_2^X + \phi_3^X - \phi_5^X - \phi_6^X) + 0.369(\phi_7^X - \phi_{10}^X) + 0.233(\phi_8^X - \phi_9^X)$
$b_{3u}$	24	$\pi^*_d$	$+0.496(\phi_1^X + \phi_4^X) - 0.267(\phi_2^X + \phi_3^X + \phi_5^X + \phi_6^X) - 0.309(\phi_7^X + \phi_{10}^X) + 0.127(\phi_8^X + \phi_9^X)$
$a_u$	25	$\pi^*_{loc}$	$+0.500(\phi_2^X - \phi_3^X + \phi_5^X - \phi_6^X)$
$b_{3g}$	27	$\sigma^*_{loc}$	$+0.483(\phi_7^Y - \phi_{10}^Y) - 0.497(\phi_8^Y - \phi_9^Y)$
$b_{2u}$	28	$\sigma^*_{loc}$	$+0.481(\phi_7^Y + \phi_{10}^Y) - 0.509(\phi_8^Y + \phi_9^Y)$

The data in Table 4.3.A. reveal that the energy difference between the A  ${}^1B_{2u}$  and B  ${}^1B_{1u}$  states is only 0.6 eV. On the basis of the Herzberg-Teller theory of vibronic coupling, it can be predicted that the B  ${}^1B_{1u}$  state

will strongly perturb the  $\tilde{A}^1B_{2u}$  state via vibrations with  $b_{3g}$  symmetry.

$\sigma \rightarrow \pi^*$  and  $\pi \rightarrow \sigma^*$  transitions

The symmetry, energy and composition of the low-lying  $^1A_u$  and  $^1B_{1g}$  states of para-DEB are given in Table 4.3.C. The transitions to these states from the ground state are forbidden,  $f = 0$  therefore. Transitions to none of these low-lying singlet states have been observed. It is interesting to note that two low-lying states of  $A_2$  symmetry were calculated for  $\phi CCH$ <sup>(57)</sup>. The introduction of another CCH group thus results in two additional low-lying states, that involve orbitals localized on the  $2p_y$  atomic orbitals of the acetylenic C-atoms. These in-plane  $\pi$ -orbitals will be discussed in detail in Section 4.4.

Table 4.3.C.

The symmetry, energy (in eV) and composition of the  $\sigma \rightarrow \pi^*$  and  $\pi \rightarrow \sigma^*$  states of para-DEB

Sym.	$\Delta E$ (eV)	Composition
$^1A_u$	3.76	$-0.570(20 \rightarrow 24) + 0.580(21 \rightarrow 26) + 0.485(20 \rightarrow 29) - 0.304(21 \rightarrow 30)$
$^1B_{1g}$	3.77	$-0.605(21 \rightarrow 24) + 0.556(20 \rightarrow 26) + 0.493(21 \rightarrow 29) - 0.286(20 \rightarrow 30)$
$^1B_{1g}$	4.75	$+0.819(23 \rightarrow 27) + 0.572(19 \rightarrow 28)$
$^1A_u$	4.80	$+0.808(23 \rightarrow 28) + 0.589(19 \rightarrow 27)$

meta-DEB  $\pi \rightarrow \pi^*$  states

The transition energies, oscillator strengths and composition of the lowest  $\pi \rightarrow \pi^*$  transitions for meta-DEB are given in Table 4.4.A. The observed energies of 4.19, 5.07 and 5.63 eV correspond to the wavelengths (295.85, 244.5 and 220.0 nm) of the origin of the 295.85 nm absorption and the first absorption

Table 4.4.A.

Symmetry, energy and composition of the lowest  $\pi \rightarrow \pi^*$  states  
of meta-DEB

Sym.	$\Delta E$ (eV)	Composition	Exptl. $\Delta E$ (eV)
${}^1B_2$	4.30(0.002)	0.736(23 $\rightarrow$ 25)-0.630(22 $\rightarrow$ 24)	4.19 ( $2 \times 10^{-4}$ )
${}^1A_1$	5.20(0.13)	0.909(23 $\rightarrow$ 24)+0.408(22 $\rightarrow$ 25)	5.07 (0.07)
${}^1B_2$	5.60(0.79)	0.630(23 $\rightarrow$ 25)+0.734(22 $\rightarrow$ 24)	5.63 (0.95)
${}^1A_1$	6.09(0.32)	0.410(23 $\rightarrow$ 24)-0.904(22 $\rightarrow$ 25)	

maxima of the 245 and 220 nm systems. The data in Table 4.4.A. reveal that the  $\pi \rightarrow \pi^*$  transitions are nearly completely determined by single-electron promotions from the bonding  $\pi$ -orbitals 22 and 23, to the antibonding  $\pi$ -orbitals 24 and 25. These molecular orbitals are given in Table 4.4.B. in terms of the atomic orbitals involved. A comparison of the  $\pi$ -MO's of benzene (Table 4.1), para-DEB (Table 4.3.B.) and meta-DEB (Table 4.4.B.) reveals that MO 24 of meta-DEB resembles closely the localized antibonding  $\pi$ -MO of para-DEB and benzene. No such correspondence is found between the bonding  $\pi$ -orbitals. The data in Table 4.4.A. show that the calculations predict correctly the transition energies of the second and third excited electronic states, as well as the ratio of the integrated intensities of these transitions. It is important to note that the introduction of a second CCH group in  $\phi$ CCH, in the meta-position, results in a minor change in the energy of the first and second excited electronic states. However, the energy of the C  ${}^1B_2$  state is appreciably lower in meta-DEB than in  $\phi$ CCH. It can be expected that the  $\tilde{A} {}^1B_2$  state will be perturbed by vibronic coupling, because of the small difference in energy between the  $\tilde{A} {}^1B_2$  and  $\tilde{B} {}^1A_1$  states and the somewhat larger difference

Table 4.4.B.

The coefficients of the 2p AO's of the MO's that are important in the single-electron promotions

that describe the  $\pi \rightarrow \pi^*$ ,  $\sigma \rightarrow \pi^*$  and  $\pi \rightarrow \sigma^*$  transition of meta-DEB

Sym.	No.	Descr.	Composition
a <sub>1</sub>	20	$\sigma_{loc}$	$-0.412(\phi_7^Y + \phi_{10}^Y) - 0.397(\phi_8^Y + \phi_9^Y) - 0.259(\phi_7^Z - \phi_{10}^Z) - 0.179(\phi_8^Z - \phi_9^Z)$
b <sub>2</sub>	21	$\sigma_{loc}$	$0.443(\phi_7^Y - \phi_{10}^Y) + 0.352(\phi_8^Y - \phi_9^Y) + 0.237(\phi_7^Z + \phi_{10}^Z) + 0.248(\phi_8^Z + \phi_9^Z)$
b <sub>1</sub>	22	$\pi_d$	$-0.586\phi_1^X - 0.259(\phi_2^X + \phi_6^X) + 0.190(\phi_3^X + \phi_5^X) + 0.424\phi_4^X + 0.239(\phi_7^X + \phi_{10}^X) + 0.220(\phi_8^X + \phi_9^X)$
a <sub>2</sub>	23	$\pi_d$	$0.362(\phi_2^X - \phi_6^X) + 0.452(\phi_3^X - \phi_5^X) - 0.335(\phi_7^X - \phi_{10}^X) - 0.226(\phi_8^X - \phi_9^X)$
a <sub>2</sub>	24	$\pi_{loc}^*$	$-0.425(\phi_2^X + \phi_6^X) - 0.481(\phi_3^X - \phi_5^X) - 0.271(\phi_7^X - \phi_{10}^X) + 0.120(\phi_8^X - \phi_9^X)$
b <sub>1</sub>	25	$\pi_d^*$	$0.600\phi_1^X - 0.291(\phi_2^X + \phi_6^X) - 0.237(\phi_3^X + \phi_5^X) + 0.512\phi_4^X + 0.197(\phi_7^X + \phi_{10}^X) - 0.096(\phi_8^X + \phi_9^X)$
a <sub>1</sub>	27	$\sigma_{loc}^*$	$0.421(\phi_7^Y + \phi_{10}^Y) - 0.436(\phi_8^Y + \phi_9^Y) + 0.240(\phi_7^Z - \phi_{10}^Z) - 0.242(\phi_8^Z - \phi_9^Z)$
b <sub>2</sub>	28	$\sigma_{loc}^*$	$-0.413(\phi_7^Y - \phi_{10}^Y) + 0.435(\phi_8^Y - \phi_9^Y) - 0.243(\phi_7^Z + \phi_{10}^Z) + 0.261(\phi_8^Z + \phi_9^Z)$

Table 4.4.C.

Symmetry, energy and composition of the  $\sigma \rightarrow \pi^*$  and  $\pi \rightarrow \sigma^*$  states of meta-DEB

Sym.	$\Delta E$ (eV)	Composition
<sup>1</sup> A <sub>2</sub>	3.77	$-0.481(20+24) - 0.382(21+25) - 0.529(21+26) + 0.497(20+29) - 0.298(21+30)$
<sup>1</sup> B <sub>1</sub>	3.78	$-0.530(21+24) - 0.324(20+25) + 0.518(21+29) - 0.504(20+26) - 0.285(20+30)$
<sup>1</sup> A <sub>2</sub>	4.91	$+0.741(23+27) + 0.514(22+28) + 0.429(19+28)$
<sup>1</sup> B <sub>1</sub>	4.92	$+0.716(23+28) + 0.541(22+27) + 0.439(19+27)$

between the  $\tilde{A}^1B_2$  and  $\tilde{C}^1B_2$  states. It can however not be predicted which of the higher energy states will perturb the  $\tilde{A}^1B_2$  state. Although the  $\tilde{B}^1A_1 \leftarrow \tilde{X}^1A_1$  transition energy is smaller than that of the  $\tilde{C}^1B_2 \leftarrow \tilde{X}^1A_1$  transition, the integrated intensity of the first transition is only one-fifth of that of the second.

$\sigma \rightarrow \pi^*$  and  $\pi \rightarrow \sigma^*$  states

Four low-lying singlet states have been predicted for the meta-DEB (see Table 4.4.C). A comparison of the data in Table 4.3.C. and 4.4.C. shows a very close correspondence between the  $\sigma \rightarrow \pi^*$  and  $\pi \rightarrow \sigma^*$  states of para- and meta-DEB. Transitions to none of these states have been observed.

ortho-DEB  $\pi \rightarrow \pi^*$  states

The results of the calculations for ortho-DEB have been presented in Table 4.5.A.1. These data show that the essentially  $\pi \rightarrow \pi^*$  transitions have a contribution from  $\sigma \rightarrow \sigma^*$  single-electron promotions. This contribution is underlined in Table 4.5.A.1. and it is seen to be negligible only for the  $\tilde{A}^1A_1$  state. The transition energies for the pure  $\pi \rightarrow \pi^*$  states of para- and meta-DEB were calculated at slightly lower energies than observed. For ortho-DEB, however, the energies of the second and third excited electronic states are predicted to have higher energies than the experimental values. The ratio of the calculated f's for the transitions to the  $\tilde{B}^1B_2$  and  $\tilde{C}^1A_1$  states, agree with the estimated ratio of the experimental integrated intensities.

It was found, in the previously reported calculations on  $\phi CCH$ , that a  $\sigma \rightarrow \sigma^*$  single-electron promotion (8.78 eV) was mixed with the totally symmetric  $\pi \rightarrow \pi^*$  states in the CI treatment. The corresponding state for  $\phi CN$  was initially not among the 30 lowest single-electron promotions. When this state (9.59 eV) was later included in the CI calculation, the energies of the lower



Table 4.5.A.1.

Symmetry, energy and composition of the lower  $\pi \rightarrow \pi^*$  states  
of ortho-DEB (40 excited states)

Sym.	$\Delta E$ (eV)	Composition	Exptl. $\Delta E$ (eV)
$^1A_1$	4.29(0.003)	0.744(23 $\rightarrow$ 25) - 0.625(22 $\rightarrow$ 24) - <u>0.017(21<math>\rightarrow</math>28)</u>	4.15 ( $10^{-4}$ )
$^1B_2$	4.69(0.10)	0.868(23 $\rightarrow$ 24) + 0.324(21 $\rightarrow$ 26)	4.74 (0.09)
$^1A_1$	5.40(0.40)	0.504(23 $\rightarrow$ 25) + 0.630(22 $\rightarrow$ 24) - 0.317(23 $\rightarrow$ 29) - <u>0.417(21<math>\rightarrow</math>28)</u>	5.63 (0.71)
$^1B_2$	5.97(0.03)	0.680(22 $\rightarrow$ 25) + 0.458(23 $\rightarrow$ 27) - <u>0.371(21<math>\rightarrow</math>26)</u>	
$^1B_2$	6.14(0.31)	0.473(23 $\rightarrow$ 24) - 0.670(22 $\rightarrow$ 25) + 0.313(23 $\rightarrow$ 27) - <u>0.374(21<math>\rightarrow</math>26)</u>	
$^1A_1$	6.41(0.26)	0.383(23 $\rightarrow$ 25) + 0.419(22 $\rightarrow$ 24) + 0.598(23 $\rightarrow$ 29) + <u>0.478(21<math>\rightarrow</math>28)</u>	

Table 4.5.A.2.

Symmetry, energy and composition of the lower  $\pi \rightarrow \pi^*$  states  
of ortho-DEB (38 excited states).

Sym.	$\Delta E$ (eV)	Composition	Expt. $\Delta E$ (eV)
$^1A_1$	4.29(0.002)	0.740(23 $\rightarrow$ 25) - 0.631(22 $\rightarrow$ 24)	4.15 ( $10^{-4}$ )
$^1B_2$	4.96(0.17)	0.954(23 $\rightarrow$ 24) + 0.289(22 $\rightarrow$ 25)	4.74 (0.09)
$^1A_1$	5.76(0.77)	0.645(23 $\rightarrow$ 25) + 0.753(22 $\rightarrow$ 24)	5.63 (0.71)
$^1B_2$	6.05(0.28)	-0.271(23 $\rightarrow$ 24) + 0.938(22 $\rightarrow$ 25)	
$^1B_2$	6.91(0.003)	0.969(23 $\rightarrow$ 27)	
$^1A_1$	7.15(0.03)	0.337(22 $\rightarrow$ 27) - 0.699(23 $\rightarrow$ 29) + 0.583(19 $\rightarrow$ 24)	

$A_1$  states were only slightly affected. In this study, contributions by  $\sigma \rightarrow \sigma^*$  single-electron promotions are found only for ortho-DEB. Instead of including these promotions in the CI treatment of para- and meta-DEB, it was decided to exclude these  $\sigma \rightarrow \sigma^*$  excitations from the  $A_1$  and  $B_2$   $\pi \rightarrow \pi^*$  promotions for ortho-DEB. The CI calculation was repeated for ortho-DEB with 38 excited

Table 4.5.B.

The coefficients of the 2p, AO's of the MO's that are important in the single-electron promotions

that describe the  $\pi \rightarrow \pi^*$ ,  $\sigma \rightarrow \pi^*$  and  $\pi \rightarrow \sigma^*$  transitions of ortho-DEB

Sym.	No.	Descr.	Composition
a <sub>1</sub>	20	$\sigma_{loc}$	$0.397(\phi_7^Y - \phi_1^Y) + 0.369(\phi_8^Y - \phi_9^Y) - 0.250(\phi_7^Z + \phi_{10}^Z) - 0.178(\phi_8^Z + \phi_9^Z)$
b <sub>2</sub>	21	$\sigma_{loc}$	$-0.459(\phi_7^Y + \phi_1^Y) - 0.378(\phi_8^Y + \phi_9^Y) + 0.246(\phi_7^Z - \phi_{10}^Z) + 0.250(\phi_8^Z - \phi_9^Z)$
a <sub>2</sub>	22	$\pi_d$	$-0.204(\phi_1^X - \phi_2^X) + 0.528(\phi_3^X - \phi_6^X) + 0.275(\phi_4^X - \phi_5^X) + 0.254(\phi_7^X - \phi_{10}^X) + 0.198(\phi_8^X - \phi_9^X)$
b <sub>1</sub>	23	$\pi_d$	$-0.421(\phi_1^X + \phi_2^X) - 0.078(\phi_3^X + \phi_6^X) + 0.353(\phi_4^X + \phi_5^X) + 0.365(\phi_7^X + \phi_{10}^X) + 0.241(\phi_8^X + \phi_9^X)$
a <sub>2</sub>	24	$\pi_d^*$	$+0.473(\phi_1^X - \phi_2^X) + 0.064(\phi_3^X - \phi_6^X) + 0.412(\phi_4^X - \phi_5^X) - 0.295(\phi_7^X - \phi_{10}^X) + 0.122(\phi_8^X - \phi_9^X)$
b <sub>1</sub>	25	$\pi_d^*$	$0.248(\phi_1^X + \phi_2^X) - 0.563(\phi_3^X + \phi_6^X) + 0.291(\phi_4^X + \phi_5^X) - 0.170(\phi_7^X + \phi_{10}^X) + 0.082(\phi_8^X + \phi_9^X)$
a <sub>2</sub>	26	$\sigma_{loc}^*$	$-0.431(\phi_7^Y - \phi_1^Y) + 0.423(\phi_8^Y - \phi_9^Y) + 0.243(\phi_7^Z + \phi_{10}^Z) - 0.238(\phi_8^Z + \phi_9^Z)$
b <sub>1</sub>	28	$\sigma_{loc}^*$	$0.402(\phi_7^Y + \phi_1^Y) - 0.446(\phi_8^Y + \phi_9^Y) - 0.239(\phi_7^Z - \phi_{10}^Z) + 0.268(\phi_8^Z - \phi_9^Z)$

Table 4.5.C.

Symmetry, energy and composition of the  $\sigma \rightarrow \pi^*$  and  $\pi \rightarrow \sigma^*$  states of ortho-DEB

Sym.	$\Delta E$ (eV)	Composition
<sup>1</sup> A <sub>2</sub>	3.77	$-0.481(20+24) - 0.382(21+25) - 0.529(21+26) + 0.497(20+29) - 0.298(21+30)$
<sup>1</sup> B <sub>1</sub>	3.78	$-0.530(21+24) - 0.325(20+25) + 0.518(21+29) - 0.504(20+26) - 0.285(20+30)$
<sup>1</sup> A <sub>2</sub>	4.91	$+0.741(23+27) + 0.514(22+28) + 0.429(19+28)$
<sup>1</sup> B <sub>1</sub>	4.92	$+0.716(23+28) + 0.541(22+27) + 0.439(19+27)$

states and using the same MO's as employed in the earlier CI calculation (see Table 4.5.B.). The result is reported in Table 4.5.A.2.

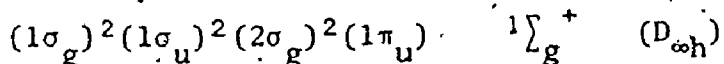
A comparison of the data in Tables 4.5.A.1. and 4.5.A.2. shows the same ordering of the excited states for both calculations. It is also seen that the ratio of the calculated f's for the  $\tilde{B}^1B_2 \leftarrow \tilde{X}^1A_1$  and  $\tilde{C}^1A_1 \leftarrow \tilde{X}^1A_1$  transitions are in agreement with the estimated experimental ratio, and that the calculated transition energies are now slightly lower in energy than the experimental values. A comparison of the data in Table 4.4.A. and 4.5.A.2. shows a large degree of correspondence between the pure  $\pi \rightarrow \pi^*$  transitions of meta- and ortho-DEB.

The above considerations do not make it possible to decide on the significance of the low-lying  $\sigma \rightarrow \sigma^*$  single-electron promotions that involve mainly the in-plane  $\pi$ -orbitals of the CCH group. This topic will be considered in more detail in Section 4.4. These in-plane  $\pi$ -orbitals play a prominent role in the calculated four low-lying  $\pi \rightarrow \sigma^*$  and  $\sigma \rightarrow \pi^*$  states. The results of the calculations for these states of ortho-DEB are given in Table 4.5.B. and it is seen that these low-lying states are very nearly identical for all three DEBs.

#### 4.4. The CNDO Parametrization of Jaffé and Del Bene

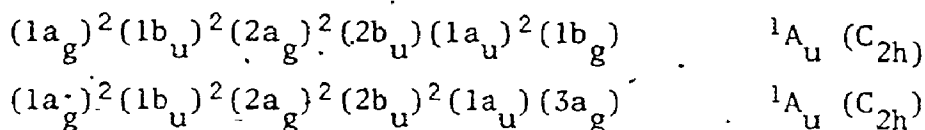
In the previous section, the question has been raised how reliable the Jaffé-Del Bene CNDO program (JDB) calculates in the in-plane  $\pi$ -orbitals of the acetylenic group. In order to further explore this, the molecules acetylene ( $H-C\equiv C-H$ ) and hydrogencyanide ( $H-C\equiv N$ ) will be considered in detail.

Acetylene is linear in the ground state, but is trans-bent in its lowest excited state<sup>(87)</sup>. The ground state configuration is given by<sup>(88)</sup>



Promotion of an electron from a  $\pi_u$  to a  $\pi_g$  orbital results in the following

configurations for the bent molecule.



The first configuration corresponds to the degenerate  ${}^1\Delta_u$  state for the linear molecule and the second to the  ${}^1\Sigma_u^+$  state ( $\pi \rightarrow \sigma^*$ ). The latter is usually accepted for the observed  ${}^1A_u$  state at 5.2 eV, on the basis of Walsh's diagrams (2,87,88). The calculations were carried out for linear acetylene with ground state bond lengths. Self-consistency was reached after 21 iterations and the CI treatment included all (25) possible single-electron promotions. The energy of the  ${}^1\Sigma_u^+$  state was calculated at 4.0 eV above the ground state. Experimentally this state has been observed at 5.2 eV (87). The calculations were next repeated for slightly distorted structures. Two trans-bent geometries were considered in which the C—H bonds made an angle of 5° and 10° respectively with the axis through the triple bond. The energy of the  ${}^1A_u$  state corresponding to the  ${}^1\Sigma_u^+$  state, was found at 4.0 eV for both structures. When the calculations were performed for acetylene with its known trans excited state geometry, the energy of this  ${}^1A_u$  state was predicted as low as 2.1 eV. The JDB program does thus not calculate a reasonable energy for the lowest excited state of acetylene.

The  ${}^1\Delta_u$  state was calculated to lie at 4.0 eV also for linear acetylene with its ground state bond lengths. The degeneracy of these states was lifted for the slightly distorted molecules. The splitting of the two components was however found to be smaller than 0.1 eV. A similar calculation on the linear molecule HCN resulted in three states at 4.8 eV, when the ground state geometry was used. The CI treatment, using self-consistent MO's, included all possible single-electron promotions. This result is very similar to the data discussed

for acetylene. The agreement with experiment is very poor. The first absorption system of HCN has been observed at 180 nm ( $\approx 6.8$  eV)<sup>(2)</sup>.

The results for  $C_2H_2$  and HCN indicate that something is basically wrong with the JDB parametrization for compounds with substituents containing triple bonds. The JDB parametrization<sup>(47)</sup> differs in two respects from the CNDO/2 parameters suggested by Pople and Sègal<sup>(89)</sup>.

1. The electron-repulsion integrals in the JDB program are calculated with the extrapolation methods employed extensively in  $\pi$ -electron type calculations. The one-center integrals are chosen semi-empirically following Pariser and Parr<sup>(90)</sup>.

2. Two types of bond integrals are distinguished, namely

$$\beta_{\mu\nu}^{\sigma} = \frac{1}{2} (\beta_A^{\sigma} + \beta_B^{\sigma}) S_{\mu\nu} \quad [4.1a]$$

$$\beta_{\mu\nu}^{\pi} = \frac{\kappa}{2} (\beta_A^{\pi} + \beta_B^{\pi}) S_{\mu\nu} \quad [4.1b]$$

Equation 1a determines the bond integral for the  $\sigma$  bonds, between the nuclei A and B. The atomic orbitals  $\mu$  and  $\nu$  of these atoms have an overlap integral equal to  $S_{\mu\nu}$ . The values  $\beta^{\sigma}$  are given by Jaffé and Del Bene<sup>(47)</sup> for H(-12 eV) C(-17 eV) and N(-26 eV). The bond integral for the  $\pi$ -bond between the nuclei A and B is given by an expression similar to the one for the  $\sigma$ -bond, but is multiplied by a scale factor  $\kappa$ . It was found by Jaffé and Del Bene<sup>(47)</sup> that the best value of  $\kappa = 0.585$ . The overlap of the acetylenic 2p functions has been calculated as 0.335 for a bond length of 1.205 Å using overlap tables<sup>(91)</sup>. With the help of the above figures it is easily found that

$$\beta_{C\equiv C}^{\sigma} = -5.695 \text{ eV} \quad \text{and} \quad \beta_{C\equiv C}^{\pi} = -3.335 \text{ eV}$$

Pople and Santry<sup>(92)</sup> have suggested the following formula for the bond integral:

$$\beta = -10.0 S \quad [4.2]$$

According to this expression, the bond integral for the acetylenic bond equals -3.35 eV. This value corresponds closely to the  $\beta_{C\equiv C}^{\pi} = -3.335$  eV used by Jaffé and Del Bene. The JDB value for  $\beta_{C\equiv C}^{\sigma}$  is grossly over-estimated according to equation [4.2]. Pariser and Parr<sup>(90)</sup> have proposed

$$\beta = -2517.5 \exp(-5.0072 * r) \quad [4.3]$$

Substitution of  $r = 1.205$  Å results in  $\beta = -6.034$  eV, for the acetylenic  $\pi$ -bond. This value compares very well with the  $\beta^{\sigma}$  value for the acetylenic bond suggested by JDB. It is very important to realize that Pariser and Parr arrived at equation [4.3] by fitting the values of the bond integrals--that predicted correctly the position of the lowest-energy excited state for ethylene and benzene--to the expression  $\beta = -A \exp(-Br)$ . Equation [4.3] is thus not calibrated for triple bonds!

The poor results obtained above for acetylene and hydrogen cyanide indicate that the  $\beta^{\sigma}$  bond integrals for the  $C\equiv C$  and  $C\equiv N$  bonds are over-estimated in the JDB parametrization scheme. Therefore,  $\sigma$  and  $\sigma^*$  MO's, localized on the in-plane  $\pi$ -orbitals of the CCH group, in the planar DEBs, cannot be relied upon. The calculated  $\sigma_{loc} \rightarrow \pi^*$  and  $\pi \rightarrow \sigma_{loc}^*$  states reported in Tables 4.3.C., 4.4.C. and 4.5.C. are thus very questionable.

The  $\sigma_{loc} \rightarrow \sigma_{loc}^*$  single-electron promotions contributing to the CI states of  $A_1$  and  $B_2$  symmetry for ortho-DEB are also doubtful. The results of the CI treatment with 38 excited states is preferred over the calculations with 40 excited states because the former does not contain contributions by the suspect in-plane  $\pi$ -orbitals. The pure  $\pi \rightarrow \pi^*$  transitions tabulated for para-, meta-, and ortho-DEB in Tables 4.3.A., 4.4.A. and 4.5.A.2. can thus be

relied upon. It should be noted that the JDB CNDO calculations are thus reduced to a pure  $\pi$ -electron type calculation for the DEBs, with Pariser-Parr bond integrals and Mataga-Nishimoto repulsion integrals.

Finally, the results of the earlier reported calculations on  $\phi$ CCH and  $\phi$ CN will be examined in the light of the above findings.

It has been discussed previously<sup>(57)</sup>, that the  $\sigma \rightarrow \sigma^*$  single-electron promotion for  $\phi$ CN was initially not included among the 30 lowest excitations in the CI treatment. When this state was included, the energies of the lowest two totally symmetric  $\pi \rightarrow \pi^*$  states were hardly affected and thus require no further comment. The two states of  $A_2$  symmetry at 5.0 eV were seen to involve mainly the MO's localized on the in-plane  $\pi$ -orbitals of the CN group. These calculated low-lying  $A_2$  states are thus doubtful. The same can be said about the low-lying states of  $A_2$  symmetry for  $\phi$ CCH (at 3.8 and 4.1 eV), because these depend nearly exclusively on excitations involving the in-plane  $\pi$ -orbitals of the CCH group.

An examination of the results obtained for the totally symmetric states of  $\phi$ CCH<sup>(57)</sup>, revealed the presence of a  $\sigma \rightarrow \sigma^*$  single-electron promotion (8.78 eV). The energy and composition of the lower  $A_1$  states of  $\phi$ CCH are detailed in Table 4.6.A.<sup>(57)</sup> The contribution by the  $\sigma \rightarrow \sigma^*$  excitation is underlined and it is seen that the transition at 4.69 and 5.69 eV involve a considerable amount of this suspect  $\sigma \rightarrow \sigma^*$  single-electron promotion.

The CI calculation of the transition energies was repeated with the same SCF-orbitals as used in Ref. 57, but without the  $\sigma \rightarrow \sigma^*$  promotion. The results are collected in Table 4.6.B. A comparison of the data in Tables 4.6.A. and 4.6.B. reveals a marked difference in the energies of the lowest-lying states of  $A_1$  symmetry. The data in Table 4.6.B. show a close corres-

Table 4.6.A.

Energy and composition of the lower  $A_1$  excited states of  $\phi$ CCH

$\Delta E$ (eV)	Composition
4.69(0.07)	$0.704(19 \rightarrow 20) - 0.382(19 \rightarrow 22) - 0.235(16 \rightarrow 20) + \underline{0.509(17 \rightarrow 23)}$
5.79(0.07)	$0.600(19 \rightarrow 20) + 0.433(18 \rightarrow 21) + 0.439(19 \rightarrow 22) + 0.223(16 \rightarrow 20) + 0.286(19 \rightarrow 24)$ $\underline{-0.358(17 \rightarrow 23)}$
6.56(0.58)	$0.348(19 \rightarrow 20) - 0.884(18 \rightarrow 21) + 0.145(19 \rightarrow 22) + 0.202(19 \rightarrow 24) - \underline{0.180(17 \rightarrow 23)}$

Table 4.6.B.

Energy and composition of the lower  $A_1$  excited states of  $\phi$ CCH,  
with the exclusion of the  $\sigma \rightarrow \sigma^*$  excitation.

$\Delta E$ (eV)	Composition
5.33(0.26)	$0.965(19 \rightarrow 20) + 0.248(18 \rightarrow 21)$
6.41(0.47)	$-0.930(18 \rightarrow 21)$
7.25(0.002)	$0.936(19 \rightarrow 22)$

pendence to the electronic energies, calculated in  $\pi$ -electron approximation by King and So<sup>(63)</sup>. In this study the bond integral for the triple bond was obtained from

$$\beta = -\frac{3.143}{r} \quad [4.4]$$

as -2.609 eV. This compares favourably with the values calculated from equations [4.1b] and [4.2].

### Conclusions

The interaction of the  $\pi$ -electrons of benzene with those in the CCH groups has been predicted to result in large redshifts of the U.V. absorptions of the DEBs with respect to the benzene absorption systems. This prediction



is based on a comparison of the spectra of benzene and its derivatives and on the CNDO/CI calculations performed. It is shown that the Jaffé and Del Bene parametrization scheme can be used confidently to calculate the transition energies of the pure  $\pi \rightarrow \pi^*$  states of the DEBs. However, not too much significance must be attached to the energies calculated for states that are composed of single-electron promotions involving in-plane  $\pi$ -orbitals.

## CHAPTER 5

### Analysis of the Electronic Spectrum

#### Introduction

Vibrational analyses of the electronic absorption systems of the three DEBs are presented in this chapter. Unfortunately, the first absorption systems of the DEBs yield very little information. The spectra will be analyzed by analogy to other substituted benzenes, by using the results of the calculations in the previous chapter and the band contour method, which is detailed in the next chapter.

#### 5.1. Analysis of the Electronic Spectrum of para-DEB

##### A. General appearance of the spectrum under low resolution

The U.V. absorption profile for para- $h_6$ , presented in Fig. 5.1, was obtained with a Cary Model 14 spectrophotometer. The two absorption systems in Fig. 5.1 will be called hereafter the 292 and 261 nm systems. The vacuum U.V. spectrum of para- $h_6$ , recorded on a McPherson Model 225 1 meter double beam scanning monochromator, is depicted in Fig. 5.2.

The oscillator strengths of the 292 and 261 nm systems have been determined from the solution spectrum of para- $h_6$  in methanol. By means of the equations given in reference 109, the oscillator strengths of the discrete 292 nm system was calculated as  $f = 3 \times 10^{-4}$  and  $f = 0.40$  for the 261 nm system. The oscillator strength of the absorption hump, extending from 185 to 150 nm was determined as  $f = 1.5$ . According to the calculations presented in Chapter 4 (Table 4.3.A.), this featureless continuum should contain the  $\tilde{C}^1B_{2u} + \tilde{X}^1A_g$  and the  $\tilde{D}^1B_{1u} + \tilde{X}^1A_g$  transitions. This prediction is consistent with the experimental oscillator strength of 1.5. The energies and oscillator strengths of the 292 and 261 nm systems are in excellent agreement with the results of the CNDO calculations. Therefore, the 292 and 261 nm systems are assigned,

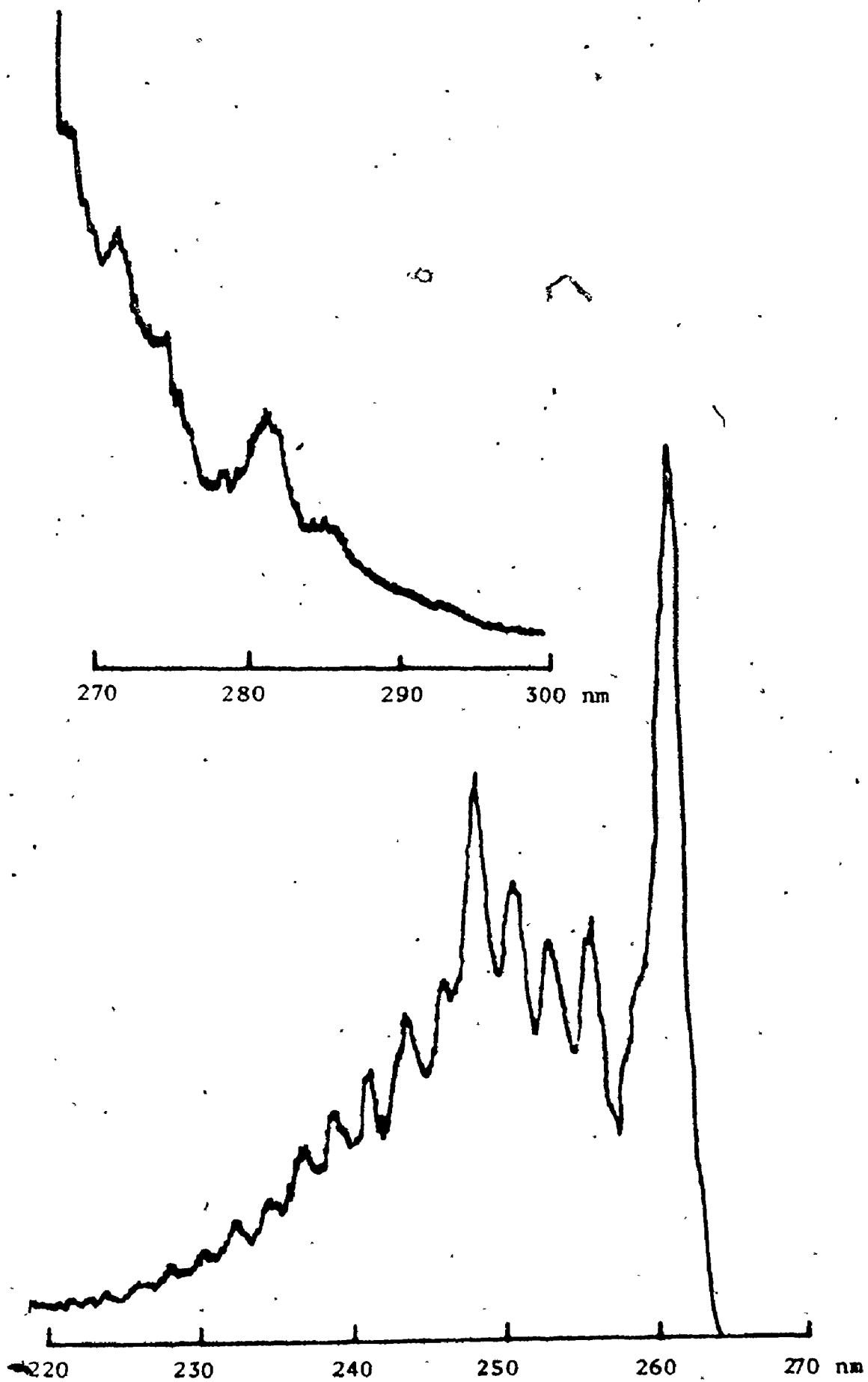


Fig. 5.1. The U.V. absorption systems of para-h<sub>6</sub>.

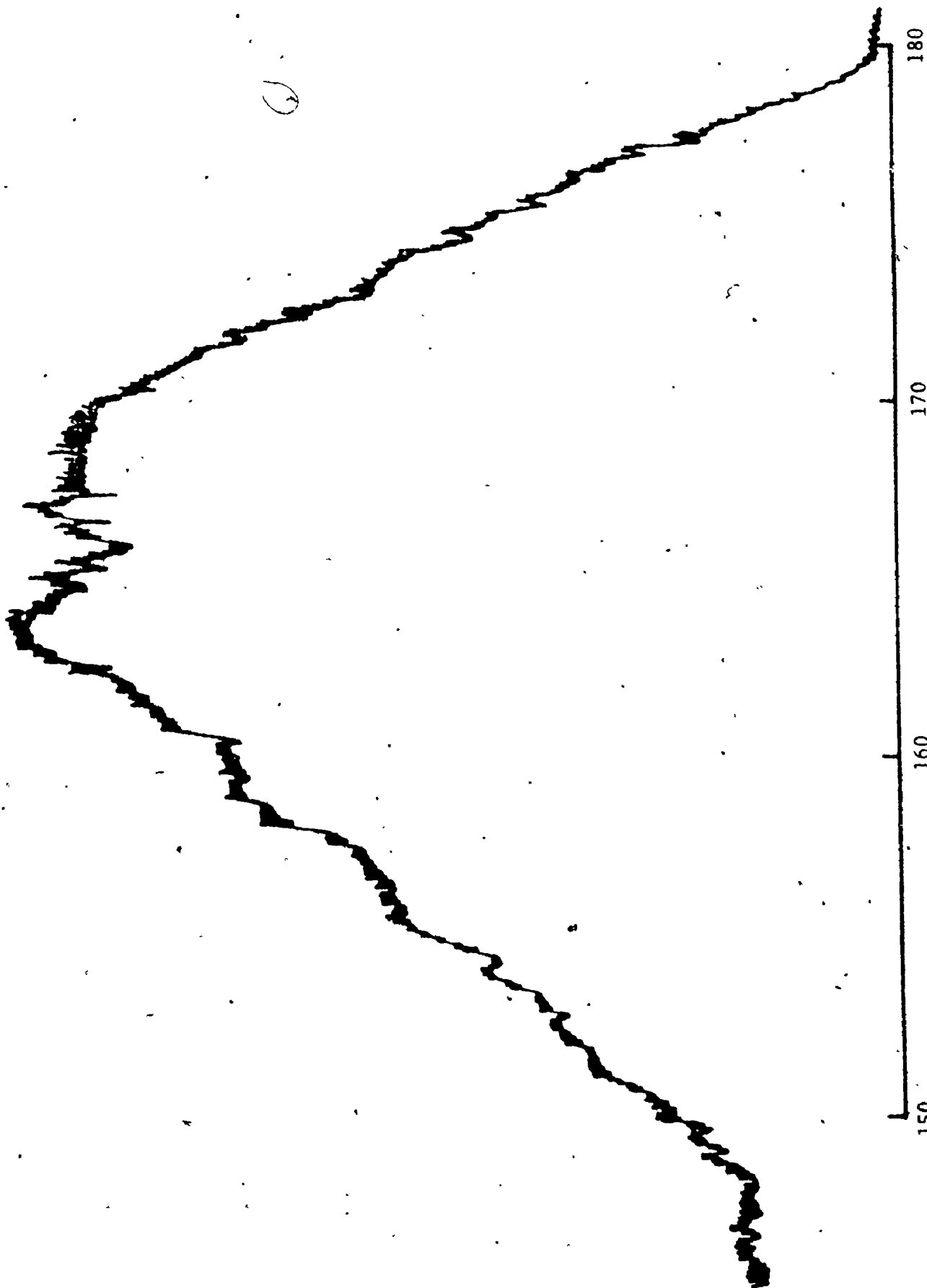


Fig. 5.2.A. The vacuum U.V. absorption systems of para-h<sub>6</sub> from 180 to 150 nm.

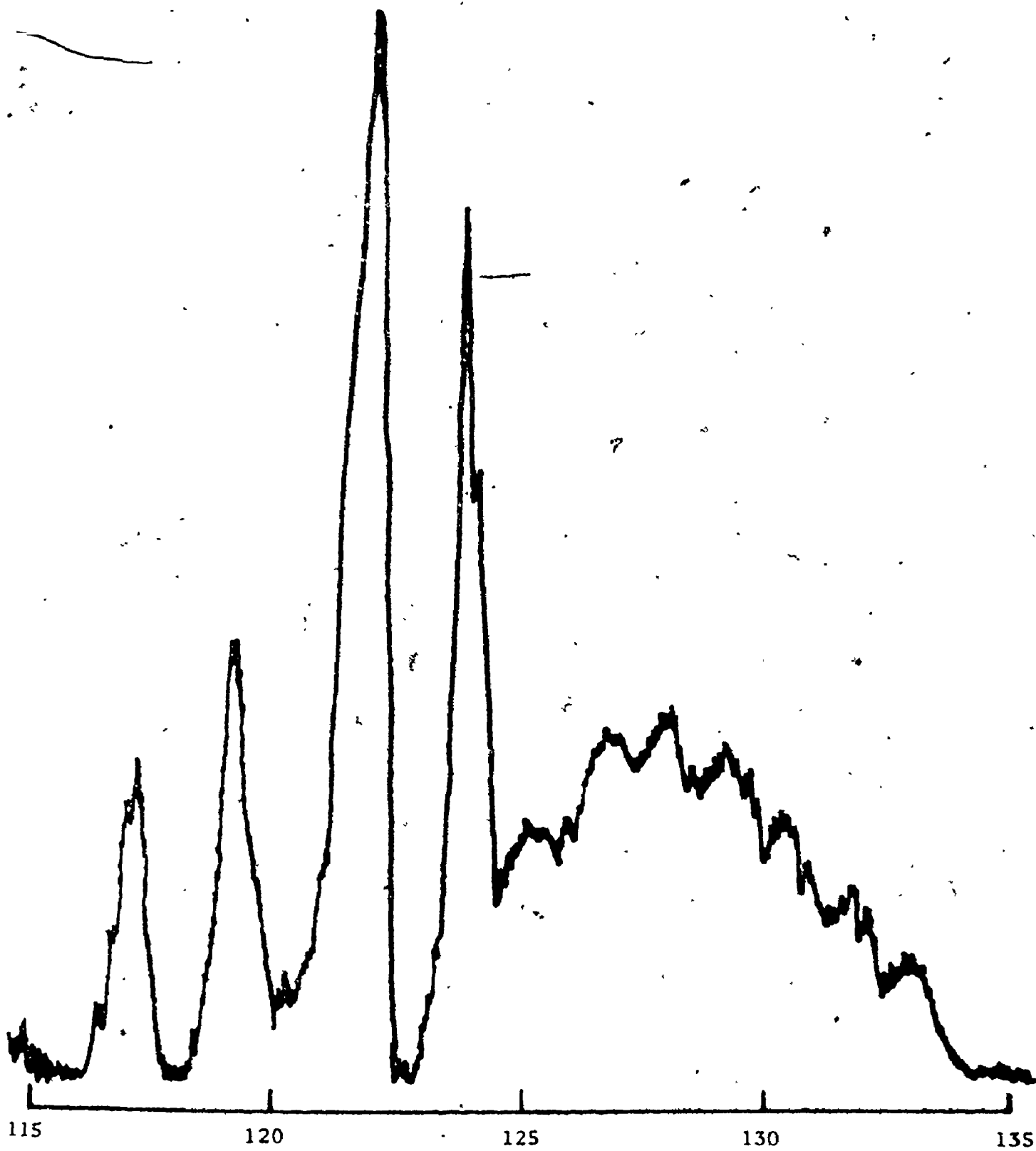


Fig. 5.2.B. The vacuum U.V. spectrum of para-h<sub>6</sub> in the region from 135 to 115 nm.

tentatively at this point, to the  $\tilde{A} \ ^1B_{2u} + \tilde{X} \ ^1A_g$  and  $\tilde{B} \ ^1B_{1u} + \tilde{X} \ ^1A_g$  transition, respectively.

No attempt has been made to analyze the region below 150 nm.

#### B. The 261 nm system

The  $\tilde{B} \ ^1B_{1u} + \tilde{X} \ ^1A_g$  transition shows vibrational structure. The vibrational bands are diffuse, even under high resolution, and have a half width of about  $100 \text{ cm}^{-1}$ . This diffuseness can be ascribed to the (pre)dissociation of para-DEB preceding polymerization.

However, the molecules  $\phi F$  and  $\phi CH_3$  for instance do not undergo photochemical decomposition, but the  $\tilde{B}$  systems for these molecules are featureless humps. Some vibrational structure can be distinguished in the  $\tilde{B}$  systems of the molecules  $\phi CH=CH_2$ ,  $\phi CN$  and  $\phi CCH$  and unusual detailed structure is found in the 261 nm system of para-DEB.

It was seen in the previous chapter that the  $\tilde{B}$  systems of  $\phi F$  and  $\phi CH_3$  are red shifted very little ( $<10 \text{ nm}$ ) with respect to the 205 nm system of benzene, while appreciable red shifts ( $\approx 30 \text{ nm}$ ) occur for the above conjugated monosubstituted benzenes. The largest red shift is found for para-DEB. There is thus a correlation between the red shift and the diffuseness of the vibrational structure in the  $\tilde{B}$  system. Since the position of the first absorption system is only slightly affected by different substituents, a correlation also exists between the diffuseness of the  $\tilde{B}$  system and the energy gap between the  $\tilde{A}$  and  $\tilde{B}$  systems. This observation suggests that the diffuseness in the second absorption system of benzene derivatives is caused by predissociation by vibrations<sup>(2)</sup>. This means that the degree of diffuseness of the vibrational bands in the  $\tilde{B}$  system is determined by the density of the vibronic levels in the first system overlapping the vibronic bands in the  $\tilde{B}$  system. This density/diffuseness increases with an increasing gap between the first and second absorption system

and also with deuteration because of the drop in frequency of the fundamentals.

With the help of the above argument, it can be rationalized that the 261 nm system of para-DEB shows a decrease in the relative intensity and in the number of vibrational bands at the blue end of the absorption system upon deuteration of the CCH groups and upon ring deuteration.

The relative intensities and the frequencies of the absorption maxima of the 261 nm system are reported in Table 5.1 for para- $h_6$  and its deuterated isotopes. The accuracy in the measured frequencies is  $\pm 15 \text{ cm}^{-1}$ .

A study of the intensities of the vibrational bands at lower temperatures showed a decrease in the relative intensity of all bands with respect to the intense, lowest-frequency band. This band is assigned as the electronic origin band of the 261 nm system.

In the spectra of all isotopes, a progression--to higher frequencies-- in  $770 \text{ cm}^{-1}$  is based on the origin band and on the intense band at 40320/40210/40340/40320  $\text{cm}^{-1}$  for para- $h_6$ /para- $d_2$ /para- $d_4$ /para- $d_6$ . The latter band is at 2010/1920/1990/1930  $\text{cm}^{-1}$  to the blue of the origin band. A similar frequency interval of about  $2000 \text{ cm}^{-1}$  has been observed also in the 220 nm system of meta- $h_6$ , the 245 and 220 nm systems of ortho- $h_6$  and in the 279 nm absorption of  $C_6H_5CCH$  and  $C_6D_5CCH$ <sup>(63)</sup>. This upper state frequency of about  $2000 \text{ cm}^{-1}$  in the spectra of the DEBs is assigned to the totally symmetric triple bond stretching mode, by analogy to  $\phi CCH$ . The ground state frequency of this fundamental is  $2108 \text{ cm}^{-1}$  for all CCH isotopes of the three isomeric DEBs. The above upper state interval is decreased by about  $90 \text{ cm}^{-1}$  in the spectra of the CCD isotopes of  $\phi CCH$  and the three DEBs. The drop in the frequency of the  $\nu(C\equiv C)$  vibration in the ground state is about  $120 \text{ cm}^{-1}$  for all above molecules. The difference in frequency of this  $\nu(C\equiv C)$  mode between ground and upper state is very small compared to the drop of almost  $500 \text{ cm}^{-1}$  between the ground and first excited

Table 5.1

Wavenumbers (in  $\text{cm}^{-1}$ ) and relative intensities of the vibrational bands  
in the diffuse 261 nm absorption system of para-DEB

para-h <sub>6</sub>		para-d <sub>2</sub>		para-d <sub>4</sub>		para-d <sub>6</sub>		Assignment
38310	vs	38290	vs	38360	vs	38390	vs	0 <sup>0</sup>
38680	sh			38680	sh	38650	sh	8 <sup>1</sup> <sub>0</sub>
39070	s	39060	s	39140	s	39150	s	7 <sup>1</sup> <sub>0</sub>
39460	s	39440	s	39580	vw	39600	vvw	5 <sup>1</sup> <sub>0</sub>
39840	s	39850	s	39920	s	39920	s	7 <sup>2</sup> <sub>0</sub>
40320	vs	40210	vs	40340	s	40320	s	3 <sup>1</sup> <sub>0</sub>
40620	s	40600	s	40615	vw	40680	vw	7 <sup>3</sup> <sub>0</sub>
41070	s	40980	m	41110	w	41070	vw	3 <sup>1</sup> <sub>0</sub> 7 <sup>1</sup> <sub>0</sub>
41410	m	41390	w	41470	vw	41530	vvw	7 <sup>4</sup> <sub>0</sub>
41860	m	41750	w	41910	vw			3 <sup>1</sup> <sub>0</sub> 7 <sup>2</sup> <sub>0</sub>
42200	w	42160	vw	42280	vvw			7 <sup>5</sup> <sub>0</sub>
42610	w	42550	vw					3 <sup>1</sup> <sub>0</sub> 7 <sup>3</sup> <sub>0</sub>
43010	vw							7 <sup>6</sup> <sub>0</sub>
43480	vw							3 <sup>1</sup> <sub>0</sub> 7 <sup>4</sup> <sub>0</sub>
43820	vw							7 <sup>7</sup> <sub>0</sub>



singlet state in acetylene<sup>(63)</sup>. This indicates that the acetylenic groups are only slightly involved in the electronic excitation.

The frequency of the above progression was found as  $770 \pm 30 \text{ cm}^{-1}$  in the spectra of the four isotopes of para-DEB. This frequency could have dropped 30 to  $40 \text{ cm}^{-1}$  on deuteration, but the accuracy was not sufficient to measure this. In the 292 nm system (see below) the following upper state intervals have been measured  $756.8/761.5/723.5/717.8 \text{ cm}^{-1}$  for para-h<sub>6</sub>/para-d<sub>2</sub>/para-d<sub>4</sub>/para-d<sub>6</sub>. Approximately identical upper state spacings in the U.V. spectra of para-DFB<sup>(82)</sup> and para-xylene<sup>(81,110)</sup>, have been assigned to a totally symmetric substituent-sensitive C—C stretching mode. The above progression for para-DEB is assigned by analogy to the totally symmetric  $\nu(\text{C—C})$  mode  $\nu_7$ . The ground state frequency of this vibration was found in the Raman spectrum as  $812/809/768/763 \text{ cm}^{-1}$ . This assignment is supported by the absence of other in-plane vibrations, of a<sub>1</sub> symmetry, with frequencies around  $800 \text{ cm}^{-1}$ .

The strong band, to the blue of the origin, at  $39460/39440 \text{ cm}^{-1}$  for para-h<sub>6</sub>/para-d<sub>2</sub>, is left to assign at this point. The frequency interval between the above band and the  $0_0^0$  band is  $1150 \text{ cm}^{-1}$  for both isotopes. The ground state frequencies in Table 3.5.A. show that this excited state frequency of  $1150 \text{ cm}^{-1}$  may arise from excitation of either the totally symmetric ( $\nu_5$ ) or the non-totally symmetric ( $\nu_{28}$ ) substituent-sensitive  $\nu(\text{C—C})$  modes with ground state frequencies of  $1176/1171/1175/1168 \text{ cm}^{-1}$  and  $1260/1260/1258/1258 \text{ cm}^{-1}$  for para-h<sub>6</sub>/para-d<sub>2</sub>/para-d<sub>4</sub>/para-d<sub>6</sub>. In the  $\tilde{A} \ ^1B_{2u} \leftarrow \tilde{X} \ ^1A_g$  transition (see below) excited state frequencies of 1170 and  $1160 \text{ cm}^{-1}$  are found for the hydrogenic and ring deuterated isotopes respectively. The above upper state frequencies are assigned to  $\nu_5$ . A very small change in frequency thus occurs upon excitation. This is consistent with the assignments of similar excited state frequency intervals in the spectra of mono-substituted and para-disubstituted

benzenes (see Chapter 4).

This assignment implies that both totally symmetric substituent-sensitive  $\nu(\text{C}-\text{C})$  vibrations ( $\nu_5$  and  $\nu_7$ ) undergo a rather small change in frequency upon excitation. This was found above also for the  $\nu(\text{C}\equiv\text{C})$  mode  $\nu_3$ . The changes in geometry upon excitation are small for benzene derivatives (see Chapter 6). Therefore, the small changes in frequency of  $\nu_3$ ,  $\nu_5$  and  $\nu_7$  on excitation, imply that neither the CCH group nor the linkage between this group and the aromatic ring are significantly affected by changes in the electronic structure on excitation.

#### C. The 292 nm system under high resolution

The 292 nm system of para-DEB shows a great resemblance to the 279 nm system of  $\phi\text{CCH}$ . The oscillator strengths for these absorption systems are nearly identical:  $f = 5 \times 10^{-4}$  for  $\phi\text{CCH}$  and  $3 \times 10^{-4}$  for para-DEB. The absorption for both molecules shows two components: a weak system with double headed bands and a strong subsystem with single headed bands. In the spectra of both molecules, the intensity is less extended to the blue for the ring deuterated isotopes, compared with the hydrogenic compounds. King and So<sup>(63)</sup> have suggested that this indicates that mainly ring vibrations are excited in vibronic transitions.

Attempts to study the variation of the intensity of bands with temperature were not successful for the following reasons. The saturated vapour pressure of para-DEB at room temperature is only 0.4 torr. No absorption could be detected at dry ice temperature ( $-78^\circ\text{C}$ ) even with path lengths of about 90 meters. The sample could not be heated to suitably high temperatures, because of the rapid polymerization which occurred.

The frequencies and the relative intensities of the bands in the 292 nm system of the isotopes of para-DEB are collected in Table 5.2.

Table 5.2

Wavenumbers ( $\text{cm}^{-1}$ ) and relative intensities of the bands  
in the  $\tilde{A} \ ^1B_{2u} \leftarrow \tilde{X} \ ^1A_g$  transition of para-DEB

para-h <sub>6</sub>		para-d <sub>2</sub>		para-d <sub>4</sub>		para-d <sub>6</sub>		Assignment
33711.9	vw	33722.2	vvw	33861.1	vw			20 <sub>1</sub> <sup>0</sup>
34250.1	w(II)	34268.9	w(II)	34377.0	w(II)	34396.7	vw(II)	0 <sub>0</sub> <sup>0</sup>
34414.2	vvw	34424.8	vvw	34535.3	vvw	34545.4	vvw	$\alpha$
34586.8	vw	34599.3	vw	34711.7	vvw	34641.8	ew	$\beta$
34738.5	vs	34768.6	vs	34846.4	vs	34889.6	w	20 <sub>0</sub> <sup>1</sup>
		34744.8	vs			34856.9	vs	19 <sub>0</sub> <sup>1</sup>
34851	vvw	34854.5	vvw					28 <sub>0</sub> <sup>1</sup>
34887.9	ew							$\alpha$ <sup>1</sup>
35009.9	w(II)	35030.4	w(II)	35100.5	w(II)	35114.5	w(II)	7 <sub>0</sub> <sup>1</sup>
35425.5	vvw			35435.7	vvw			5 <sub>0</sub> <sup>1</sup>
35498.0	m	35497.2	s	35570.0	w	35576.7	m	20 <sub>0</sub> <sup>17</sup> <sub>0</sub> <sup>1</sup>
		35520.4	s			35610.4	vw	19 <sub>0</sub> <sup>17</sup> <sub>0</sub> <sup>1</sup>
35609.0	vvw							28 <sub>0</sub> <sup>17</sup> <sub>0</sub> <sup>1</sup>
35914.2	m	35911.3	m			36012.6	vw	20 <sub>0</sub> <sup>15</sup> <sub>0</sub> <sup>1</sup>
		35935.0	m			36037.9	vw	19 <sub>0</sub> <sup>15</sup> <sub>0</sub> <sup>1</sup>
36167.8	vvw							5 <sub>0</sub> <sup>17</sup> <sub>0</sub> <sup>1</sup>
36258.8	ew	36245.0	ew			36293.2	vvw	20 <sub>0</sub> <sup>17</sup> <sub>0</sub> <sup>2</sup>
		36267.4	ew					19 <sub>0</sub> <sup>17</sup> <sub>0</sub> <sup>2</sup>
36672.4	vvw							20 <sub>0</sub> <sup>15</sup> <sub>0</sub> <sup>17</sup> <sub>0</sub> <sup>1</sup>

The origin band of the 292 nm system of para-DEB can be assigned readily by analogy to the assignment of the  $0_0^0$  band of the 279 nm absorption system of  $\phi$ CCH. At the red end of the absorption system of para- $h_6$ /para- $d_2$ // $\phi$ CCH/ $\phi$ CCD, a double band is found at  $+488.4/499.7//490.2/503.6 \text{ cm}^{-1}$  from the most intense band in the spectrum and single headed bands are observed at  $-538.2/546.7//513.5/526.9 \text{ cm}^{-1}$  from the above double headed band. The latter separation corresponds to the  $b_{3g}/b_2$  fundamental of the acetylenic skeletal bending mode  $\nu_{20}/\nu_{35}$ , whose ground state frequency is  $537/545//513/531 \text{ cm}^{-1}$ . The above double headed band has been assigned as  $0_0^0$  for  $\phi$ CCH. By analogy, the  $0_0^0$  band of para-DEB is assigned to the double headed band at  $34250.1/34268.9/34377.0/34396.7 \text{ cm}^{-1}$  for para- $h_6$ /para- $d_2$ /para- $d_4$ /para- $d_6$ . This assignment is supported by the following arguments:

1. The blue shift of the origin band is  $+10 \text{ cm}^{-1}$  per acetylenic D atom and  $+32 \text{ cm}^{-1}$  per aromatic D atom. These figures agree very well with the shifts observed for  $\phi$ CCH and other benzene derivatives<sup>(63)</sup>.
2. The acetylenic skeletal bending mode  $\nu_{20}$  is the only vibration whose ground- and upper state fundamental frequency increases upon deuteration of the CCH groups.
3. It is shown in the next chapter on band contour analysis that the  $0_0^0$  and  $20_0^1$  bands are type B and type A bands respectively:

By analogy to the analysis for  $\phi$ CCH<sup>(63)</sup>, it is suggested that the 292 nm system of para-DEB should be interpreted in terms of a weak allowed component and a very intense forbidden subsystem. This forbidden part of the spectrum is based on the single quantum excitation in the upper state of the  $\beta(\text{C}-\text{C}\equiv\text{C})$  vibration ( $\nu_{20}$ ) for the CCH isotopes. In the spectra of the CCD isotopes, this  $\nu_{20}$  as well as the  $\beta(\equiv\text{C}-\text{D})$  vibration ( $\nu_{19}$ ) is excited. These two vibrations fall into the  $b_{3g}$  symmetry class. The above can be explained by the Herzberg-

Teller theory of vibronic coupling. First, the forbidden component in the 292 nm system of para-DEB is more intense than the forbidden subsystem in the 279 nm absorption of  $\phi$ CCH, because of the difference in energy between the A and B systems is smaller for para-DEB (0.6 eV) than for  $\phi$ CCH (0.9 eV).

Second, the  $\tilde{A} \ ^1B_{2u} \leftarrow \tilde{X} \ ^1A_g$  transition borrows intensity from the  $\tilde{B} \ ^1B_{1u} \leftarrow \tilde{X} \ ^1A_g$  transition via vibrations with  $b_{3g}$  symmetry for para-DEB.

The first absorption system of para-DEB contains a rather small number of vibrational bands to the blue of the  $0_0^0$  band, in addition to the bands discussed above. Most of the bands in the spectrum can be analyzed in terms of excited state frequencies of 760/752/722/718  $\text{cm}^{-1}$  and 1175/1166/1160/1155  $\text{cm}^{-1}$  for para- $h_6$ /para- $d_2$ /para- $d_4$ /para- $d_6$  in combination with the  $0_0^0$  band and the false origins in  $\nu_{19}$  and  $\nu_{20}$ . These frequencies have been assigned to the totally symmetric substituent-sensitive C—C stretching modes  $\nu_5$  and  $\nu_7$  for reasons outlined above under B.

The ring deformation  $\nu_{28}$  that plays such an important role in the 260 nm system of benzene (see Chapter 4) falls into the  $b_{3g}$  class of vibrations for para-DEB. The extremely weak bands at 34851.1/34854.5  $\text{cm}^{-1}$  for para- $h_6$ /para- $d_2$  have been tentatively assigned to this vibration.

Finally, very weak bands are found at +164.1/155.9/158.3/148.7  $\text{cm}^{-1}$  and at +336.7/330.4/334.7/331.3  $\text{cm}^{-1}$  from the  $0_0^0$  band. These bands will be called the  $\alpha$  and  $\beta$  bands respectively, hereafter. For para- $h_6$ , the  $\alpha$  and  $\beta$  bands are also associated with the most intense band in the spectrum at 34738.5  $\text{cm}^{-1}$ . The  $\alpha$  and  $\beta$  bands will be discussed later.

The small number of observed vibrational bands can be ascribed to two factors. First, the energy gap between the weak A and the very intense B system is very small (0.6 eV). No vibrational structure could be found to the blue of 272 nm, because of absorption by the long-wave tail of the 261 nm

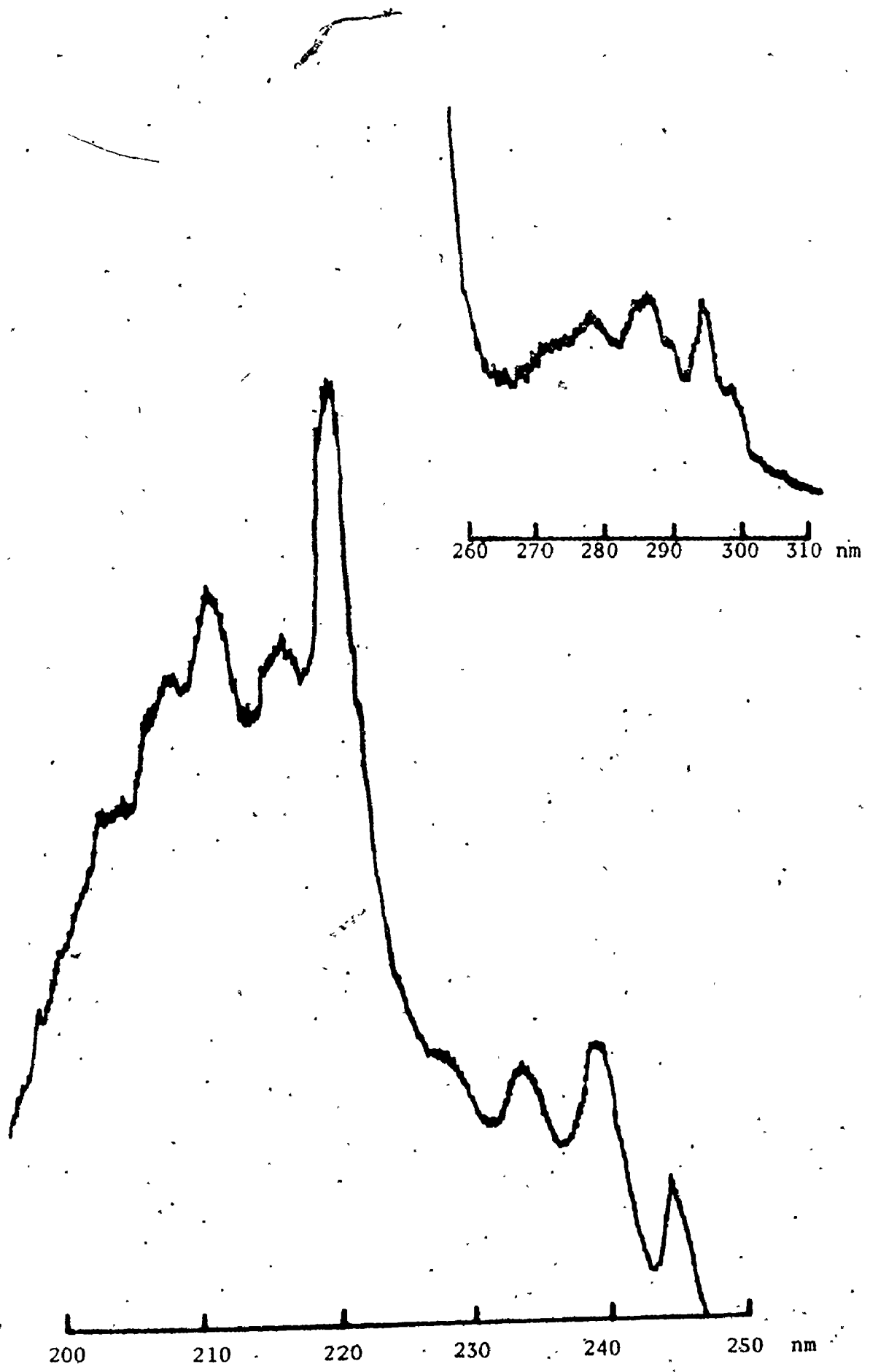
singlet system. Second, the strong bands in the spectra of all isotopes are accompanied by 7 to 8 members of a sequence in about  $-16 \text{ cm}^{-1}$ . The first  $16 \text{ cm}^{-1}$  sequence band contains four members of a sequence in about  $-2 \text{ cm}^{-1}$ . (The possibility that the structure within each  $16 \text{ cm}^{-1}$  sequence is due to rotational structure is excluded in Chapter 6 on the basis of band contour analysis.) The higher members of the  $-16 \text{ cm}^{-1}$  sequence have the  $-2 \text{ cm}^{-1}$  sequence stacked upon them to the blue as well as to the red. Weak bands in the 292 nm system could only be detected with difficulty because of these sequence bands. It should be noted in this respect that the low resolution spectra of the CCD isotopes are diffuse below 278 nm. The high resolution spectra of these isotopes have revealed that this (apparent) diffuseness is caused by sequence congestion.

The relatively high intensity of the  $-16 \text{ cm}^{-1}$  and the  $-2 \text{ cm}^{-1}$  sequence indicate that these sequences originate on vibrational levels of low energy in the ground state. The sequences are only very slightly affected by deuteration of the acetylenic and aromatic protons. They have therefore been ascribed to the very low frequency out-of-plane bending modes of the whole CCH group. These are the  $\gamma(\text{C}-\text{CCH})$  vibrations of  $b_{2g}$  symmetry ( $\nu_{14}$ ) and of  $b_{3u}$  symmetry ( $\nu_{42}$ ), whose ground state values are  $197/182/186/177 \text{ cm}^{-1}$  and  $68/68/64/63 \text{ cm}^{-1}$  for para- $\text{h}_6$ /para- $\text{d}_2$ /para- $\text{d}_4$ /para- $\text{d}_6$ .

## 5.2. Analysis of the Electronic Spectrum of meta-DEB

### A. General appearance of the spectrum under low resolution

Three electronic absorption systems have been recorded in the U.V. for meta-DEB on the Cary. These systems will be called the 296, 245 and 220 nm absorption systems. The profiles of the 245 and 220-nm systems, presented in Fig. 5.3, curve B, were obtained using a 10 cm cell with the sample in the side arm at a temperature of about  $-25^\circ\text{C}$ . The 296 nm system, curve A in Fig. 5.3,



was obtained using a solution of meta-DEB in methanol in a 1 cm path length quartz U.V. cell.

The oscillator strengths of the three absorption systems have been determined from the solution spectrum of meta-DEB in methanol. The oscillator strength of the discrete 296 nm system was calculated as  $f = 2 \times 10^{-4}$ ,  $f = 0.08$  for the 245 nm absorption, and  $f = 0.95$  for the very intense 220 nm transition.

The transition energies and oscillator strengths calculated in Chapter 4 (Table 4.4.A) are in excellent agreement with the position and intensity of the above three transitions. The 296, 245 and 220 nm systems of meta-DEB are assigned, tentatively at present, to the  $\tilde{A} \ ^1B_2 + \tilde{X} \ ^1A_1$ ,  $\tilde{B} \ ^1A_1 + \tilde{X} \ ^1A_1$  and  $\tilde{C} \ ^1B_2 + \tilde{X} \ ^1A_1$  transitions respectively.

The 220 nm system shows some coarse vibrational structure. This structure could not be analyzed from the spectra recorded in this study because the bands are very weak and broad, except for the intense bands at 45450 and 47430  $\text{cm}^{-1}$ . The frequency interval between these prominent peaks is about 2000  $\text{cm}^{-1}$ . This spacing is assigned to the excited state frequency of the totally symmetric triple bond stretching mode  $\nu_3$  for reasons outlined above in Section 5.1.B.

Four broad, diffuse vibrational humps appear at 244.4 (medium), 239.0 (strong), 233.6 (medium) and 228.5 (weak) nm in the 245 nm system. The frequency interval between these peaks is about 950  $\text{cm}^{-1}$ . As discussed in Chapter 3, the totally symmetric ring breathing vibration occurs at about 1000  $\text{cm}^{-1}$  in the ground state for benzene and all mono-, meta- and 1,3,5-substituted benzenes. According to the review in Chapter 4, this ring breathing vibration plays an important role in the U.V. spectra of the above molecules. The upper state frequency of this vibration is about 950  $\text{cm}^{-1}$  for all molecules. The above four peaks in the 245 nm system of meta-DEB therefore almost certainly represent



a progression in this totally symmetric ring breathing vibration ( $\nu_{10}$ ) in the upper state.

#### B. The 296 nm system under high resolution

The  $\tilde{A} \ ^1B_2 \leftarrow \tilde{X} \ ^1A_1$  transition of meta- $h_6$  and meta- $d_2$  contains a rather limited number of vibronic bands compared to the wealth of structure present in the analogous transition for other derivatives of benzene. It was impossible to detect any structure at frequencies higher than  $35720 \text{ cm}^{-1}$  for both isotopes, because of the steeply increasing absorption of the long-wave tail of the 245 nm absorption system. No bands could be observed at frequencies lower than  $33400 \text{ cm}^{-1}$  with the sample at its saturated vapour pressure of 0.35 torr at room temperature and path lengths up to 90 meters. The frequencies and relative intensities of the measured bands are collected in Table 5.3. Not listed in this table are the sequences in  $-2.5$ ,  $-5.5$ ,  $-30$  and  $-35 \text{ cm}^{-1}$  that are observed up to the fourth member for strong bands. The higher frequency sequence bands have the sequences in  $-2.5$  and  $-5.5 \text{ cm}^{-1}$  stacked upon them, to the red as well as to the blue. This observation makes it unlikely that the structure within the  $-30$  and  $-35 \text{ cm}^{-1}$  sequence bands is due to rotational transitions (see below). The high relative intensity of the sequences suggests that they originate on low frequency vibrations. The sequence intervals are small; the vibrations involved are thus only slightly affected by electronic excitation. The intervals do not change on deuteration of the CCH groups.

The sequences in  $-5$  and  $-35 \text{ cm}^{-1}$  found in the 279 nm system of  $\phi\text{CCH}^{(63)}$ , have analogous features as the above sequences for meta-DEB. The two sequences for  $\phi\text{CCH}$  have been ascribed to the two low frequency out-of-plane bending modes  $\gamma(\text{C}-\text{CCH})$  and  $\gamma(\text{C}-\text{C}\equiv\text{C})$ ; whose ground state frequencies are  $162/154/161/146 \text{ cm}^{-1}$  and  $349/340/330/322 \text{ cm}^{-1}$  respectively. The introduction of a second CCH group in  $\phi\text{CCH}$  results in a total of four low-frequency out-of-plane  $\text{C}-\text{C}\equiv\text{C}$

Table 5.3

Wavenumbers ( $\text{cm}^{-1}$ ) and relative intensities of the vibrational bands  
in the 296 nm transition of meta-DLB

meta-h <sub>6</sub>	meta-d <sub>2</sub>	Assignment
33314.9 vvw	33353.5 vvw	$14_1^0$
33346.8 vvw	33370.7 vvw	$41_1^0$
33800.0 vw	33824.2 vw	$0_0^0$
33905.9 vvw	33923.0 vvw	$\alpha$
34264.5 vs	34271.3 vs	$14_0^1$
	34326.1 vvs	$39_0^1/40_0^1$
34462.3 s	34482.0 s	$11_0^1$
	34746.0 vvw	$38_0^1$
34924.7 vw	34928.9 vw	$14_0^1 11_0^1$
35211.6 w	35211.8 w	$14_0^1 10_0^1$
35512.0 w	35513.0 w	$14_0^1 8_0^1$
35710.1 vvw	35718.4 vvw	$11_0^1 8_0^1$

and CCH bending modes with ground state frequencies of 185/172, 122/119, 366/358, and 343/333  $\text{cm}^{-1}$ . These four vibrations can be grouped into two sets of out-of-plane vibrations, similar to the set given above for  $\phi\text{CCH}$ . The observation of two sets of two sequences in the spectrum of meta-DEB that resemble closely the two sequences found for  $\phi\text{CCH}$ , strongly suggests that the sequences for meta-DEB originate on the above four low-frequency vibrations.

Only single headed bands have been observed in the spectra of meta- $\text{h}_6$  and meta- $\text{d}_2$ . The band contours for benzene derivatives are discussed in detail in Chapter 6 and it will be seen there that the A-type bands are single headed for all 27 substituted benzenes studied to date. The single headed bands in the spectra of meta- $\text{h}_6$  and meta- $\text{d}_2$  are thus probably type A bands. Likewise, double headed bands are almost certainly type B bands. This is confirmed by a calculation of the rotational profiles of type A and type B bands for meta- $\text{h}_6$ . These contours were calculated (see Chapter 6 for details) with the ground state rotational constants estimated in Chapter 1. It will be shown in the next chapter that no accurate values can be obtained for the excited state geometries at  $\phi\text{CCH}$  and para-DEB. The excited state geometry of meta-DEB—and thus the rotational constants—can therefore not be estimated. However, for ortho- $\text{h}_6$  double headed bands have been observed with a separation of 1.8  $\text{cm}^{-1}$  (see below), while double headed bands with a band head separation of 2.2  $\text{cm}^{-1}$  have been calculated for ortho-DFB<sup>(84)</sup>. The changes in rotational constants for meta- $\text{h}_6$  were chosen as  $\Delta A = -0.005 \text{ cm}^{-1}$  and  $\Delta B = -0.007$ , because similar values have been determined for meta-DFB<sup>(84)</sup>. The calculations resulted in a single headed type A band and a double headed type B band, with a separation of 1.1  $\text{cm}^{-1}$  between the two absorption maxima. The origin band is assigned to the weak band at 33800.0/33824.2  $\text{cm}^{-1}$  for meta- $\text{h}_6$ /meta- $\text{d}_2$  for the following

reasons.

The blue shift of this band is  $+12 \text{ cm}^{-1}$  per acetylenic D-atom, which is close to the values found for  $\phi\text{CCH}$  ( $+13 \text{ cm}^{-1}$ ) and for para-DEB ( $+10 \text{ cm}^{-1}$ ). If the most intense band in the spectrum at  $34264.5/34271.3 \text{ cm}^{-1}$  is assigned as the  $0_0^0$  band, the bands to the red are not at separations corresponding to ground state frequencies. This difficulty does not arise if the weak band at  $33800.0/33824.2 \text{ cm}^{-1}$  is assigned as  $0_0^0$ . With this assignment, the most intense band occurs at  $+464.5/457.1 \text{ cm}^{-1}$  from the  $0_0^0$  band. By analogy to the analyses for meta-DFB and meta-xylene, this interval is assigned to the upper state frequency of the totally symmetric ring deformation  $\nu_{14}$ , whose Raman value is  $482/473 \text{ cm}^{-1}$ . The very weak band at  $-485.1/470.7 \text{ cm}^{-1}$  from the  $0_0^0$  has been assigned to the ground state frequency of  $\nu_{14}$ . The extremely weak band at  $-453.1/453.5 \text{ cm}^{-1}$  from the  $0_0^0$  is assigned to the non-totally symmetric ring deformation  $\nu_{41}$ , whose I.R. frequency is  $455/454 \text{ cm}^{-1}$ .

The bands at the blue end of the spectrum can be described as involving the excitation of vibrations with upper state frequencies of  $660/657$ ,  $947/949$  and  $1247/1242 \text{ cm}^{-1}$ . These vibrations are based on the strongest band in the spectrum at  $34264.5/34271.3 \text{ cm}^{-1}$  and on the  $0_0^0$  bands at  $33800.0/33824.2 \text{ cm}^{-1}$ . The above upper state frequency intervals are assigned to the totally symmetric  $\nu(\text{C}-\text{C})$  modes  $\nu_8$ ,  $\nu_{10}$  and  $\nu_{11}$ , whose ground state frequencies are  $703/700$ ,  $998/997$  and  $1236/1233 \text{ cm}^{-1}$ . The totally symmetric ring breathing mode  $\nu_{10}$  has been discussed in detail in the previous section. As discussed in Chapter 4, the totally symmetric substituent-sensitive C—C stretching modes play an important role in the U.V. spectra of meta-DFB and meta-xylene. The upper state frequencies of these vibrations for the latter molecules are approximately equal to the upper state frequencies given above for meta-DEB. The assignment is further supported by the absence of other in-plane vibrations with frequencies

in the immediate vicinity of the ground state frequencies of the  $\nu(\text{C}-\text{C})$  modes of vibration. Finally, the very weak band at  $105.9/98.8 \text{ cm}^{-1}$  is called the  $\alpha$ -band hereafter and will be discussed later.

According to the above analysis, the 296 nm system of meta-DEB consists of an allowed and a forbidden component that is based on the single quantum excitation of the totally symmetric ring deformation  $\nu_{14}$ . The vibration is also active in the first absorption systems of meta-DFB and meta-xylene. In the spectra of the latter molecules, this false origin—and the forbidden subsystem built on it—is much weaker than for meta-DEB. From the Herzberg-Teller theory of vibronic coupling, this intensity difference can be explained by the energies of the higher excited electronic states. The  $\tilde{B}$  and  $\tilde{C}$  systems for meta-DEB namely occur at 245 and 220 nm, while the analogous transitions for both meta-xylene and meta-DFB are found at 215 and 195 nm. A considerable red shift is thus found for the  $\tilde{B}$  and  $\tilde{C}$  systems of meta-DEB with respect to those for meta-xylene and meta-DFB.

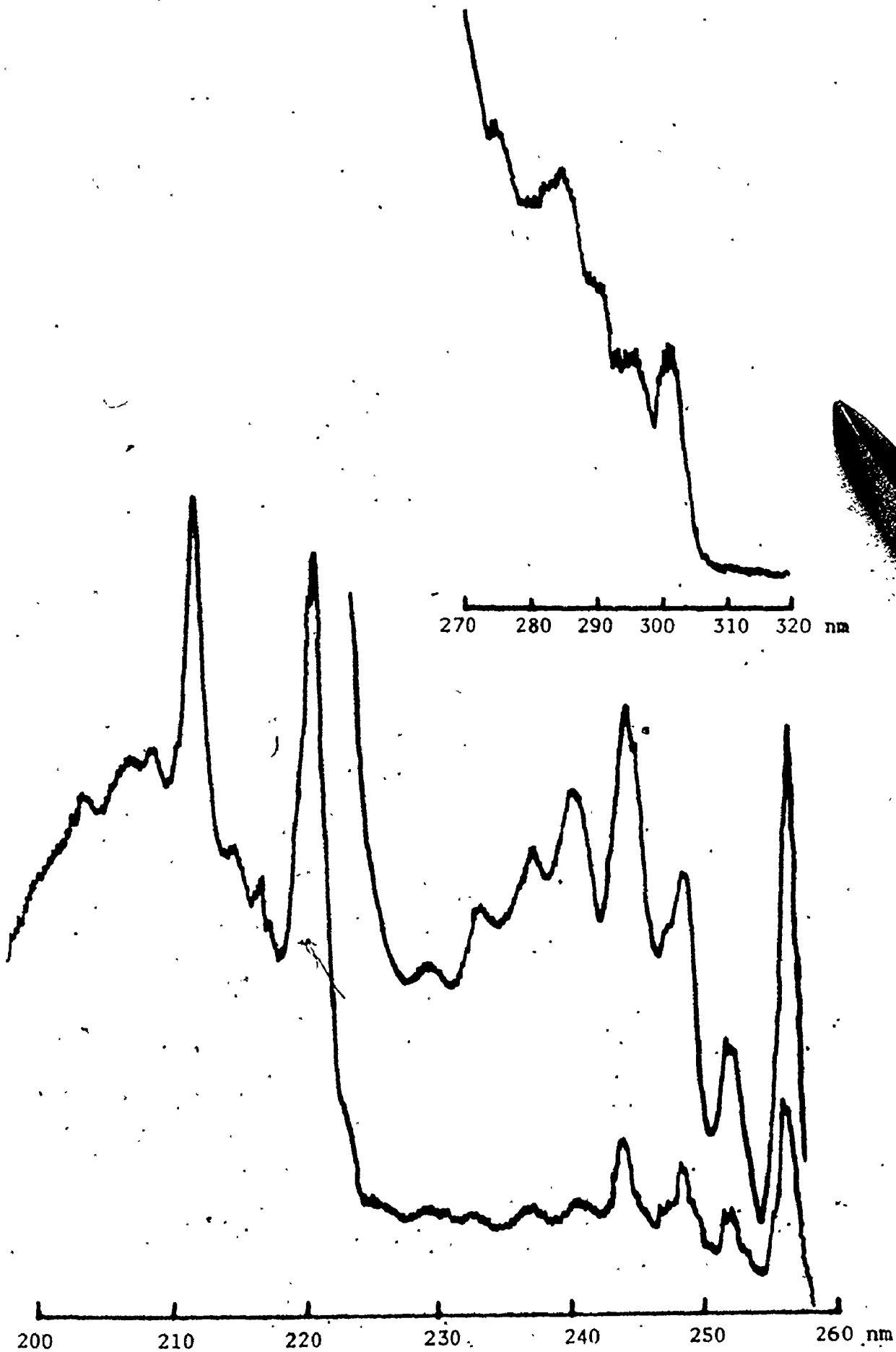
### 5.3. Analysis of the Electronic Spectrum of ortho-DEB

#### A. General appearance of the spectrum under low resolution

Three electronic absorption systems have been recorded for ortho-DEB on the Cary. These three transitions will be referred to below as the 220, 256 and 298 nm systems. The profiles of these three absorption systems are presented in Fig. 5.4.

The oscillator strengths have been determined from the solution spectrum of ortho-DEB in methanol as  $f = 10^{-4}$ , 0.13 and 0.90 for the 298, 256 and 220 nm system respectively. In accordance with the calculations and discussion in Chapter 4, the 298, 256 and 220 nm absorption systems have been assigned to the  $\tilde{A} \ ^1A_1 + \tilde{X} \ ^1A_1$ ,  $\tilde{B} \ ^1B_2 + \tilde{X} \ ^1A_1$  and  $\tilde{C} \ ^1A_1 + \tilde{X} \ ^1A_1$  transitions respectively.

The very intense 220 nm system contains two prominent peaks, namely at



45500  $\text{cm}^{-1}$ , and 2000  $\text{cm}^{-1}$  to the blue of this band. This interval is assigned to the upper state frequency of the totally symmetric  $\nu(\text{C}\equiv\text{C})$  vibration  $\nu_4$ , by analogy to the intervals of 2000  $\text{cm}^{-1}$  measured in the spectra of  $\phi\text{CCH}$ , para- and meta-DEB (see Section 5.1.B.). The other weak bands in the 220 nm system could not be analyzed.

The frequencies of the maxima of the vibrational peaks measured in the 256 nm system of ortho- $\text{h}_6$  are collected in Table 5.4, together with their relative intensities. The spectra of the ring deuterated isotopes were not recorded because only small amounts of sample were available. The accuracy of the frequencies listed is  $\pm 20 \text{ cm}^{-1}$ . The 256 nm  $\tilde{\text{B}}, ^1\text{B}_2 + \tilde{\text{X}}, ^1\text{A}_1$  transition also shows two prominent peaks with a separation of about 2000  $\text{cm}^{-1}$ , namely the most intense, lowest-frequency band in the system at 39060  $\text{cm}^{-1}$  and the strong band—2020  $\text{cm}^{-1}$  to the blue of the strongest band—at 40280  $\text{cm}^{-1}$ . This spacing is assigned here also to the upper state frequency of the totally symmetric  $\nu(\text{C}\equiv\text{C})$  mode  $\nu_4$ . All other bands in Table 5.4 can be described with upper state frequencies of 650 and 1230  $\text{cm}^{-1}$  in combination with the above two prominent bands. These same separations have been measured also in the 298 Å  $^1\text{A}_1 + \tilde{\text{X}}, ^1\text{A}_1$  transition (see below). Similar frequency intervals have been observed in the first absorption systems of ortho-DFB<sup>(86)</sup> and ortho-xylene<sup>(28)</sup>. It is suggested, on the basis of these analogies, that the separations of 650 and 1230  $\text{cm}^{-1}$  in the 256 nm system should be assigned to the totally symmetric, substituent-sensitive C—C stretching modes  $\nu_8$  and  $\nu_{11}$ , whose ground state frequencies are 706 and 1204  $\text{cm}^{-1}$ .

#### B. The 298 nm system under high resolution

The 298 nm system of ortho- $\text{h}_6$ /ortho- $\text{d}_4$ /ortho- $\text{d}_6$  was photographed under high resolution using a 1.83 m multiple reflection cell, containing the sample at the saturated vapour pressure at room temperature (0.35 torr). Maximum path

lengths used were about 96 meters (52 traversals). The spectra of the isotopes of ortho-DEB have the following features in common with the spectra described in Section 5.2 for the isotopes of meta-DEB.

The spectra of the isotopes of ortho-DEB show sequences in  $-3.5$ ,  $-5.5$ ,  $-28$  and  $-33 \text{ cm}^{-1}$ , that can be described analogously as the sequences in  $-2.5$ ,  $-5.5$ ,  $-30$  and  $-32 \text{ cm}^{-1}$  for meta-DEB discussed in Section 5.2.B. These sequences of ortho-DEB are therefore attributed to the four low-frequency  $\gamma(\text{C}-\text{C}\equiv\text{C})$  and  $\gamma(\text{C}-\text{CCH})$  vibrations with ground state frequencies of  $130/130/123 \text{ cm}^{-1}$ ,  $182/170/162 \text{ cm}^{-1}$ ,  $335/325/316 \text{ cm}^{-1}$  and  $371/337/338 \text{ cm}^{-1}$ . Weak bands could only be detected with difficulty for the same reasons as outlined for para- and meta-DEB. Also, the spectra of ring deuterated molecules showed a much less extended intensity distribution than observed for ortho- $\text{h}_6$ . Two types of bands can be distinguished in the 298 nm transition. Type I bands are single headed, while type II bands are double headed. The two absorption maxima in the type II bands are separated by  $1.8/1.4 \text{ cm}^{-1}$  for ortho- $\text{h}_6$ /ortho- $\text{d}_4$ . As discussed in Section 5.2.B., it is almost certain that the single headed type I bands are polarized along the inertial a axis and that the double headed type II bands are type B. This could not be confirmed for ortho-DEB, because the band contour programs available to this author did not reproduce the profile calculated for ortho-DFB<sup>(84)</sup> (see Chapter 6).

The origin band is assigned to the type I band at  $33507.2/33612.9/33639.8 \text{ cm}^{-1}$  for ortho- $\text{h}_6$ /ortho- $\text{d}_4$ /ortho- $\text{h}_6$  for the following reasons.

The blue shift of this band is  $+9 \text{ cm}^{-1}$  per acetylenic D-atom, which compared favourably with the values of  $+10 \text{ cm}^{-1}$  for para-DEB,  $+12 \text{ cm}^{-1}$  for meta-DEB and  $+13 \text{ cm}^{-1}$  for  $\phi\text{CCH}$ . The blue shift of this band is  $+27 \text{ cm}^{-1}$  per aromatic D-atom. This figure agrees very well with the shift of  $+32 \text{ cm}^{-1}$  per aromatic D-atom for para-DEB and of  $+31 \text{ cm}^{-1}$  for  $\phi\text{CCH}$ .



If the weak type II band at 33093.5/33202.4  $\text{cm}^{-1}$  for ortho- $\text{h}_6$ /ortho- $\text{d}_4$  is assigned as the origin band by analogy to the assignment for para- and meta-DEB, then the separations of the bands to the red of this band do not correspond to ground state frequencies. This difficulty disappears if the most intense band at 33507.2/33612.9  $\text{cm}^{-1}$  is assigned as  $0_0^0$ . The weak type II bands at +366/358  $\text{cm}^{-1}$  from the  $0_0^0$  can then be assigned as the upper state frequency of the non-totally symmetric ring deformation ( $\nu_{41}$ ), by analogy to the assignment for ortho-DFB<sup>(86)</sup> and ortho-xylene<sup>(28)</sup>. The ground state frequency of this ring deformation for ortho- $\text{h}_6$ /ortho- $\text{d}_4$  is 414/411  $\text{cm}^{-1}$ . The weak type II band at -413.7/410.5  $\text{cm}^{-1}$  from the  $0_0^0$  has been assigned to this ground state frequency. The very weak band at +426.8/423.3  $\text{cm}^{-1}$  from the  $0_0^0$  is assigned to the upper state frequency of the totally symmetric acetylenic bending mode  $\nu_{15}$ , whose Raman frequency is 440/438  $\text{cm}^{-1}$ . The band at +974/814  $\text{cm}^{-1}$  from the  $0_0^0$  shows a blue shift of 150  $\text{cm}^{-1}$  upon ring deuteration. This drop in frequency is of the same order of magnitude as the decrease in frequency in the ground state of the in-plane aromatic  $\beta(\text{C}-\text{H})$  vibrations on ring deuteration. This suggests that the above band arises from the excitation in the upper state of the aromatic  $\beta(\text{C}-\text{H})/\beta(\text{C}-\text{D})$  vibration of  $a_1$  symmetry ( $\nu_{10}$ ), whose Raman values are 1037/833  $\text{cm}^{-1}$  for ortho- $\text{h}_6$ /ortho- $\text{d}_4$ . This bending mode is also active in the spectra of ortho-xylene<sup>(4,28)</sup> and ortho-DFB<sup>(4,86)</sup>. The very weak bands at +786.0/747.9  $\text{cm}^{-1}$  from the  $0_0^0$  can be described as involving single quantum excitation of the substituent-sensitive  $\nu(\text{C}-\text{C})$  vibration ( $\nu_{38}$ ), of  $b_2$  symmetry, with a ground state frequency of 807/760  $\text{cm}^{-1}$ . The above assignments together support the proposed assignment for the  $0_0^0$ .

The remaining bands to the blue of the  $0_0^0$  band can be described as involving the excitation of vibrations with upper state frequencies of 663/633 and 1200/1128  $\text{cm}^{-1}$  for ortho- $\text{h}_6$ /ortho- $\text{d}_4$ , in combination with the origin band.

The above frequency intervals are assigned to the upper state frequencies of the totally symmetric substituent-sensitive C—C stretches  $\nu_{11}$  and  $\nu_8$ , whose ground state values are 706/678 and 1204/1128  $\text{cm}^{-1}$  respectively. This assignment is made by analogy to the analyses presented for ortho-DFB and ortho-xylene. . .

Finally, the bands to the red of the  $O_0^0$  will be considered except the type II band at  $-413.7/410.5 \text{ cm}^{-1}$ , which was assigned above. All these bands are very weak and single headed. They are, however, different from the type I band described earlier in this section in that they show three sequences only, namely in  $-3$ ,  $-10$  and  $-56 \text{ cm}^{-1}$ . The band at  $32457.8/32510.3/32510.4 \text{ cm}^{-1}$  for ortho- $h_6$ /ortho- $d_4$ /ortho- $d_6$  is peculiar, since it is not affected by deuteration of the CCH groups, although the  $O_0^0$  band of ortho- $d_6$  is blue shifted by  $26.7 \text{ cm}^{-1}$  with respect to the  $O_0^0$  band of ortho- $d_4$ .

As discussed in Chapter 3, the sample of ortho-DEB contained a phthaldehyde impurity (starting material for the synthesis), as well as some (mixture of) hydrocarbon(s) with a high boiling point. The latter impurity was introduced in the last step of the synthesis via the commercial n-butyllithium solution in hydrocarbons, of which n-hexane was the major component. In order to find out whether the bands to the red of the  $O_0^0$  are caused by this hydrocarbon impurity, the n-butyllithium—in 10 cc of the hydrocarbon solution—was decomposed with water. The lithium hydroxide was removed by filtration and the n-hexane was distilled off. A Cary tracing of the U.V. spectrum of all the residue in methanol showed a gradually increasing absorption starting around 350 nm. Upon dilution this absorption was blue shifted but no absorption maximum could be found above 190 nm. This observation, in combination with the frequency data in Table 5.5, makes it more likely that the very weak bands presently under discussion are caused by the starting material for the synthesis

Table 5.4

Wavenumbers ( $\text{cm}^{-1}$ ) and relative intensities of the vibrational bands  
in the 256 nm system of ortho-DEB

ortho-h <sub>6</sub>		Assignment
39060	vs	$0_0^0$
39700	s	$11_0^1$
40300	s	$8_0^1$
40950	sh	$8_0^1 11_0^1$
41060	vs	$3_0^1$
41700	s	$3_0^1 11_0^1$
42290	w	$3_0^1 8_0^1$
42930	w	$3_0^1 8_0^1 11_0^1$
43630	vw	$3_0^1 8_0^2 11_0^1$

Table 5.5

Wavenumbers ( $\text{cm}^{-1}$ ) and relative intensities of the bands  
measured in the 298 nm system of ortho-DEB

ortho-h <sub>6</sub>		ortho-d <sub>4</sub>		ortho-d <sub>6</sub>		Assignment
32457.8	vvw(III)	32510.3	vvw(IFI)	32510.4	vvw	phthaldehyde
32722.1	vvw	32746.9	vvw			phthaldehyde
32931.2	vvw(III)	32960.5	vvw(III)			phthaldehyde
33093.5	vvw(II)	33202.4	vvw(II)			41 <sup>0</sup> <sub>1</sub>
33158.6	vvw(III)	33168.9	vvw			phthaldehyde
33507.2	vs(I)	33612.9	vs(I)	33639.8	s(I)	0 <sup>0</sup> <sub>0</sub>
33873.0	w(II)	33971.3	w(II)	33973.9	vvw	41 <sup>1</sup> <sub>0</sub>
33934.0	vw	34036.2	vw(I)			15 <sup>1</sup> <sub>0</sub>
34170.4	vs(I)	34245.6	vs(I)	34267.7	m	11 <sup>1</sup> <sub>0</sub>
34293.2	vvw(II)	34350.8	vvw			38 <sup>1</sup> <sub>0</sub>
34481.4	vvw	34426.7	vvw			10 <sup>1</sup> <sub>0</sub>
34534.7	vvw(II)					41 <sup>1</sup> <sub>0</sub> 11 <sup>1</sup> <sub>0</sub>
34708.3	vw	34727.6	vw			8 <sup>1</sup> <sub>0</sub>
34833.0	w(I)	34910.2	w(I)			11 <sup>2</sup> <sub>0</sub>
34956	vvw	35087	vvw			30 <sup>1</sup> <sub>0</sub> 11 <sup>1</sup> <sub>0</sub>
35071	vvw					41 <sup>1</sup> <sub>0</sub> 8 <sup>1</sup> <sub>0</sub>
35144	vvw					10 <sup>1</sup> <sub>0</sub> 11 <sup>1</sup> <sub>0</sub>
35369.4	vvw	35362	vvw			11 <sup>1</sup> <sub>0</sub> 8 <sup>1</sup> <sub>0</sub>
35504	vvw	35546	vvw			11 <sup>3</sup> <sub>0</sub>

(phthaldehyde) than by the hydrocarbon impurity. A Cary tracing of the U.V. spectrum of phthaldehyde in methanol did reveal some absorption around 300 nm. No attempts have been made to determine whether this absorption is due to an  $n \rightarrow \pi^*$  transition or whether it is the long-wave tail of the  $\pi \rightarrow \pi^*$  transitions with absorption maxima to lower wavelengths.

#### The $\alpha$ and $\beta$ bands

In the previous sections the  $\alpha$  and  $\beta$  bands have been mentioned. These will be discussed below, together with the analogous bands for  $\phi\text{CCH}$ .

In the spectra of  $\text{C}_6\text{H}_5\text{CCH}/\text{C}_6\text{H}_5\text{CCD}/\text{C}_6\text{D}_5\text{CCH}/\text{C}_6\text{D}_5\text{CCD}$  the single headed  $\alpha$  bands have been observed at  $+146.4/138.5/141.4/133.8 \text{ cm}^{-1}$  and the single headed  $\beta$  bands at  $+334.5/348.0/340.8/358.2 \text{ cm}^{-1}$  from the  $\text{O}_0^0$  bands. Weak bands were found at separations of  $-156/155/136/136 \text{ cm}^{-1}$  from the strongest bands, including the  $\text{O}_0^0$  band. The frequency interval between the latter bands to the red of the  $\text{O}_0^0$  and the  $\beta$  bands is equal to the upper state frequency of the nontotally symmetric ( $b_2$ ) acetylenic skeletal bending mode  $\nu_{35}$ .

In the spectra of para- $\text{h}_6$ /para- $\text{d}_2$ /para- $\text{d}_4$ /para- $\text{d}_6$  the very weak  $\alpha$  bands occur at  $+164.1/155.8/158.3/142.4 \text{ cm}^{-1}$  and the  $\beta$  bands at  $+336.7/330.3/334.7/295.1 \text{ cm}^{-1}$  from the origin band. The very intense  $20_0^1$  band in the spectrum of para- $\text{h}_6$  was associated by a very weak  $\alpha$  band at a separation of  $+149.4 \text{ cm}^{-1}$ .

In the spectrum of meta- $\text{h}_6$ /meta- $\text{d}_2$ , the very weak  $\alpha$  bands have been found at  $+105.9/98.8 \text{ cm}^{-1}$  from the  $\text{O}_0^0$ . No  $\beta$  bands could be detected. Neither the  $\alpha$  nor the  $\beta$  bands have been observed in the spectra of the isotopes of ortho-DEB.

Notwithstanding the large number of vibronic bands measured in the spectrum of  $\phi\text{CCH}$ , only a tentative assignment could be proposed for the  $\alpha$  and the  $\beta$  bands. The spectra of the DEBs do not contain sufficient information to propose an explanation. It is only observed here that the  $\alpha$ -bands for  $\phi\text{CCH}$ ,

para-DEB and meta-DEB occur at separations from the respective  $0_0^0$  bands that are about  $20 \text{ cm}^{-1}$  smaller than the ground state frequency of a very low-frequency out-of-plane [ $\gamma(\text{C}-\text{CCH})$ ] vibration for each of these molecules.

### Conclusions

Three electronic absorption systems have been observed for each of the three DEBs. The very intense second and third transitions of the DEBs are red shifted by about 30 nm with respect to the analogous absorption in benzene and other benzene derivatives, while the very weak first transition is only slightly red shifted. The discrete vibrational structure in the very weak first absorption system can only be observed over a small wavenumber range, because of the proximity of the intense higher transitions.

The analysis of the rather limited vibrational structure is made largely by comparison with related molecules, and with the calculations presented in the previous chapter. The calculated and experimental transition energies and oscillator strengths are in excellent agreement. The totally symmetric C—C stretching modes— $\nu_5$  and  $\nu_7$  for para-DEB;  $\nu_8$ ,  $\nu_{10}$  and  $\nu_{11}$  for meta-DEB; and  $\nu_8$  and  $\nu_{11}$  for ortho-DEB—play an important role in the first and second absorption systems of the DEBs.

## CHAPTER 6

### Band Contour Analysis and Excited State Geometry

#### Introduction

In this chapter the changes in rotational constants upon excitation will be determined for the isotopes para-h<sub>6</sub>, para-d<sub>4</sub> and ring-deuterated phenylacetylene via the band contour method. The results obtained will be used, in combination with literature data, to obtain information on the geometry of the aromatic ring in the lowest excited electronic state of various benzene derivatives.

#### 6.1. Band Contour Analysis

##### A. General features of the rotational profiles

The rotational analysis of the electronic spectra of benzene derivatives has been reviewed recently by Ross<sup>(59)</sup>. Only those features of the rotational fine structure of substituted benzenes that are relevant for the discussion later in this chapter will be mentioned here.

The following empirical observations have been made upon the infrared spectra of all large polyatomics--such as benzene derivatives--that are asymmetric tops: bands polarized along the b inertial axis are double peaked (B-type) and bands polarized parallel to the a (type A) and c (type C) inertial axes show only one absorption maximum. Both single and double peaked bands have been found in the U.V. spectra of benzene derivatives. Computer simulation techniques for the rotational contours have revealed that:

1. The changes in rotational constants upon electronic excitation are always very small, although larger than the changes found for purely vibrational excitation. The changes in rotational constants upon electronic excitation for 13 benzene derivatives, as given by Ross<sup>(59)</sup>, have been reproduced in

Table 6.1

The changes in rotational constants (in  $\text{cm}^{-1}$ ) for benzene  
and various benzene derivatives


			$\Delta A$ ( $\text{cm}^{-1}$ )	$\Delta B$ ( $\text{cm}^{-1}$ )	$\Delta C$ ( $\text{cm}^{-1}$ )	Ref.
H	H <sub>4</sub>	F	-0.01122	-0.00101	-0.00159	59
F	H <sub>4</sub>	F	-0.0118	+0.00022	-0.00037	98
F	H <sub>4</sub>	F	-0.0119	+0.00023	-0.00036	99
H	H <sub>4</sub>	Cl	-0.01095	-0.00030	-0.00064	59
Cl	H <sub>4</sub>	Cl	-0.01050	+0.00017	+0.00001	59
F	H <sub>4</sub>	Cl	-0.01120	+0.00025	-0.00007	59
H	H <sub>4</sub>	OH	-0.01135		-0.00116	61
H	H <sub>4</sub>	OH	-0.01118	+0.00014	-0.00111	59
F	H <sub>4</sub>	OH	-0.01110	+0.00099	+0.00008	59
H	H <sub>4</sub>	Br	-0.00955	-0.00002	-0.00023	59
H	H <sub>4</sub>	NH <sub>2</sub>	-0.01118	+0.00136	-0.00059	59
F	H <sub>4</sub>	NH <sub>2</sub>	-0.0125	+0.00099	-0.00011	59
H	H <sub>4</sub>	H	-0.0086	-0.0086	-0.0043	59
D	D <sub>4</sub>	D	-0.0064	-0.0064	-0.0032	59
H	H <sub>4</sub>	NC	-0.00789	-0.00101	-0.00101	68
H	H <sub>4</sub>	CCH	-0.00710	-0.00092	-0.00089	59
D	D <sub>4</sub>	CCH	-0.0054	-0.00106	-0.00092	
CCH	H <sub>4</sub>	CCH	-0.0071	-0.00035	-0.00036	
CCH	D <sub>4</sub>	CCH	-0.0054	-0.00037	-0.00038	
H	H <sub>4</sub>	HC=CH <sub>2</sub>	-0.00615	-0.00062	-0.00072	59
H	H <sub>4</sub>	CN	-0.00610	-0.00120	-0.00103	59
D	H <sub>4</sub>	CN	-0.0062	-0.0012	-0.00101	97
H	H <sub>4</sub>	CH <sub>2</sub>	-0.00440	-0.00175	-0.00127	93
H	H <sub>4</sub>	CD <sub>2</sub>	-0.00420	-0.00182	-0.00127	93
D	D <sub>4</sub>	CD <sub>2</sub>	-0.00319	-0.00157	-0.00105	93
ortho-C <sub>6</sub> H <sub>4</sub> F <sub>2</sub>			-0.00449	-0.00082	-0.00084	84
meta-C <sub>6</sub> H <sub>4</sub> F <sub>2</sub>			-0.00370	-0.00128	-0.00106	84



Table 6.1. This table has been updated with the results obtained recently for phenylisocyanate ( $\phi\text{NC}$ )<sup>(68)</sup>, the benzyl-radical ( $\phi\dot{\text{C}}\text{H}_2$ )<sup>(93)</sup>, ortho- and meta-difluoro benzene (DFB)<sup>(84)</sup> and para-DEB (see below).

2. The electronic origin bands for all monosubstituted and all para-disubstituted compounds that have been studied to date are double headed and have been assigned as type B bands. Therefore, the lowest excited singlet states of these molecules have to be designated as  $\tilde{\text{A}}^1\text{B}_2$  in the notation of the  $\text{C}_{2v}$  point group. The electronic origin bands of the first absorption systems of ortho- and meta-DFB are single headed and have been shown to be of type A<sup>(84)</sup>. These observations imply that the lowest-energy transitions of monosubstituted and para-disubstituted benzenes are polarized along the Y axis, which has the same direction as the inertial b axis. For meta- and ortho-DFB, the lowest-energy transition is polarized parallel to the Y and Z axes respectively. These correspond to the direction of the inertial a axis for each type of molecule.

The position of the low-frequency head of the double peaked type B band for monosubstituted and para-disubstituted molecules has been shown<sup>(59)</sup> to depend nearly exclusively on  $\Delta\text{C}$ , while the position of the high frequency head is determined by  $\Delta\text{A}$ . The intensity and width of the high frequency head however is  $\Delta\text{C}$  dependent.

#### B. Application to para-DEB

Two programs were available for the calculation of rotational profiles, namely Parkin's approximate asymmetric rotor program<sup>(94)</sup> (maximum J equal to 110) and Pierce's, still unpublished, exact calculation (maximum J is 50). A copy of the latter program reached the author via an unknown path and some modifications may have been made along this route. The observed type A and

type B bands of  $\phi\text{CGH}^{(63)}$  were reproduced satisfactorily with Pierce's program. Also, similar type B bands were calculated for para-DEB with the two above programs using the same input parameters. But the B and C type bands, calculated with Pierce's program for formaldehyde, are identical and neither agrees with the experimental profile for B and C type bands. It was found that levels for  $J > 50$  contributed considerably to the type B contour for para-DEB. Therefore, Parkin's program was used for computing the band contours for para-DEB.

Input parameters were: nuclear statistical weights of 6 and 10 for even and odd  $K$  respectively for type B bands, and 10 and 6 for type A bands respectively, a computational resolution of  $0.07\text{ cm}^{-1}$ , a line width of  $0.10\text{ cm}^{-1}$ , a linear intensity scale and the ground state rotational constants estimated in Chapter 1. Contours were calculated for selected values of  $\Delta A$  and  $\Delta C$  and  $\Delta B$  was calculated from the planarity condition.

The provision in Parkin's program for using the symmetric rotor approximation could be used to full advantage, since no difference was detected between the contours calculated (a) in asymmetric rotor approximation with  $J \leq 110$ ,  $K = 70$  and the symmetric rotor approximation for  $K$  from 71 to 110, and (b) with  $K$  up to 12 in the asymmetric part and from 13 to 110 in the symmetric rotor formulation.

Microdensitometer tracings of the  $0_0^0$  and  $20_0^1$  bands are presented in Figs. 6.1 and 6.2 respectively. These profiles are rather similar in two respects. First, they contain hardly any line-like rotational fine structure. This lack of detail can be explained as follows. para-DEB is a very large molecule with, consequently, very small rotational constants. This results in a large number of rotational transitions per  $\text{cm}^{-1}$  in the spectrum. The Doppler line widths of rotational transitions are typically  $0.02$  to  $0.03\text{ cm}^{-1}$ .

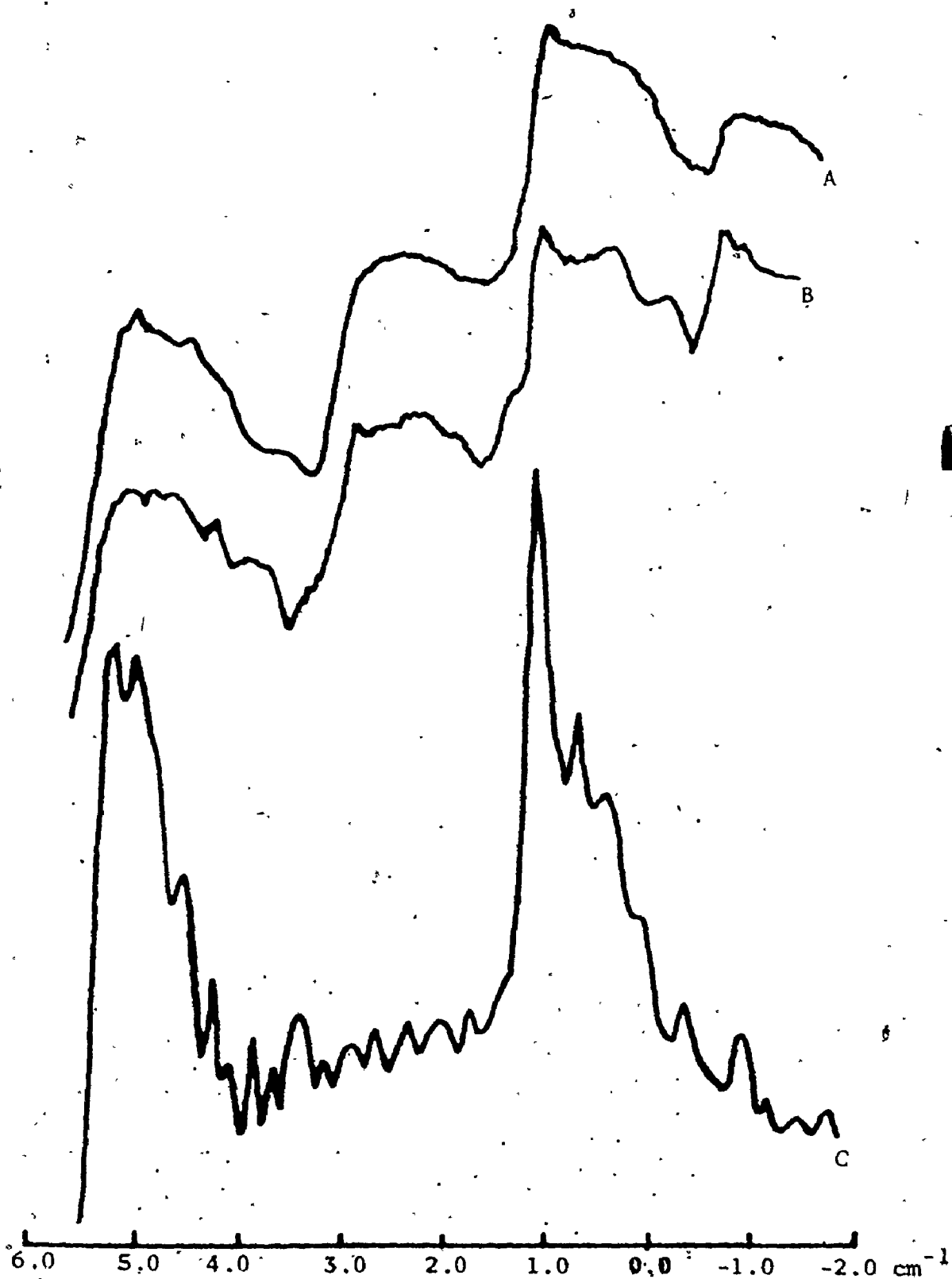


Fig. 6.1. The  $O_0^0$  band (B-type) of para- $h_6$ . (Curves A and B are microdensitometer tracings and curve C is a calculated contour.)

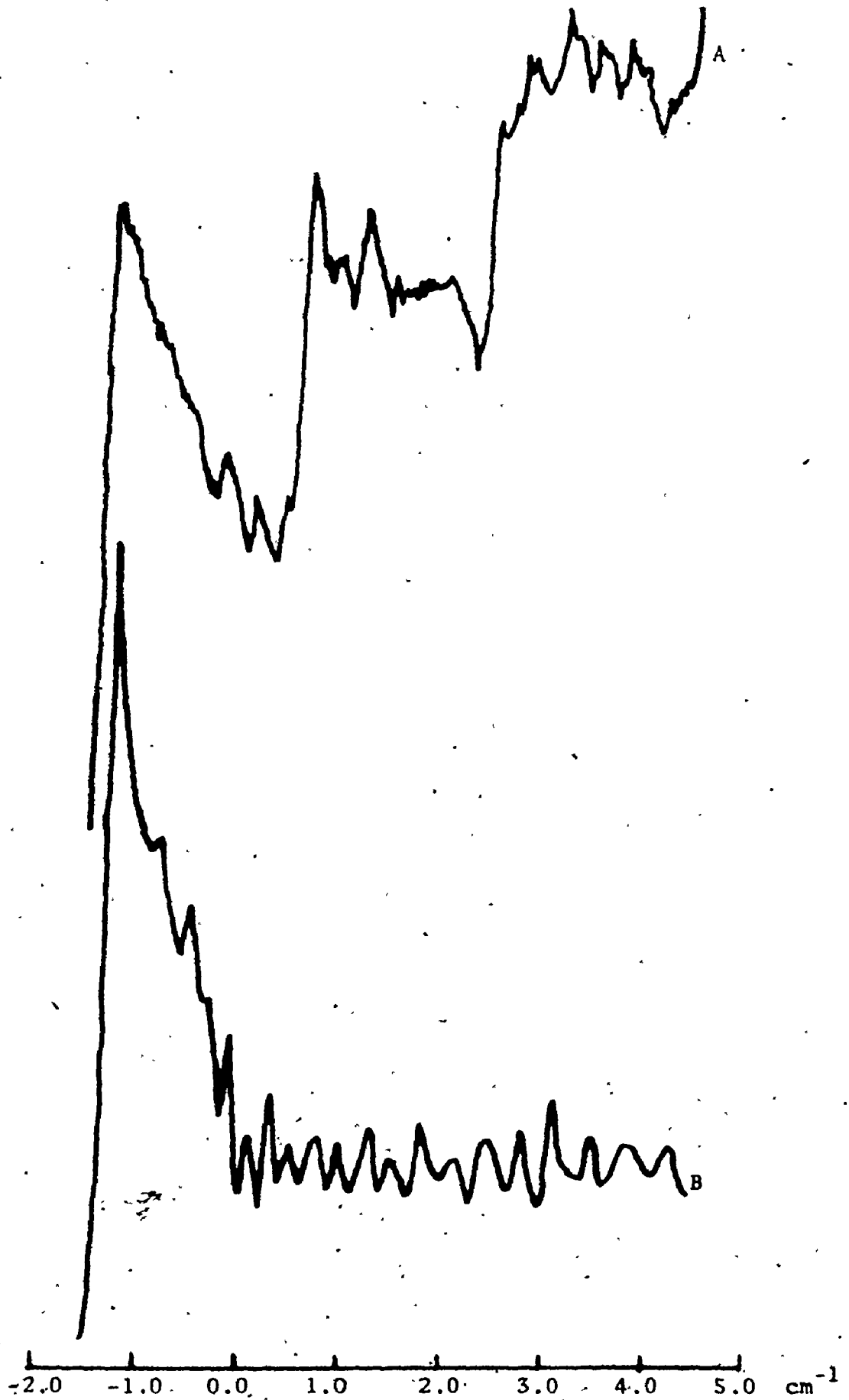


Fig. 6.2. The  $20_0^1$  (A-type) band of para- $\text{h}_6$ . (Curve A is a tracing and

and it is thus not surprising that the vibronic bands in the spectra of very large molecules generally show an unresolved envelope, even under the highest spectroscopic resolution. This is certainly true for  $\phi\text{Cl}$ ,  $\phi\text{Br}$  and para- $\text{C}_6\text{H}_6$ .

Second, both profiles show several absorption maxima separated by  $2.0\text{ cm}^{-1}$ . The tracings for the  $\text{O}_0^0$  band in Fig. 6.1 reveal an additional absorption maximum at about  $4.1\text{ cm}^{-1}$  from the band head. The position of this maximum was determined as  $-4.15 \pm 0.05\text{ cm}^{-1}$  from the high frequency head of the band for both para- $\text{h}_6$  and para- $\text{d}_2$ . This separation was measured on a number of different plates with a travelling microscope. Similar measurements for the ring deuterated isotopes para- $\text{d}_4$  and para- $\text{d}_6$  resulted in a frequency interval of  $3.65 \pm 0.03\text{ cm}^{-1}$  between the two type B heads.

The intensity ratio and the  $2.0\text{ cm}^{-1}$  separation of the first two bands in the profile of the  $\text{O}_0^0$  band of para- $\text{h}_6$  was reproduced (with Parkin's program) for  $\Delta A \approx -0.015\text{ cm}^{-1}$  and  $\Delta E \approx -0.0005\text{ cm}^{-1}$ . The calculated type B contour did however show these two absorption maxima only, and the calculated type A contour revealed only one absorption peak. Further calculations on type B bands showed that values of  $\Delta A$  smaller than  $-0.015\text{ cm}^{-1}$  resulted in a separation between the two peaks smaller than  $2.0\text{ cm}^{-1}$ , while the frequency interval increased for larger  $\Delta A$ . For  $\Delta A = -0.007\text{ cm}^{-1}$  a separation of about  $4.0\text{ cm}^{-1}$  was found between the two B type heads. Line-like rotational structure, which should be experimentally resolvable, was calculated for very small  $\Delta A$  ( $< 0.002\text{ cm}^{-1}$ ). All calculated type A bands were single headed. On the basis of these results, it was concluded that the spectrum of para- $\text{h}_6$  contains a sequence in  $2.0\text{ cm}^{-1}$  and that the absorption maximum of  $4.15\text{ cm}^{-1}$  from the band head corresponds to the low frequency head of the double peaked origin band.

It was seen in Section 6.1.A. that the band head separation for type B bands is determined by  $\Delta C$  and that the relative intensity of the type B peaks is governed by  $\Delta A$ .  $\Delta A$  has therefore been determined by reproducing as closely as possible the head separation of  $4.15$  and  $3.65 \text{ cm}^{-1}$  for para- $\text{h}_6$  and para- $\text{d}_4$  respectively. Unfortunately the intensity ratio of the two peaks cannot be used to find  $\Delta C$  because of the intense sequence bands with unknown Boltzmann factors and the limited latitude of the very fine grain film used. However, the width of the high frequency head is  $\Delta C$  dependent (see 6.1.A.). The  $\Delta C$  upon excitation has been chosen to correspond to the  $\Delta C$  value for which this high frequency band approximates as closely as possible the shape and the half width of the experimental profile.

The approximately correct frequency interval between the two absorption maxima of the  $0_0^0$  band was found above for  $\Delta A = -0.007 \text{ cm}^{-1}$ . The data in Table 6.1 for other para-disubstituted benzenes suggests the value of  $\Delta C$  to lie within the range from  $-0.0001$  to  $-0.0005 \text{ cm}^{-1}$ . Therefore a grid search was made in which  $\Delta A$  varied from  $-0.005 \text{ cm}^{-1}$  to  $-0.009 \text{ cm}^{-1}$  in steps of  $0.0005 \text{ cm}^{-1}$ . For each value of  $\Delta A$ ,  $\Delta C$  was varied from  $-0.0002$  to  $-0.0005 \text{ cm}^{-1}$  in steps of  $0.00004 \text{ cm}^{-1}$ .

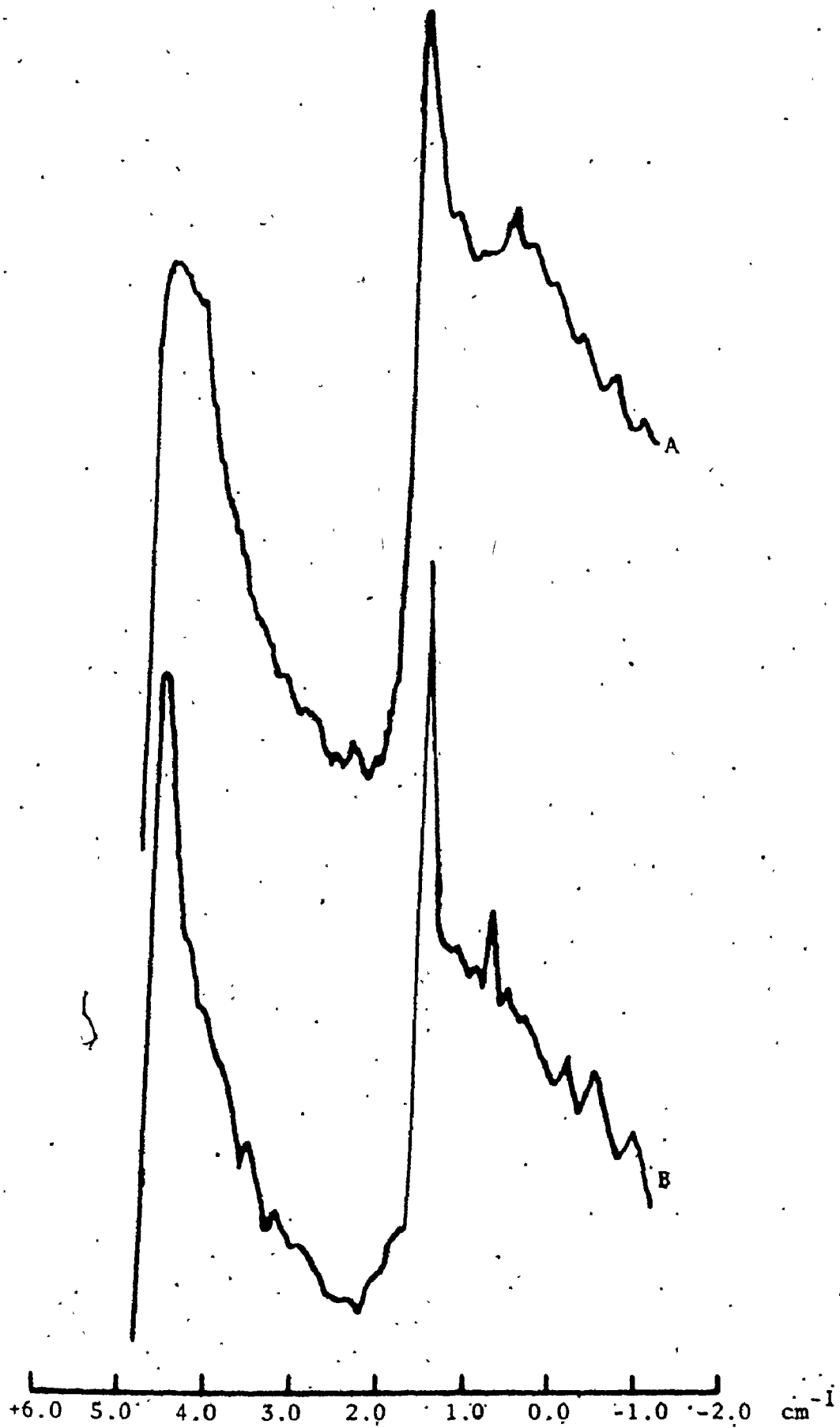
For low values of  $\Delta C$ , the high frequency head was calculated to have a half width of about  $1 \text{ cm}^{-1}$  and a very low intensity. For high values of  $\Delta C$ , this head showed a small half width and a high intensity. The intensity and half width of this head went through a maximum simultaneously for intermediate  $\Delta C$ . It was assumed that the  $\Delta C$  value corresponding to these maxima represents the  $\Delta C$  upon electronic excitation. A fine grid search then showed that reasonable fits were bracketed by  $\Delta A = -0.0071 \pm 0.0001 \text{ cm}^{-1}$  and  $\Delta C = -0.00036 \pm 0.00002 \text{ cm}^{-1}$  for para- $\text{h}_6$  and by  $\Delta A = -0.0054 \pm 0.0001 \text{ cm}^{-1}$  and  $\Delta C =$

$-0.00038 \pm 0.00002 \text{ cm}^{-1}$  for para- $d_4$ . The lack of detail in the profile did not enable a more accurate determination of the changes in rotational constants upon electronic excitation. The calculated type B band is presented in Fig. 6.1 for para- $h_6$ . It was not considered worthwhile to superimpose the  $2.0 \text{ cm}^{-1}$  sequence bands on the calculated contour. The profile of the type A band calculated with the above  $\Delta A$  and  $\Delta C$  values is presented in Fig. 6.2.

The following similarities between  $\phi\text{CCH}$  and para-DEB are worth noting. First, So<sup>(10)</sup> also observed a difference of  $0.5 \text{ cm}^{-1}$  in the separation between the two type B heads for  $\phi\text{CCH-}h_6$  and  $\phi\text{CCH-}d_5$ . Second, the  $\Delta A$  value for para- $h_6$  is equal to the  $\Delta A$  for  $\phi\text{CCH-}h_6$  and, third, the intensity ratio of the type B heads is calculated as 75:100 for both hydrogenic molecules. Because of these similarities, the above analysis for para-DEB would be supported if the excited state rotational constants for the isotope  $\phi\text{CCH-}d_5$  would be predicted correctly by the above results, namely an increase in  $\Delta A$  of  $0.0017 \text{ cm}^{-1}$  and a very slight decrease in  $\Delta C$  of about  $0.00002 \text{ cm}^{-1}$ , with respect to the hydrogenic compound.

A microdensitometer tracing of the  $O_0^0$  band of  $\phi\text{CCH-}d_5$  (Fig. 6.3) has been made from a plate photographed by So. Also presented in Fig. 6.3 is the contour calculated for the above changes in rotational constants and all other input parameters as used by So. The agreement between the calculated and observed profile could not be improved by slightly varying  $\Delta A$  and  $\Delta C$ . The results obtained are included in Table 6.1. The origin band for meta- $h_6$  is presented in Fig. 6.4 and the  $O_0^0$  band for ortho- $h_6$  in Fig. 6.5. The lack of line-like rotational structure and the presence of sequence bands, make it impossible to use these bands for band contour work.

No type B bands have been found in the spectrum of meta-DEB. Very



00

(C) is a mic



33835.0  $\text{cm}^{-1}$

33804.0  $\text{cm}^{-1}$

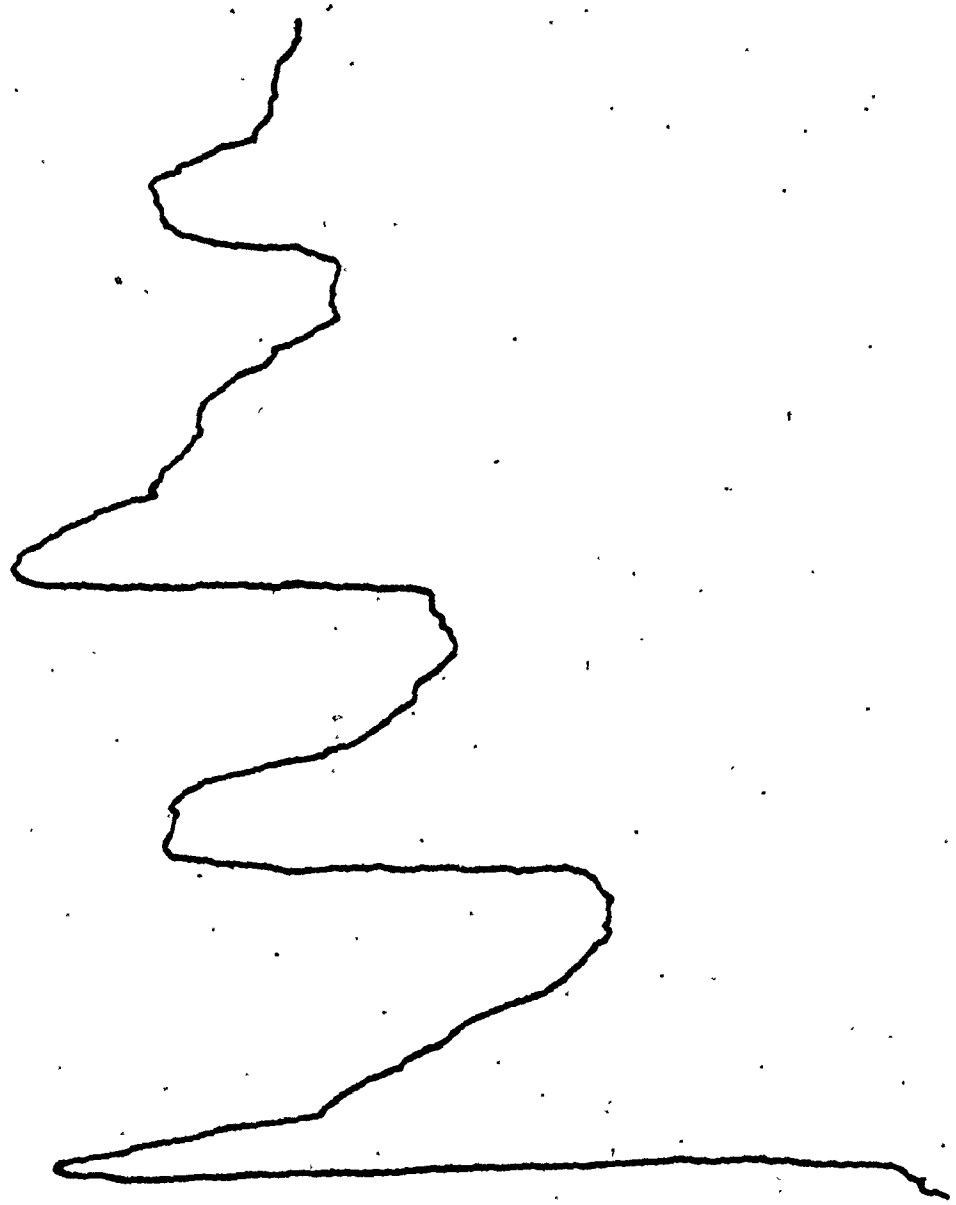


Fig. 6.4. A microdensitometer tracing of the  $O_0$  band of meta- $h_6$ .

33495.1  $\text{cm}^{-1}$

33507.1  $\text{cm}^{-1}$

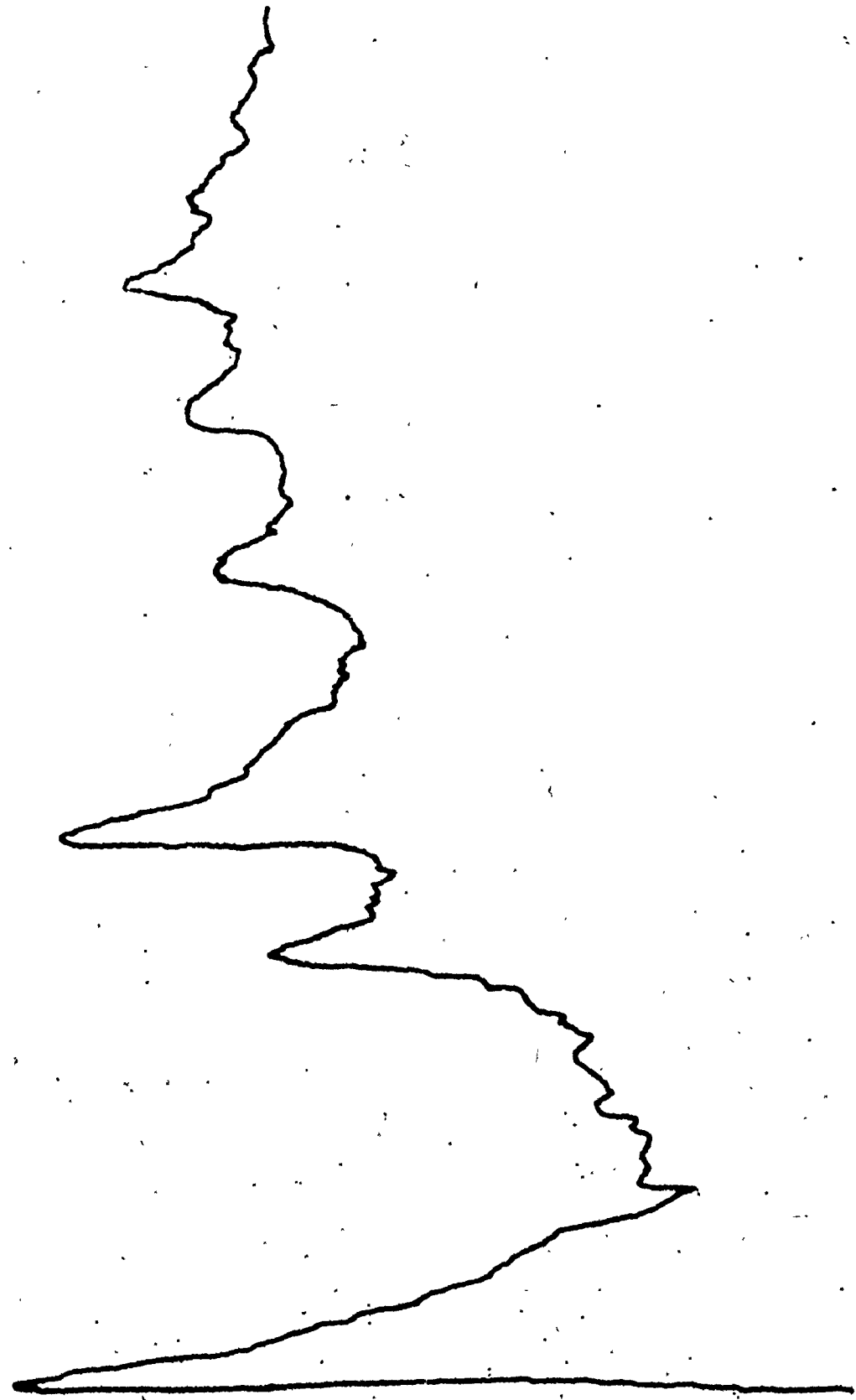


Fig. 6.5. A microdensitometer tracing of the  $0_0^0$  band of ortho- $\text{h}_6$ .

weak double-headed bands with a band head separation of 1.8 and 1.4  $\text{cm}^{-1}$  have been observed in the spectrum of ortho- $\text{h}_6$  and ortho- $\text{d}_4$  respectively. The band contour method has not been used to determine the polarization and the rotational constants for these bands for two reasons. First, not enough sample was available to obtain a band with a reasonable contrast. Second, neither the Parkin nor the Pierce program available reproduced satisfactorily the type B contour reported for ortho-DFB<sup>(84)</sup>.

## 6.2: Excited State Geometries

### A. Benzene

Callomon et al<sup>(51)</sup> have analyzed the rotational structure of the bands in the 260 nm absorption system of  $\text{C}_6\text{H}_6$  and  $\text{C}_6\text{D}_6$ , that arise from the excitation of one quantum of the lowest frequency  $e_{2g}$  vibration in the ground and excited electronic state. The position of all nuclei in the first excited state of benzene can be calculated from the data obtained. It can be shown that

$$\Delta X = -X + \sqrt{X^2 + \frac{1}{48} (2\Delta I_A^H - \Delta I_A^D)} \quad [6.1]$$

where  $\Delta I_A = 16.85689 \frac{A'' - A'}{A'' * A'}$  with A in  $\text{cm}^{-1}$ , X stands for the distance (in Å) of the C-nuclei 2, 3, 5 and 6 from the line joining the C-atoms 1 and 4 in the ground state, while the same distance in the excited state is equal to  $X + \Delta X$ .

Insertion of  $X = 1.397 \text{ \AA}$ , the C—C bond length in the ground state, gives  $\Delta X = +0.033 \text{ \AA}$ . This implies that the C—C bond length has increased by 0.038 Å upon excitation. This result is in excellent agreement with the values derived via Franck-Condon analysis. McKenzie et al<sup>(95)</sup> calculated the increase in C—C bond length as 0.037 Å, using different force fields for the ground and

excited states. Craig<sup>(96)</sup> arrived at a value of 0.035 to 0.036 Å via a simpler procedure in which ground state parameters only were used and in which the C-H grouping was considered as one mass-unit.

#### B. Substituted benzenes

Among the score of derivatives of benzene previously studied in absorption, there is only one isotopically substituted compound, namely  $\phi\text{CN-d}_4$ . Brand and Knight<sup>(97)</sup> found that the changes in rotational constants for this molecule were less than the accuracy to which the rotational constants are known for  $\phi\text{CN}$ . Cossart-Magos and Leach<sup>(93)</sup> have studied the rotational structure in the high resolution gas phase emission spectra of  $\text{C}_6\text{H}_5\text{CH}_2$  (I),  $\text{C}_6\text{H}_5\text{CD}_2$  (II) and  $\text{C}_6\text{D}_5\text{CD}_2$  (III). The changes in the rotational constants upon excitation can be used to calculate the  $r_s$  position of the methylenic protons and the average change in the distance of the nuclei 2, 3, 5 and 6 from the line joining the C-atoms 1 and 4. Insertion of the data for the isotopes II and III into equation [6.1] gives  $\overline{\Delta X} = +0.017$  Å. The results obtained in this study make it possible to calculate  $\Delta X = +0.027$  Å for para-DEB. This value of  $\Delta X$  is independent of  $X$  in the range  $X = 1.397 \pm 0.010$  Å. Likewise, the same average increase ( $\overline{\Delta X} = +0.027$  Å) is found for  $\phi\text{CCH}$  using the results for  $\phi\text{CCH-h}_6$  and  $\phi\text{CCH-d}_5$ . The corresponding increase for benzene was found earlier as 0.033 Å. The difference amounts thus to only 0.006 Å between para-DEB and benzene. This constitutes the only quantitative statement to date concerning the excited state geometry of benzene derivatives. Further information on the substitution structure of benzene derivatives can only be obtained by studying isotopes with  $^{13}\text{C}$  nuclei. A small uncertainty will remain in the position of the C-nuclei because of the uncertainty in the changes in the rotational constants obtained via the band contour method.

These uncertainties have been estimated as:  $\Delta A$ ,  $\pm 0.0001 \text{ cm}^{-1}$ ;  $\Delta B$ ,  $\pm 0.00002$  to  $\pm 0.00003 \text{ cm}^{-1}$ ; and  $\Delta C$ ,  $\pm 0.00001$  to  $\pm 0.00002 \text{ cm}^{-1}$ . The magnitude of these estimated errors is confirmed by the results of the independent studies on para-DFB<sup>(98,99,100)</sup> and  $\phi\text{OH}$ <sup>(61,101)</sup>. These uncertainties do not make it possible to use the inertial defect for establishing the planarity or non-planarity of the ring. The in-plane distortion of the aromatic ring upon excitation determines the change in moment of inertia along the a axis. No unique structural information can however be obtained from only two independent rotational constants, because A is determined--in first approximation-- by four bond lengths ( $r_{1,2}$ ,  $r_{3,4}$ ,  $r_{4,5}$  and  $r_{5,6}$ ) and two bond angles ( $\angle C_6C_1C_2$  and  $\angle C_3C_4C_5$ ), if the C-H grouping is considered as one mass-unit (c.f. Craig<sup>(96)</sup>). Because of ring-strain, the maximum change in bond angle is about 4 degrees. If both above bond angles would increase by this amount upon excitation, then  $\Delta A = -0.006 \text{ cm}^{-1}$ . The experimental values of  $\Delta A$  (Table 6.1) are all larger than this value, except for the benzyl radical. An increase in bond length thus almost certainly occurs upon excitation.

Two simple, extreme models can be used to explain the observed changes in  $\Delta A$ .

1. The bond angles in the ground and excited state of benzene derivatives are equal to  $120^\circ$  and the substituents affect only the bond lengths, and only slightly.
2. The bond lengths in the ground and excited state of all benzene derivatives are set equal to those for the corresponding states of benzene. The substituents cause small changes in the angles only.

A third, more complex model would be that

3. all four bond lengths and both bond angles, that define A, undergo apprec-

able changes upon excitation. The changes in bond length are not the same as those occurring for benzene. Of course, different substituted benzenes may approach more closely to either model 1 or model 2.

The above models will now be considered from different points of view.

#### Chemical intuition.

The main difficulty in models 1 and 2 is which choice of initial assumptions is more plausible. For para- $\phi F_2$ , for instance, the changes in rotational constants have been determined in three independent studies (98,99,100) and a different excited state geometry is postulated in each study. Model 1 and 2 are inconsistent with the observation (see Table 6.1) that the  $\Delta A$ 's are very nearly equal for  $\phi Cl$  and para- $\phi Cl_2$ ,  $\phi F$  and para- $\phi F_2$ , and  $\phi CCH$  and para-DEB. Cvitas et al<sup>(19)</sup> have predicted excited state geometries for a number of benzene derivatives that show almost identical changes in rotational constants upon excitation. It has been argued in detail in Chapter 1 that such small differences in rotational constants cannot be used to arrive at unambiguous structural information.

#### Franck-Condon analysis

No Franck-Condon analysis has been reported to date for the lowest  $\pi \rightarrow \pi^*$  transition of any substituted benzene. It is worthwhile to estimate the magnitude of the ring distortion that can be derived from a simple Franck-Condon analysis analogous to Gray's simplified procedure, viz. the excited state geometry is derived from the intensity distribution in the totally symmetric ring breathing vibration using a ground state force field.

Scherer<sup>(102)</sup> has derived a force field for the ground state of  $\phi Cl$  by studying the complete range of chlorinated aromatic molecules  $C_6H_xCl_{6-x}$ . The suggested force field resulted in a mean frequency error of  $\pm 2 \text{ cm}^{-1}$  for the

calculated and experimental fundamental frequencies. The importance of Scherer's study lies in the fact that he did not only calculate the Cartesian displacements for the single quantum excitation of the ring breathing mode, but also the uncertainties in these displacements. If the ring C-nuclei in  $\phi\text{C}_6\text{H}_6$  are numbered as in Fig. 1.1 for  $\phi\text{CCH}$ , Scherer's result can be summarized as follows:

The uncertainties in the displacements of the C-nuclei 2, 4 and 6 are much smaller than the displacements themselves, while the reverse is true for the C-atoms 1, 3 and 5. Nothing can thus be said about the motions of the latter nuclei.

The difference in  $\Delta A$  between  $\phi\text{C}_2$  and  $\phi$  equals  $-0.00235 \text{ cm}^{-1}$ . This value corresponds to a total increase of  $0.04 \text{ \AA}$  in four bond lengths, if model 1 is assumed. Likewise, in model 2, a total increase of 3.4 degrees should occur in two bond angles. It is doubtful that the above Franck-Condon procedure could distinguish between these two possibilities.

### Theoretical considerations

Several formulae have been proposed to calculate bond lengths from bond orders<sup>(5,6,103)</sup>, calculated in  $\pi$ -electron approximation. The change in  $\pi$ -bond order upon electronic excitation for benzene<sup>(5)</sup> is approximately equal to the change calculated for a number of substituted benzenes<sup>(104)</sup>. According to these calculations, the changes in bond length upon excitation are very nearly equal for benzene and its derivatives and the differences in  $\Delta A$  must thus arise from changes in bond angles (model 2). These changes cannot be evaluated without the inclusion of  $\sigma$ -electrons in the calculation. It was decided therefore to calculate--in CNDO approximation--the changes in geometry from the bond lengths and bond angles for which the energy was minimal for the

ground and excited state.

The CNDO/2 parametrization proposed by Pople and Segal<sup>(92)</sup> has been applied successfully to calculate bond lengths and bond angles. This scheme appears to fail however for calculating vertical excitation energies<sup>(47,92,105)</sup>. Jaffé and Del Bene<sup>(47)</sup> have proposed a parametrization scheme in order to calculate electronic transitions more accurately. Excellent agreement between predicted and experimental  $\pi + \pi^*$  transition energies was found for the DEBs in Chapter 4. The Jaffé and Del Bene scheme did not, however, result in reliable  $\sigma$ -MO's for the CCH groups. The CNDO/2 parameters were therefore used to compute bond lengths and bond angles. No additional calculations were carried out to find vertical excitation energies.

Ground state geometries were calculated with a closed shell CNDO/2 program, kindly provided by Dr. D. P. Santry. Self-consistency was assumed when the difference in energy between two successive iterations was less than  $10^{-5}$  a.u. This criterion was satisfied after about 10 iterations, when the eigenvectors of the Hamiltonian were used as initial MO's. Self-consistency was achieved much faster (3 to 4 iterations), when the SCF-MO's for a slightly different geometry were used as initial MO's.

Excited state geometries were computed with the open shell CNDO/2 program described by Kroto and Santry<sup>(106)</sup>. Two changes were introduced into this program. First, the Fock-matrices of the Nth and (N-1)th iteration were averaged, whenever the difference in energy between two successive iterations was smaller than zero. The same procedure has been used previously to bring about convergence<sup>(57,105)</sup>. Second, strict orthogonality was maintained between the closed and open shell orbitals by using the virtual orbitals of the closed shell calculation as a basis for the open-shell calculations<sup>(107)</sup>.



Self-consistency ( $\Delta E < 5 \times 10^{-5}$  a.u.) was usually achieved after about 12 iterations, if the eigenvectors of the Hamiltonian were used as initial MO's. Half this number of iterations was sufficient, when the calculations were started with the SCF-MO's obtained for a slightly different geometry.

Open-shell CNDO/2 calculations on several small molecules have reproduced satisfactorily the experimental excited state geometries<sup>(105-108)</sup>. No such calculations have been reported for such large polyatomics, as the benzene derivatives considered in this study. Computations were carried out for the molecules  $\phi$ ,  $\phi F$ ,  $\phi CCH$  and para-DEB. The  $r_s$  ground state geometry of the first three molecules is known and the changes in  $\Delta A$  for  $\phi F$  and  $\phi CCH$  deviate in opposite directions from the  $\phi$  value. In order to be useful, this theoretical approach should predict correctly, at least, the order of magnitude of  $\Delta A$  for  $\phi$ ,  $\phi F$ ,  $\phi CCH$  and para-DEB.

The results of the calculations are presented in Table 6.2. The ground state geometries have been discussed in detail in Chapter 1. It is sufficient to state here only that the ring C—C bond lengths for the ground states were systematically too short by 0.01 Å. This systematic error is probably caused by the neglect of differential overlap and all ring C—C bond lengths were incremented by 0.01 Å in the ground and excited electronic states. It is no use to discuss in any detail the calculated excited state geometries. The data in Table 6.2 namely show that the calculated  $\Delta A$ 's for  $\phi$  and  $\phi F$  are both about 25% lower than the experimental values, while the theoretical  $\Delta A$ 's for  $\phi CCH$  and para-DEB are about 40% higher than the observed  $\Delta A$ 's. It is impossible to say whether bond lengths or bond angles are responsible for the poor agreement, although the latter are rather large (about 5 degrees) for  $\phi CCH$  and para-DEB.

Table 6.2

Calculated ground and excited state geometries for  $\phi$ ,  $\phi F$ ,  $\phi CCH$  and para-DEB

	$r_{1,2}(\text{\AA})$	$r_{2,3}(\text{\AA})$	$r_{3,4}(\text{\AA})$	$r_{7,8}(\text{\AA})$	$r_{1,8}(\text{\AA})$	$\angle C_6C_1C_2$	$\angle C_3C_4C_5$	$\Delta A_{\text{calc.}}(\text{cm}^{-1})$	$\Delta A_{\text{exp.}}(\text{cm}^{-1})$
$\tilde{X}^1A_{1g}$	1.397	1.397	1.397	-	-	120.0	120.0	-0.0065	-0.0086
$\tilde{A}^1B_{2u}$	1.424	1.424	1.424	-	-	120.0	120.0		
$\tilde{X}^1A_1$	1.397	1.395	1.395	-	1.348	122.5	119.5	-0.0090	-0.0118
$\tilde{A}^1B_2$	1.422	1.405	1.418	-	1.324	125.5	121.0		
$\tilde{X}^1A_1$	1.405	1.395	1.396	1.423	1.209	118.5	120.0	-0.0103	-0.0071
$\tilde{A}^1B_2$	1.432	1.405	1.415	1.385	1.224	121.0	123.5		
$\tilde{X}^1A_1$	1.406	1.395	1.406	1.423	1.209	118.6	118.6	-0.0116	-0.0071
$\tilde{A}^1B_{2u}$	1.425	1.407	1.425	1.398	1.222	123.0	123.0		

It can be concluded that the rotational constants of the first excited electronic state of benzene derivatives, that have been determined to date, cannot be used to shed further light on the structure of the aromatic ring.

#### Further experimental work

The data in Table 6.1 contain the following information. First, it is seen that  $\Delta C$  for monosubstitution is much larger than  $\Delta C$  for para-disubstitution and that the  $\Delta C$  values for the latter molecules fall within a rather narrow wave number range. (This observation was very helpful for finding  $\Delta C$  for para-DEB.) Second, the observed  $\Delta A$  values fall into two classes. Class I is defined by  $\Delta A = -0.011 \pm 0.001 \text{ cm}^{-1}$  and contains the halogenobenzenes, phenol and para-fluorophenol, aniline and para-fluoroaniline. Class II is defined by  $\Delta A = -0.007 \pm 0.001 \text{ cm}^{-1}$  and contains benzene derivatives with two  $\pi$ -electrons. para-DEB is the first compound studied with two such substituents. No hybrid compound, such as para-fluoroethynylbenzene (para-F $\phi$ CCH) for instance, has been studied to date. Yet, this class of molecules can provide useful information. If  $\Delta A$  for para-F $\phi$ CCH were found to be equal to approximately the sum of the  $\Delta A$ 's for  $\phi$ CCH and  $\phi$ F, it can be concluded that substituent effects are localized and that the excited state geometry can be described best with model 3. If  $\Delta A$  were to have a value between  $-0.007$  and  $-0.012 \text{ cm}^{-1}$ , it seems likely that slight distortions of the aromatic ring occur upon substitution in ground and excited electronic states (model 1 and 2). It is unlikely that  $\Delta A$  for para-F CCH would be smaller than the  $\Delta A$  for  $\phi$ CCH.

#### Conclusions

The change in the moment of inertia along the a axis upon electronic excitation has been determined for the isotopes para- $\text{h}_6$  and para- $\text{d}_4$ . The distance of the unsubstituted C-nuclei from the main symmetry axis has been

calculated to increase by  $0.027 \text{ \AA}$  upon electronic excitation. The analogous increase for benzene is  $0.033 \text{ \AA}$ .

It is shown that nothing definitive can be said about the geometry of the aromatic ring in the first excited electronic state of benzene derivatives, notwithstanding the score of such molecules studied to date. Further experimental studies are suggested to gain an insight into the changes in the ring geometry upon excitation.

## CONCLUSIONS

The vibrational spectra of a total of nine isotopes of the three isomeric diethynylbenzenes have been investigated over the 60 to 4000  $\text{cm}^{-1}$  region. The analysis of the infrared and Raman spectra has resulted in the assignment of the 42 fundamental frequencies of each of the diethynylbenzenes. The analysis has established the occurrence of a coupling between the out-of-plane skeletal bending modes of the acetylenic groups with out-of-plane benzene vibrations. The ambiguities in the assignments of the bands measured in the far infrared region of the monosubstituted benzenes  $\phi\text{CCH}$  and  $\phi\text{CN}$  are explained by this interaction.

For each diethynylbenzene, three low energy  $\pi \rightarrow \pi^*$  transitions are observed in the near and far ultraviolet regions. The longest wavelength absorption systems show some discrete vibrational structure, while the other transitions contain diffuse vibrational bands. In order to aid the interpretation of the observed spectra, a review is presented of the analyses reported for benzene and its mono- and disubstituted derivatives. Molecular orbital calculations--in CNDO approximation--are carried out to support the evidence obtained from the review that the lower  $\pi \rightarrow \pi^*$  electronic states of the diethynylbenzenes show large redshifts with respect to the corresponding transitions in other substituted benzenes.

The three lowest calculated transitions should be assigned as follows according to these calculations:  $\tilde{A} \ ^1B_{2u} + \tilde{X} \ ^1A_g$ ,  $\tilde{B} \ ^1B_{1u} + \tilde{X} \ ^1A_g$  and  $\tilde{C} \ ^1B_{2u} + \tilde{X} \ ^1A_g$  for para-diethynylbenzene;  $\tilde{A} \ ^1B_2 + \tilde{X} \ ^1A_1$ ,  $\tilde{B} \ ^1A_1 + \tilde{X} \ ^1A_1$  and  $\tilde{C} \ ^1B_2 + \tilde{X} \ ^1A_1$  for meta-diethynylbenzene; and  $\tilde{A} \ ^1A_1 + \tilde{X} \ ^1A_1$ ,  $\tilde{B} \ ^1B_2 + \tilde{X} \ ^1A_1$  and  $\tilde{C} \ ^1A_1 + \tilde{X} \ ^1A_1$  for ortho-diethynylbenzene in order of increasing transition energies. The B and C systems are predicted to show redshifts of as much as

40 to 50 nm, while the A systems show minor redshifts with respect to the analogous transitions in benzene and its substituted derivatives.

The agreement between the calculated and observed transition energies and oscillator strengths is quite good for each diethynylbenzene. The predicted ( $B_{2u}$ ) symmetry of the first excited electronic state of para-diethynylbenzene is supported by a band contour analysis of the double headed origin band. The proposed ( $B_{1u}$ ) symmetry of the second excited electronic state is consistent with the ( $b_{3g}$ ) symmetry of the vibration via which the very weak A system borrows intensity from the intense B system. No band contour analyses could be carried out on the  $O_0^0$  bands of ortho- and meta-diethynylbenzene, because these bands show an unresolved rotational envelope with only one absorption maximum. A similar single headed profile has been observed for the  $O_0^0$  bands of the lowest-energy transitions of ortho- and meta-difluorobenzene. The calculation of these profiles<sup>(84)</sup> has shown that the lowest-energy transitions in ortho- and meta-difluorobenzene have the same symmetry as predicted for ortho- and meta-diethynylbenzene.

This theoretical and experimental evidence provides support for the correlation between the higher excited electronic states of benzene and those of its derivatives. Previous studies have been limited to the first excited electronic state mainly.

The aim of spectroscopy is the elucidation of molecular structure in ground and excited electronic states. These structures for benzene and its derivatives are discussed in Chapters 1 and 6 respectively. It is shown in Chapter 1 that neither isotopic substitution nor chemical intuition and CNDO calculations have revealed how substitution affects the geometry of the aromatic ring. The unknown distortion of the hexagonal ring is estimated to result in

an uncertainty of 0.5 to 1.0% in the ground state rotational constants. In Chapter 6, the changes in the rotational constants B and C upon electronic excitation are seen to fall within the above margin of 0.5 to 1.0% for all substituted benzenes. However, the change in the rotational constant A ( $\Delta A$ ) amounts to 4% for benzene. For conjugated derivatives of benzene, such as styrene, benzonitrile, phenylacetylene and para-diethynylbenzene,  $\Delta A$  equals 3% and  $\Delta A \approx 5\%$  for all other substituted benzenes. The differences between the  $\Delta A$  for benzene and its derivatives is thus only  $\pm 1\%$ . This change is of the order of magnitude of that induced by purely vibrational excitation. It is not surprising, therefore, that it has not been possible to find the distortions of the regular hexagonal excited state ring geometry of benzene caused by the substituents, via arguments based on chemical intuition, Franck-Condon analysis and theoretical considerations. With the help of the data obtained in this study for para-diethynylbenzene and perdeutero para-diethynylbenzene, the distance of the unsubstituted C-nuclei from the main symmetry axis has been calculated to differ only 0.006 Å from the analogous increase for benzene. The determination of the molecular structure of benzene derivatives thus requires almost certainly a study of heavy atom isotopes.

## BIBLIOGRAPHY

1. G. Herzberg, "Infrared and Raman Spectra", D. van Nostrand Co., Inc., New York, 1968.
2. G. Herzberg, "The Electronic Spectra of Polyatomic Molecules", D. van Nostrand Co., Inc., Princeton, New Jersey, 1967.
3. G. W. King, "Spectroscopy and Molecular Structure", Holt, Rinehard and Winston, Inc., New York, 1964.
4. G. Varsanyi, "Vibrational Spectra of Benzene Derivatives", Academic Press, New York, 1969.
5. R. G. Parr, "Quantum Theory of Molecular Electronic Structure", W. A. Benjamin, Inc., New York, 1963.
6. M. J. S. Dewar, "The Molecular Orbital Theory of Organic Chemistry", McGraw Hill, Inc., New York, 1969.
7. (a) T. Oka, J. Phys. Soc. Japan, 15, 2274 (1953).  
(b) J. Kraitchman, Am. J. Phys., 21, 17 (1953).
8. A. A. Westenberg, G. H. Goldstein and E. B. Wilson, J. Chem. Phys., 17, 1319 (1949).
9. J. H. Callomon and B. P. Stoicheff, Can. J. Phys., 35, 373 (1957).
10. S. P. So, Ph.D. Thesis, McMaster University, 1969.
11. B. P. Stoicheff, Tetrahedron, 17, 135 (1962).
12. J. K. Tyler and J. Sheridan, Trans. Far. Soc., 59, 2661 (1963).
13. D. R. Lide, Tetrahedron, 17, 125 (1962).
14. C. C. Costain, J. Chem. Phys., 29, 864 (1958).
15. L. Nygaard, I. Bojesen, T. Pedersen and J. Rastrup-Anderson, J. Mol. Struct., 2, 209 (1968).
16. J. Casado, L. Nygaard and G. O. Sorenson, J. Mol. Struct., 8, 211 (1971).
17. B. Bak, D. Christensen, W. B. Dixon, L. H. Nygaard and J. Rastrup-Anderson, J. Chem. Phys., 37, 2027 (1962).
18. J. Trotter, Acta Cryst., 13, 86 (1960).
19. T. Cvitas, J. M. Hollas and G. H. Kirby, Mol. Physics, 19, 305 (1970).
20. T. L. Jacobs, Org. Reactions, V, 1 (1949).



22. J. M. Watson, *Macromol.*, 5, 331 (1972).
23. R. E. Dessy, Y. Okuzumi and A. Chen, *J. Am. Chem. Soc.*, 84, 2899 (1962).
24. G. W. Chantry, H. M. Evans, J. W. Fleming and H. A. Gebbie, *Infrared Physics*, 9, 31 (1969).
25. G. W. King, *J. Sci. Instr.*, 35, 11 (1958).
26. W. Bracke, *J. Polym. Science A1*, 10, 2097 (1972).
27. G. W. King and S. P. So, *J. Mol. Spectrosc.*, 36, 468 (1970).
28. C. D. Cooper and H. Spomer, *J. Chem. Phys.*, 20, 1248 (1952).
29. R. A. Nyquist and W. J. Potts, *Spectrochim. Acta*, 16, 419 (1960).
30. J. H. S. Green, *Spectrochim. Acta*, 26A, 1913, 1503, 1523 (1970).
31. C. Garrigou-Lagrange, M. Chehata and J. Lascombe, *J. Chim. Phys.*, 63, 552 (1966).
32. C. Garrigou-Lagrange, J-M. Lebas and M. Josien, *Spectrochim. Acta*, 12, 305 (1958).
33. P. N. Gates, R. Radcliffe and D. Steele, *Spectrochim. Acta*, 25A, 507 (1969).
34. A. Stojiljkovic and D. H. Whiffen, *Spectrochim. Acta*, 12, 47 (1958).
35. J. C. Evans and R. A. Nyquist, *Spectrochim. Acta*, 16, 918 (1960).
36. M. R. Padhye and B. S. Rao, *J. Sci. Ind. Res., Sect. B.*, 18, 499 (1959).
37. K. M. Danchinov, A. N. Rodionov, E. A. Gastilovich and D. N. Shigorin, *Opt. Spectrosc.*, 31, 648 (1971).
38. R. J. Jacobsen, *Spectrochim. Acta*, 21, 127 (1965).
39. R. J. Jacobsen and F. F. Bentley, *Appl. Spectry.*, 18, 88 (1964).
40. H. W. Wilson and J. E. Bloor, *Spectrochim. Acta*, 21, 45 (1965).
41. A. D. Allen and C. D. Cook, *Can. J. Chem.*, 41, 1084 (1963).
42. D. H. Whiffen, *J. Chem. Soc.*, 1350 (1956).
43. D. H. Whiffen, *Spectrochim. Acta*, 7, 253 (1955).
44. R. A. Nalepa and J. D. Laposa, accepted for publication in the *Journal of Molecular Spectroscopy*.

46. C. S. Parmenter, *Adv. Chem. Phys.*, XXII, 365 (1972).
47. J. Del Bene and H. H. Jaffé, *J. Chem. Phys.*, 48, 1807 (1968).
48. S. D. Peyerimhoff and R. J. Buenker, *Theor. Chim. Acta (Berlin)*, 19, 1 (1970).
49. S. P. McGlynn, T. Azumi and M. Kinoshita, "Molecular Spectroscopy of the Triplet State", Prentice Hall, Englewood Cliffs, N.J., 1969.
50. L. Burnelle and M. J. Kranepool, *J. Mol. Spectrosc.*, 37, 383 (1971).
51. J. H. Callomon, T. M. Dunn and I. M. Mills, *Phil. Trans. Roy. Soc. London, Ser. A*, 259, 499 (1966).
52. B. Katz, M. Brith, B. Sharf and J. Jortner, *J. Chem. Phys.*, 52, 88 (1970).
53. G. W. King and E. H. Pennington, *J. Mol. Spectrosc.*, 15, 394 (1965).
54. A. A. Gwaiz, M. A. El-Sayed and D. S. Tinti, *Chem. Phys. Letters*, 9, 454 (1971).
55. A. L. Sklar, *J. Chem. Phys.*, 10, 135 (1942).
56. J. Petrushka, *J. Chem. Phys.*, 34, 1111, 1120 (1961).
57. G. W. King and A. A. G. van Putten, *J. Mol. Spectrosc.*, 42, 514 (1972).
58. G. W. King and A. A. G. van Putten, *J. Mol. Spectrosc.*, 44, 286 (1972).
59. I. G. Ross', *Adv. Chem. Phys.*, XXV, 341 (1973).
60. J. C. D. Brand, D. R. Williams and T. J. Cook, *J. Mol. Spectrosc.*, 20, 359 (1966).
61. H. D. Bist, J. C. D. Brand and D. R. Williams, *J. Mol. Spectrosc.*, 21, 76 (1966); 24, 413 (1967).
62. J. C. D. Brand, S. Califano and D. R. Williams, *J. Mol. Spectrosc.*, 26, 398 (1968).
63. G. W. King and S. P. So, *J. Mol. Spectrosc.*, 37, 543 (1971).
64. N. Ginsburg, W. W. Robertson and F. A. Matsen, *J. Chem. Phys.*, 14, 511 (1946).
65. S. H. Wollman, *J. Chem. Phys.*, 14, 123 (1946).
66. R. C. Hirt and J. P. Howe, *J. Chem. Phys.*, 16, 480 (1948).
67. W. W. Robertson, J. F. Music and F. A. Matsen, *J. Am. Chem. Soc.*, 72, 5260 (1960).

68. A. R. Muirhead, A. Hartford, Jr., K. Huang and J. R. Lombardi, *J. Chem. Phys.*, 56, 4385 (1972).
69. S. Prakash and N. L. Singh, *J. Scient. Ind. Res.*, B21, 512 (1962).
70. H. Sponer and S. J. Wolfman, *J. Chem. Phys.*, 9, 816 (1941).
71. K. Kimura and S. Nagakura, *Theor. Chim. Acta (Berlin)*, 3, 164 (1965).
72. K. Kimura and S. Nagakura, *Mol. Phys.*, 9, 117 (1965).
73. J. R. Lombardi, *J. Chem. Phys.*, 56, 2278 (1972).
74. K. Huang and J. R. Lombardi, *J. Chem. Phys.*, 55, 4072 (1971).
75. G. L. LeBel and J. D. Laposa, *J. Mol. Spectrosc.*, 41, 249 (1972).
76. H. Singh and J. D. Laposa, *Journ. of Luminesc.*, 3, 287 (1971).
77. R. A. Nalepa and J. D. Laposa, accepted for publication in the *Journal of Luminescence*.
78. A. H. Kalantar and A. C. Albrecht, *Ber. Bunsengesellsch. Physik. Chemie*, 68, 361 (1964).
79. B. Ford, *Theor. Chim. Acta (Berlin)*, 10, 342 (1968).
80. H. E. Popkie and J. B. Moffat, *Can. J. Chem.*, 43, 624 (1965).
81. C. D. Cooper and M. L. N. Sastri, *J. Chem. Phys.*, 20, 607 (1952).
82. C. D. Cooper, *J. Chem. Phys.*, 21, 379 (1953).
83. B. Katz, M. Brith, B. Sharf and J. Jortner, *J. Chem. Phys.*, 54, 3924 (1971).
84. A. Hartford and J. R. Lombardi, *J. Mol. Spectrosc.*, 40, 262 (1971).
85. P. D. Singh and A. N. Pathak, *Ind. J. Pure Appl. Phys.*, 7, 39 (1969).
86. L. N. Tripath and A. N. Pathak, *Curr. Sci.*, 36, 230 (1967).
87. C. K. Ingold and G. W. King, *J. Chem. Soc.*, 2708 (1958).
88. H. Howard and G. W. King, *Can. J. Chem.*, 37, 700 (1959).
89. J. A. Pople and G. A. Segal, *J. Chem. Phys.*, 43, S136 (1965); 44, 3289 (1966).
90. R. Pariser and R. G. Parr, *J. Chem. Phys.*, 21, 466, 767 (1953).
91. R. S. Mulliken, C. A. Rieke, D. Orloff and H. Orloff, *J. Chem. Phys.*, 17, 1248 (1979).

93. C. Cossart-Magos and S. Leach, *J. Chem. Phys.*, 56, 1534 (1972).
94. J. E. Parkin, *J. Mol. Spectrosc.*, 15, 483 (1965).
95. R. D. McKenzie, I. W. Watkins and J. B. Coon, *Spectrochim. Acta*, 18, 1357 (1962).
96. D. P. Craig, *J. Chem. Soc.*, 2146 (1950).
97. J. C. D. Brand and P. D. Knight, *J. Mol. Spectrosc.*, 36, 328 (1970).
98. Y. Udagawa, M. Ito and S. Nagakura, *J. Mol. Spectrosc.*, 36, 541 (1970).
99. T. Cvitas and J. M. Hollas, *Mol. Phys.*, 18, 793 (1970).
100. S. N. Thakur and N. L. Singh, *Ind. J. Pure Appl. Phys.*, 7, 765 (1969).
101. J. Christofferson, J. M. Hollas and G. H. Kirby, *Proc. Roy. Soc.*, A307, 97 (1968).
102. J. R. Scherer, *Spectrochim. Acta*, 22, 1179 (1966).
103. A. Julg and O. Julg, *Theor. Chim. Acta (Berlin)*, 22, 353 (1971).
104. P. C. Mishra, S. N. Thakur and D. K. Rai, *J. Cryst. Mol. Structure*, 1, 99 (1971).
105. G. A. Segal, *J. Chem. Phys.*, 52, 3530 (1970).
106. H. W. Kroto and D. P. Santry, *J. Chem. Phys.*, 47, 2736 (1967).
107. G. A. Segal, *J. Chem. Phys.*, 53, 360 (1970).
108. G. H. Kirby and K. Miller, *J. Mol. Struct.*, 8, 373 (1971).
109. "Methods of Experimental Physics", editor Dudley Williams, Academic Press, New York 1962, Vol. 3.
110. B. Katz, M. Brith, B. Sharf and J. Jortner, *J. Chem. Phys.*, 54, 3924 (1971).